# TRIBOLOGICAL STUDIES OF ULTRA-THIN FILMS AT HEAD/MEDIA INTERFACE FOR MAGNETIC DATA STORAGE SYSTEMS

**EHSAN RISMANI-YAZDI**

**NATIONAL UNIVERSITY OF SINGAPORE**

**2012**

# TRIBOLOGICAL STUDIES OF ULTRA-THIN FILMS AT HEAD/MEDIA INTERFACE FOR MAGNETIC DATA STORAGE SYSTEMS

**EHSAN RISMANI-YAZDI**

*(B. E, Isfahan University of Technology, Isfahan, Iran)*
*(M.S., Isfahan University of Technology, Isfahan, Iran)*

**A THESIS SUBMITTED**

**FOR THE DEGREE OF DOCTOR OF PHILOSOPHY**
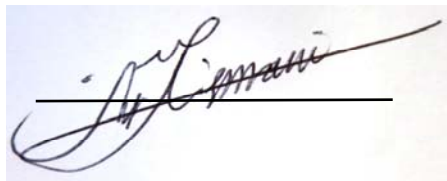
**DEPARTMENT OF MECHANICAL ENGINEERING**

**NATIONAL UNIVERSITY OF SINGAPORE**

**2012**

# Declaration

I hereby declare that this thesis is my original work and it has been written by me in its entirety. I have duly acknowledged all the sources of information which have been used in the thesis.

This thesis has also not been submitted for any degree in any university previously.

**Ehsan Rismani-Yazdi**

# List of Publications

1- **E Rismani**, S. K. Sinha, H. Yang, S. Tripathy, and C. S. Bhatia, "*Effect of pre-treatment of the substrate surface by energetic $C^+$ ion bombardment on structure and nano-tribological characteristics of ultrathin tetrahedral amorphous carbon (ta-C) protective coatings*" Journal of Physics D: applied physics, 44, 115502 (2011)

2- **Ehsan Rismani**, S. K. Sinha, H. Yang, and C. S. Bhatia "*Effect of pre-treatment of Si interlayer by energetic $C^+$ ions on the improved tribo-mechanical properties of magnetic head overcoat*", Journal of Applied Physics, 111, 084902 (2012)

3- **Ehsan Rismani**, S. K. Sinha, H. Yang, and C. S. Bhatia "*Development of a ta-C wear resistant coating with composite interlayer for recording heads of magnetic tape drives*", Tribology Letters, 46, (3), pp. 221-232 (2012)

4- **Ehsan Rismani**, M. Abdul Samad, Sujeet K. Sinha, Reuben Yeo, Hyunsoo Yang, and C. Singh Bhatia, "*Ultrathin Si/C graded layer to improve tribological properties of Co magnetic films*", Applied Physics Letters, 101, 191601 (2012);

5- M. Abdul Samad, **E. Rismani**, H. Yang, S. K. Sinha & C. S. Bhatia, "*Overcoat Free Magnetic Media for Lower Magnetic Spacing and Improved Tribological Properties for Higher Areal Densities*", Tribology Letters, **43**:247–256, (2011)

6- **Ehsan Rismani**, Reuben Yeo, S. K. Sinha, W. Ming, Kwek, H. Yang, and C. S. Bhatia, "*Developing a Composite Al-TiN$_x$C$_y$ Interlayer to Improve the*

*Durability of ta-C Coating for Magnetic Recording Heads*", (manuscript is submitted to Tribology letters, September 2012)

**Conference Presentations**

7- **Ehsan Rismani**, S. K. Sinha, and C. S. Bhatia*, "Improvement of nano-tribological characteristics of ultra-thin tetrahedral amorphous carbon (ta-C) protective coatings of the magnetic head by formation of an Al-C-Si composite interlayer*", ASME/STLE international Joint Tribology Conference, October 2011, Los Angeles, USA.

8- **E. Rismani**, M. Abdul Samad, H. Yang, S. K. Sinha & C. S. Bhatia, "*Improved Tribological Properties of the Magnetic Disk Media: Surface Modification with a Mixture of Si and C Atoms*", Accepted in International Magnetics Conference (INTERMAG), April 2012, Vancouver, Canada.

9- M. Abdul Samad, **E. Rismani**, H. Yang, S. K. Sinha and C. S. Bhatia, "*A novel approach of carbon embedding in magnetic media for future hard/disk interface*", <u>INVITED TALK</u> at TMRC Conference, August − 2011, Univ. of Minnesota, Minneapolis, USA

10- **Ehsan Rismani**, M. Abdul Samad, S. K. Sinha, H. Yang, W. Ming Kwek, and C. S. Bhatia, "*A bi-level $C^+$ ion embedment approach for surface modification of magnetic media*", International Conference on Diamond and Carbon Materials, September, 2012, Granada, Spain

11- **E. Rismani**, S. K. Sinha, W. Ming, Kwek, H. Yang, and C. S. Bhatia, "*Developing a Composite Al-TiN$_x$C$_y$ Interlayer to Improve the Durability of ta-C Coating for Magnetic Recording Heads*", 2012 ASME-ISPS /JSME-IIP Joint International Conference on Micromechatronics for Information and Precision

Equipment MIPE2012 June 18-20, 2012, Santa Clara, California, USA (<u>won ASME ISPS division graduate student fellowship award of US$1250</u>)

**Book Chapter**

12- C. S, Bhatia, **Ehsan Rismani**, S. K. Sinha, and Aaron J. Danner, "*Application of Diamond-Like Carbon Films in Magnetic Recording Tribology*", Book Chapter (Chapter No.: 992) in Encyclopedia of Tribology, 1$^{st}$ edition, Springer, March 2012.

**Patents**

13- C. S, Bhatia, **Ehsan. Rismani**, and S. K. Sinha, "Development of a durable wear resistant overcoat for magnetic recording systems", PCT Patent Application No. PCT/SG2011/000304, published on 15 March 2012, publication number WO/2012/033465.

# Acknowledgements

manufacturing several parts required for test setups. I would also like to express my gratitude to the graduate office staffs, Ms. Teo Lay Tin, Sharen and Ms. Thong Siew Fah, for their support.

Finally, I would like to thank my dear wife, Khatereh, for her support and encouragement and having patience and stamina to support me throughout my PhD candidature. No words are sufficient to express my gratitude and thanks for her support and understanding.

Last but not least, I would like to thank GOD and my parents for all their blessings and support.

# Table of content

# Summary

The main goal of this work is to develop ultrathin wear-resistant overcoats to improve the tribological performance of the next generation of magnetic recording systems (hard disk drives (HDDs) and magnetic tape drives) with extremely high data storage capacity. Tetrahedral amorphous carbon (ta-C) films developed by filtered cathodic vacuum arc (FCVA) were used as the key material. Different surface treatment (modification) techniques were developed to improve wear resistance of the ta-C coatings while keeping their thickness within an acceptable range ($\leq$10nm for the tape drive heads and $\leq$1 nm for HDD magnetic media). Using these surface treatment techniques, the overcoat was chemically bonded to the surface of the recording head. This remarkably enhanced the durability of the overcoat compared to that of conventional coatings. In addition, effect of different environmental conditions was studied on the tribological performance of the developed coatings. Surface modification of the media led to better wear performance in comparison with the existing commercial hard disk and tape media.

# List of Tables

# List of Figures

# List of symbols

| | |
|---|---|
| a. u. | Arbitrary unit |
| a-C | Amorphous carbon |
| a-C:H | Hydrogenated amorphous carbon |
| a-C:N | Nitrogenated amorphous carbon |
| AES | Auger electron spectroscopy |
| AFM | Atomic force microscopy |
| AMR | Anisotropic magnetoresistive |
| ARXPS | Angle resolved c-ray photo electron spectroscopy |
| B. E. | Binding energy |
| BaFe | Barium Ferrite |
| BPI | Bit be inch |
| COC | Carbon overcoat |
| CVD | Chemical vapor deposition |
| CZT | Cobalt Zirconium Tantalum |
| DAQ | Data acquisition card |
| DC | Direct current |
| DLC | Diamond like carbon |
| e. V. | Electron Volt |
| ECWR | Electron cyclotron wave resonance |
| EDM | Electric discharge machining |
| EELS | Electron energy loss spectroscopy |
| ESCA | Electron Spectroscopy for Chemical Analysis |
| FCVA | Filtered cathodic vacuum arc |

| | |
|---|---|
| GMR | Giant magnetoresistive |
| HCA | Head cleaning agent |
| HDD | Hard disk drive |
| HDI | Head disk interface |
| HMS | Head media spacing |
| IBD | Ion beam deposition |
| ICP | Inductively coupled plasma |
| INSIC | Information storage industry consortium |
| IPA | Isopropyl alcohol |
| km | Kilometer |
| LTO | Linear tape open |
| ME | Metal evaporated |
| MEMS | Micro-electro-mechanical systems |
| MP | Metal particle |
| MPa | Mega Pascal |
| MR | Magnetoresistive |
| nm | Nanometer |
| PECVD | Plasma enhanced chemical vapor deposition |
| PFPE | Perfluoropolyether |
| PLD | Pulsed laser deposition |
| PTR | Pole tip recession |
| RBS | Rutherford backscattering spectrometry |
| RF | Radio frequency |
| RH | Relative humidity |
| sccm | Standard Cubic Centimeters per Minute |

| | |
|---|---|
| SEM | Scanning electron microscopy |
| SNR | Signal to noise ratio |
| SPM | Scanning probe microscopy |
| ta-C | Tetrahedral amorphous carbon |
| ta-C:N | Nitrogenated tetrahedral amorphous carbon |
| Tbit/in$^2$ | Terabit per square inch |
| TEM | Transmission electron microscopy |
| TOF-SIMS | Time of flight secondary ion mass spectroscopy |
| TPI | Track per inch |
| TRIM | Transport of ions in matter |
| VCR | Video cassette recorder |
| XPS | X-ray photoelectron spectroscopy |

# Chapter 1: Introduction

Magnetic data storage (hard disk and magnetic tape drives) has been the most efficient, high capacity, and low-cost form of information storage technology. In order to maintain its usefulness over time, the magnetic spacing between the head and magnetic media of the tape or the hard disk should be decreased. Decreasing the magnetic spacing and maintaining it to narrow tolerances is very challenging in this technology. Given that tape drives are contact recording systems, there is also mechanical wear of the head as well as corrosion of the head read/write elements, which are the major causes of increased magnetic spacing. One way to overcome the tribological problems at the head/tape interface in magnetic tape drives is to provide an ultra-thin protective coating (no thicker than 10 nm) on the head surface in order to reduce direct interactions of the head materials with the tape media components. So far, many different types of wear resistant oxides, nitrides, carbides, or diamond-like-carbons (DLC) fabricated by different deposition techniques have been applied to the recording heads of magnetic tape drives. However, because of their poor durability and/or unacceptable thicknesses, most of these coating materials and methods have not been successful in producing a commercially viable solution. Tetrahedral amorphous carbon (ta-C), which is a type of DLC with a high fraction of diamond-like ($sp^3$) C-C bonds, has shown promising tribo-mechanical properties, which have made it a potential material of choice for protecting magnetic heads in tape drives. However, the serious drawback of ta-C coatings, like for all other DLC films, is their poor durability and adhesion to the $Al_2O_3$/TiC (AlTiC) ceramic substrate of the head, which may cause delamination of the coating off the substrate and abrupt failure of the coating.

Hard disk drives (HDDs) of the next generation aim to achieve magnetic recording areal densities beyond 1 Tbit/in$^2$, which requires the magnetic spacing between the magnetic head and the hard disk to be reduced to less than 4 nm. This requires the development of a protective overcoat (currently diamond-like carbon (DLC)) with a thickness of less than 2 nm. The properties of the overcoat on the air bearing of the recording head and disk media are very critical for wear and corrosion protection. Decreasing the thickness of conventional carbon overcoats poses significant issues to their tribological and corrosion performance. This necessitates the development of new processes (in terms of deposition techniques and materials) which can help in decreasing the thickness of the overcoat while improving its desired properties required for the next generation of magnetic recording systems.

The main goal of this PhD research work is to investigate and develop various strategies to enhance the durability of ta-C coatings (thinner than 10 nm) deposited by filtered cathodic vacuum arc (FCVA) technique for magnetic tape heads and also to develop ultrathin ($\leq$ 1nm) protective layers for hard disk media.

In this work, three different methods as listed below were adopted to synthesize durable protective coatings (or surface modification techniques) on the recording heads of tape drives or magnetic disk media:

1- **Pre-treatment of the head surface by bombarding the surface with energetic carbon ions (C$^+$ ions)**

In this technique, the surface of the heads was bombarded (pre-treated) by energetic carbon ions of 350 eV prior to deposition of a 10 nm ta-C overcoat. The effect of this surface treatment on the structure of the ta-C/AlTiC interface, chemical state of the overcoat and wear resistance of the coating was studied (this method is discussed in Chapter 5).

## 2- Modification of the head surface by means of formation of an Al-Si-C interlayer between head substrate and ta-C overcoat

In this method, a thin layer of Si was used as an adhesion layer between the head and ta-C overcoat. In this work, the mechanism responsible for the adhesion of Si to the AlTiC substrate was studied. Knowing this mechanism, one can enhance the adhesion of the ta-C overcoat to the head substrate by bombarding the Si-coated head (thickness of Si layer is less than 2 nm) with energetic $C^+$ ions. The structure of this Si interlayer with and without energetic $C^+$ ion pre-treatment and its effect on the tribological performance of the ta-C overcoat were also studied. This concept of pre-treatment but without an overcoat has also been studied as a potential surface modification technique for magnetic hard disk media (this method is discussed in Chapter 6).

## 3- Development of a Al-TiNₓCᵧ interlayer to chemically bound the ta-C overcoat to the head surface

In this work, an atomically mixed interlayer between the head substrate and the ta-C overcoat was developed by means of bombardment of a thin TiN film with $C^+$ ions. Mechanical and tribological tests were performed to investigate the performance of the developed coating. Chemical and physical characteristics of the film were studied by means of different characterization methods and were correlated to the mechanical and tribological behaviours of the coating in actual (in-situ) and experimental test conditions (this method is discussed in Chapter 7).

In this thesis a brief background about magnetic recording systems, their tribological challenges and proposed strategies to address these problems are presented in Chapter 2. In Chapter 3, an introduction on carbon and its different allotropes is provided. This is followed by a discussion of amorphous carbon films and different methods of deposition. At the end of the chapter, key applications of DLC films in hard disc drives

and their potential use as a protective coating on the heads of magnetic tape drives are discussed. In Chapter 4, various common experimental methods used for fundamental physical, chemical, mechanical and tribological characterizations of the films developed in this research are described. In Chapters 5, 6, and 7, different surface treatment-modification techniques that we have developed (as described above) to provide protective coatings with improved tribological performance are discussed. In Chapter 8, the effects of these developed techniques on the tribological performance of the 10 nm ta-C coatings applied on the magnetic tape heads in real head/tape interface are studied. The effect of relative humidity (RH) of the working environment on the tribological performance (wear durability and friction) of the ta-C coating is discussed in chapter 9. In Chapter 10, the concept of bombarding the Si layer with C ions (which is explained in Chapter 6) to form a mixed layer was used to develop a $\leq 1$ nm Si/C mixed layer to modify the tribological properties of the Co-based hard disk media. Finally Chapter 11 provides the conclusion for this PhD research work and the potential works for future studies are suggested in Chapter 12.

# Chapter 2: Magnetic recording technology (past, present, and future)

Magnetic storage (recording) is defined as recording information by local magnetization of a thin film of ferromagnetic material in opposing directions by an external magnetic field. This ferromagnetic material is known as the "magnetic media" and can be coated on flexible polymeric substrates (magnetic tapes), rigid glass or aluminum plates (hard disks). The recording magnetic field is induced by a write head which is moving with respect to the magnetic media (Figure 2-1). This head can then read the recorded information by measuring the variations of the magnetic field above the film surface.
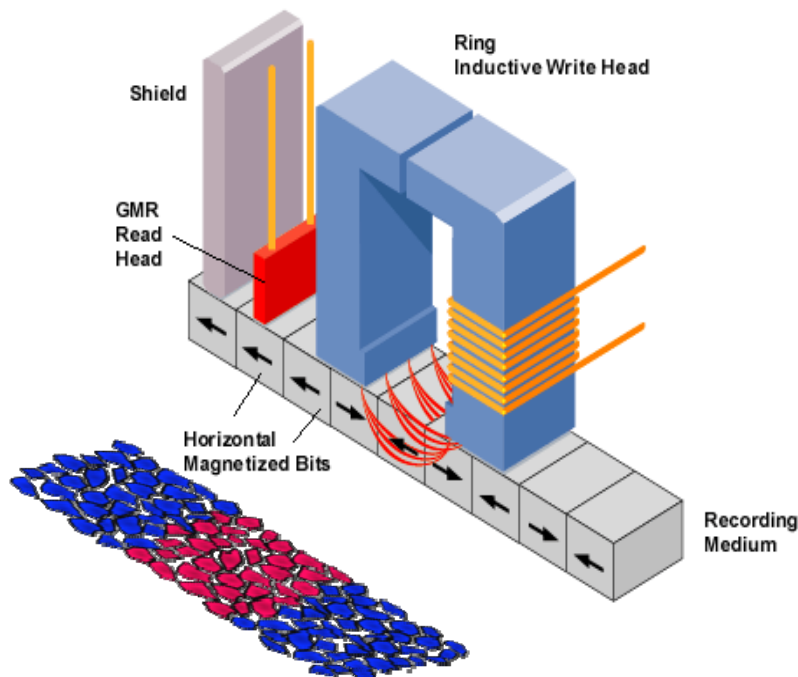


**Figure 2-1** Schematic view of magnetic recording concept showing the head recording element and magnetic medium

Data bits are written along the tracks. Each data bit is written by magnetization of a number of ferromagnetic grains of the media. The areal density is defined as the number of bits along one inch of a track (bits per inch or BPI) multiplied by the

number of tracks per inch (TPI) of the media. The ratio of TPI and BPI is called the bit aspect ratio.

In hard disk drives (HDDs), the head is not in contact with the media and flies in close proximity over the rotating rigid disk. However, magnetic tape drives are contact recording systems in which the head has full continuous contact with the moving flexible media.

## 2.1 Magnetic Hard Disk

Presently, hard disk drives (HDDs) are the most common devices for mass storage of information. Hard drives are magnetic storage devices in which data is recorded as magnetized bits on the surface of a thin layer of ferromagnetic material such as cobalt or its alloys (e.g. Co-Cr-Pt) deposited (sputtered) on the surface of a very smooth glass or aluminum alloy substrate. A read-write head flying a few nanometers above the surface of this magnetic media is responsible for writing and reading the recorded data on the disk (Figure 2-2).
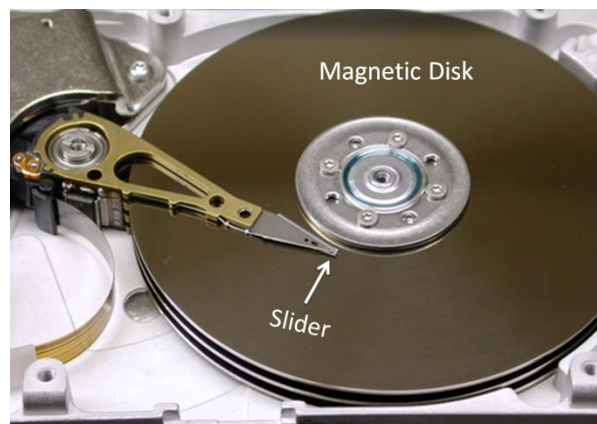


**Figure 2-2** Configurations of disc and slider in hard disk drive

The disk rotates at a speed of approximately 5400-15000 rpm. The read-write head consists of many thin film layers. The head is not in contact with the media and flies in close proximity over the rotating disk. An $Al_2O_3/TiC$ (AlTiC) ceramic slider supports the magnetic sensing elements. AlTiC is a hard composite ceramic consisting of about

70% by weight of $Al_2O_3$ and 30% by weight of TiC. This ceramic part is the main bearing surface when the head is flying above the media or when any crash occurs between head and disk. Figure 2-3 shows a schematic view of the head/media interface of a hard disk drive.
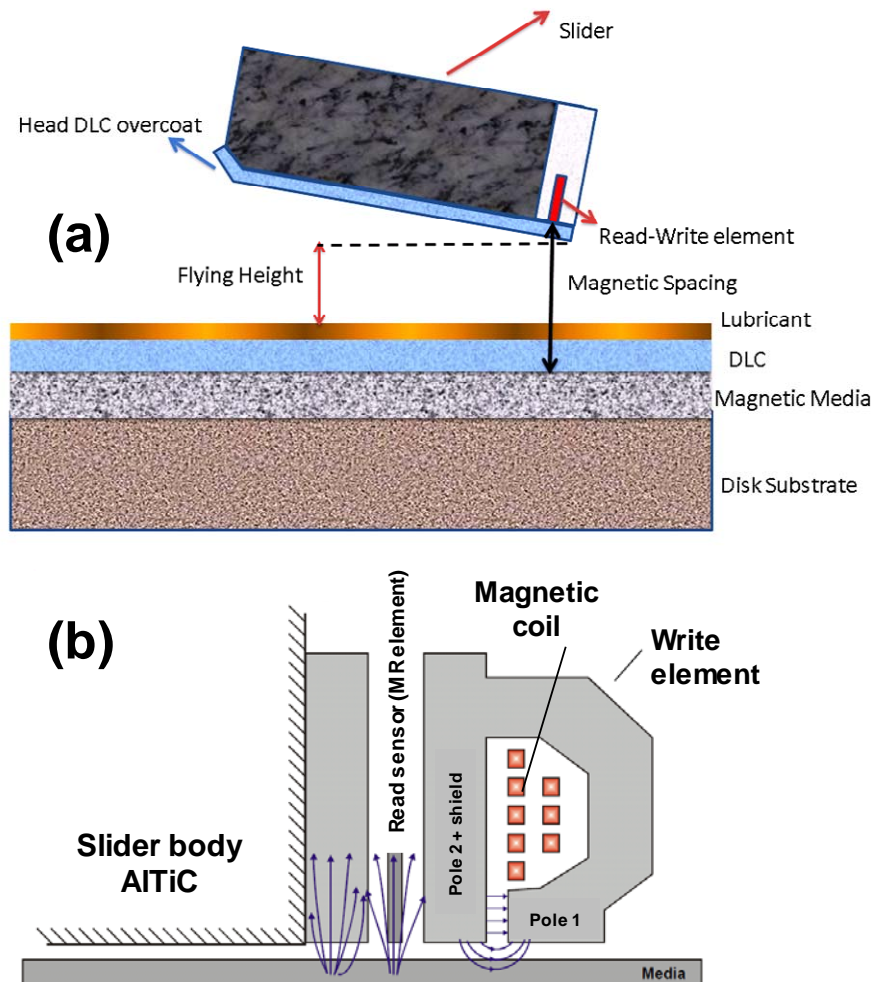


**Figure 2-3** Schematic view of (a) the head-media interface and (b) head read/write elements

To prevent the magnetic medium and the head read-write elements (reader sensor and writing poles) from oxidation and wear, the surfaces of the media and head are coated with a thin diamond-like carbon (DLC) overcoat (Figure 2-2). The top surface of the DLC layer is covered by a very thin layer of lubricant. This lubricant should have low vapor pressure, good lubricity and high thermal stability. It should also be chemically inert and should not react with the other materials in the head-media interface.

Perfluoropolyethers (PFPEs) such as ZDOL or ZTetraol have all of these superior properties and are extensively used as lubricants on the surfaces of the magnetic media in disk drives. The combination of the lubricant and hard DLC coating can lower the friction and wear between the media and head when they are in contact for any reason. The lubricant can also prevent media corrosion.

### 2.1.1 Tribological challenges at the head/disk interface of hard disk drives

Since its invention by IBM in 1956, the areal density of hard disc drives has continuously increased every year from 0.002 Mbits/in$^2$ to about 1 Tbits/in$^2$ today (Figure 2-4). This has been achieved by reducing the size of bits (reduction of the bit aspect ratio) and magnetic grains, improving the signal processing methods to recover the recorded data with higher signal to noise ratio, and using magnetic materials with higher coercivities [1].
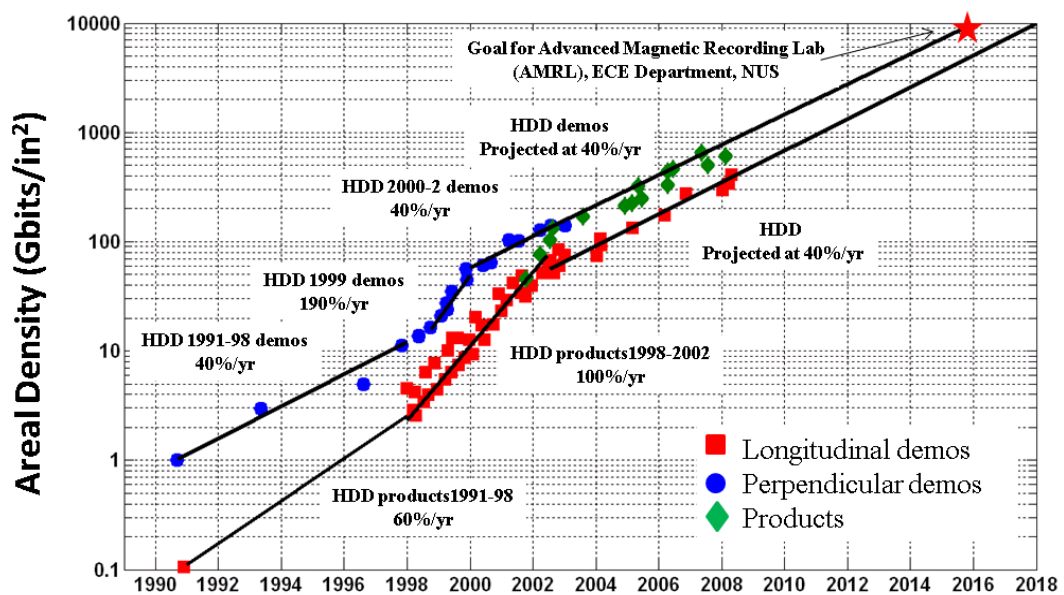


**Figure 2-4** Increasing recording density of hard disk drives over time

The vertical distance between the read-write elements of the head and magnetic media is known as the magnetic spacing (also known as head-media spacing or HMS) which consists of the flying height of the head, the thicknesses of the carbon overcoat and

lubricant, and the surface roughness of the head and media (Figure 2-3). According to the Wallace equation [2], bit size – and therefore the data storage density – increases exponentially with a decrease in the magnetic spacing. Head-media spacing can be reduced by decreasing the fly height as well as the thickness of the carbon overcoat (COC). Figure 2-5 shows the evolution of various components of the magnetic spacing with time.

|  | HMS | Disk OC/ Surface Mod | Lube / Inhibitor | Head OC / Surface Mod | Fly Height (FH) | TOH/ Glide Avalanche | Nominal Clearance |
|---|---|---|---|---|---|---|---|
| 100 Gb/in² | 10 | 2 | 1 | 2 | 5 | 2.5 | 2.5 |
| 1 Tb/in² | 6 | 1 | 0.75 | 1 | 3 | 1.75 | 1.25 |
| 10 Tb/in² | 3 | 0.5 | 0.75 | 0.5 | 1.25 | 0.75 | 0.5 |

**Legend:**
- Head OC / Surface Mod.
- Nominal Clearance
- TOH / Glide Avalanche
- Lube / Inhibitor
- Disk OC / Surface Mod.
- HMS
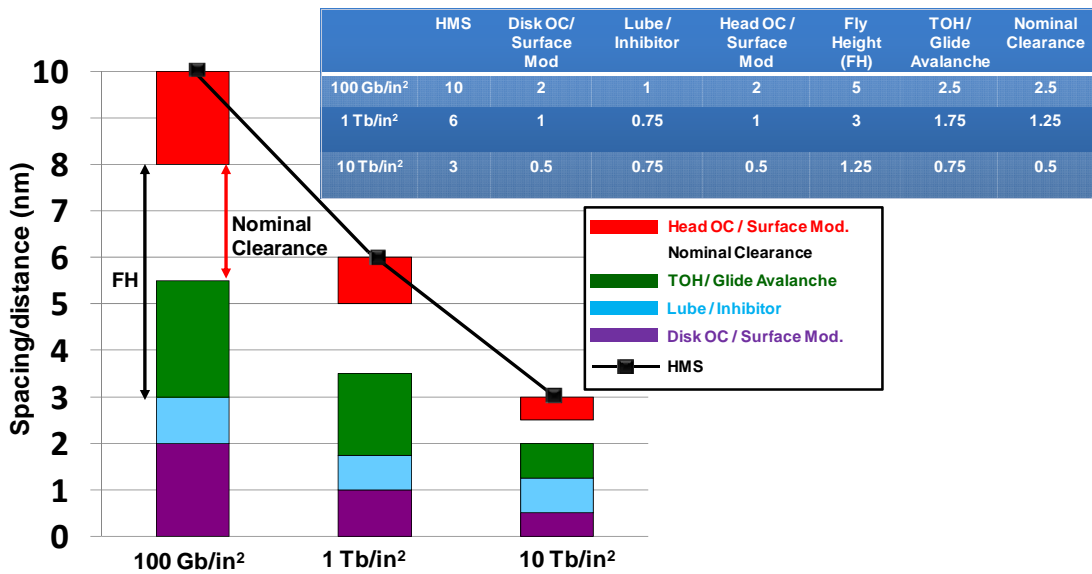
**Figure 2-5** Evolution of various components of the magnetic spacing with time

To protect the head/media interface, the protective film (carbon overcoat) should be extremely thin, hard, atomically dense, continuous (free of pin holes), and also chemically inert. A continuous reduction in the thickness of the carbon coatings still requires preserving their unique mechanical and chemical properties. However, a decrease in the magnetic spacing will give rise to many other tribological and corrosion- related challenges. This has necessitated improvements in the preliminary procedures, compositions and deposition methods of these protective carbon films. Different developments (in terms of materials and surface treatment techniques) will be discussed in Section 3-4.

## 2.2 Magnetic tape drive

Magnetic tape recording for digital data storage has existed since the early 1950's. It was the first magnetic information storage device replacing the likes of paper tape and punch cards [3, 4]. Magnetic tape storage has been the most efficient, high capacity, low-cost information storage technology and has spanned the range of computing platforms from desktops to supercomputers. For several decades, it has been unmatched in terms of price, performance and capacity, especially for back-up, archive and data protection applications.

A typical magnetic tape medium comprises a long, narrow, flexible and thin polymer (plastic) substrate and a thin layer of ferromagnetic material also known as the magnetic coating. The magnetic layer of the tape can either be a thin layer of magnetic particles, which are embedded in a polymer binder (this is known as metal particle (MP) tape) [5], or a thin layer of sputtered or evaporated magnetic metal films (this is known as metal evaporated (ME) magnetic tape) [6] deposited on the plastic substrate. In the present work, the discussion will be mainly focused on MP media, because of their predominant position in data recording today.

### 2.2.1 Magnetic tape media

Tape substrate is conventionally made of polyethylene teraphthalate (PET), but in order to have thinner films, polyethylene naphthalate (PEN) or polyaramides with higher elastic modulus is also being used [5]. The magnetic coating of a particulate medium is usually applied to the substrate as a slurry containing mostly magnetic particles (at up to 80% by weight, 50% by volume) bound together by means of a polymeric resin. The magnetic particles are generally iron-cobalt-based acicular metal particles (MP). However, hexagonal ferrite, generally known as barium ferrite (BaFe), has been used in some recent impressive demonstrations of very high areal density and

is considered as the magnetic particle of choice to be used in the next generations of magnetic tape [7-9]. In addition to magnetic particles and the polymeric binder, a typical magnetic tape consists of relatively large abrasive particles such as aluminum oxide or zirconium oxide known as head-cleaning agent (HCA). The main purpose of using these cleaning particles is to remove the contaminants adhered to the head surface. In order to prevent surface charging (electrostatic charges), carbon black is usually incorporated into the tape surface. And last but not the least, the magnetic coating consist of an essential lubricant (typically fatty acid esters) which fills its porous structure [10, 11]. The main use of the lubricant is to decrease the static (stiction) and dynamic friction at the head tape interface. Finally, a backside coating is applied to the tape to provide antistatic protection, prevent adhesion of the tape during the winding/unwinding process, and most importantly, to give it its desired mechanical and tribological properties.

## 2.2.2  Magnetic recording head

The structure of recording heads in tape drives is very similar to that of magnetoresistive (MR) heads in hard disk-drives (Figure 2-6) [6, 12].
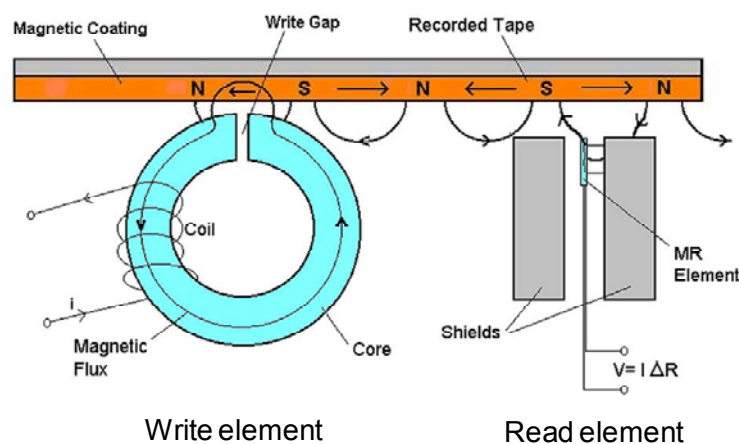


**Figure 2-6** Structure of recording heads in tape drives showing read and write concepts [6]

Tape heads are made from rings of ferromagnetic material (Cobalt Zirconium Tantalum (CZT) alloy) with a gap where the tape contacts it so the magnetic field can fringe out to magnetize the magnetic particles on the tape. A coil of wire around the ring carries the current (writing signal) to produce a magnetic field proportional to the signal to be recorded. Rapid reversals in the current as the tape moves against the magnetic gap will record transitions between the two magnetized states (N and S magnetized bits).

The older generations of read/write heads are inductive heads which used the same write coil to read data. In these heads, a voltage was induced to the coil when the read/write gap was passed by the magnetic transitions recorded on the medium. The heads currently available use a separate read element to recover the recorded data based on the MR effect [6, 12]. The MR effect gives rise to a change in the electrical resistance of a material in the presence of a magnetic field. The resistance change depends on the direction of the applied field (more precisely, orientation of magnetization) with respect to the current direction. MR heads are able to read very small magnetic features reliably by detecting the flux transitions in the media and converting them back to electrical signals which can be interpreted as data. The basic structure of the MR read head comprises a thin, rectangular film of Permalloy ($Ni_{81}Fe_{19}$) with a thickness of about 10-40 nm, sandwiched in between magnetically permeable cobalt-zirconium-tantalum (CZT) shields. The shields provide the necessary resolution of closely spaced transitions by shielding the element from the fields from upstream and downstream bits. A schematic view of an MR read sensor is shown in Figures 2-6 and 2-7.
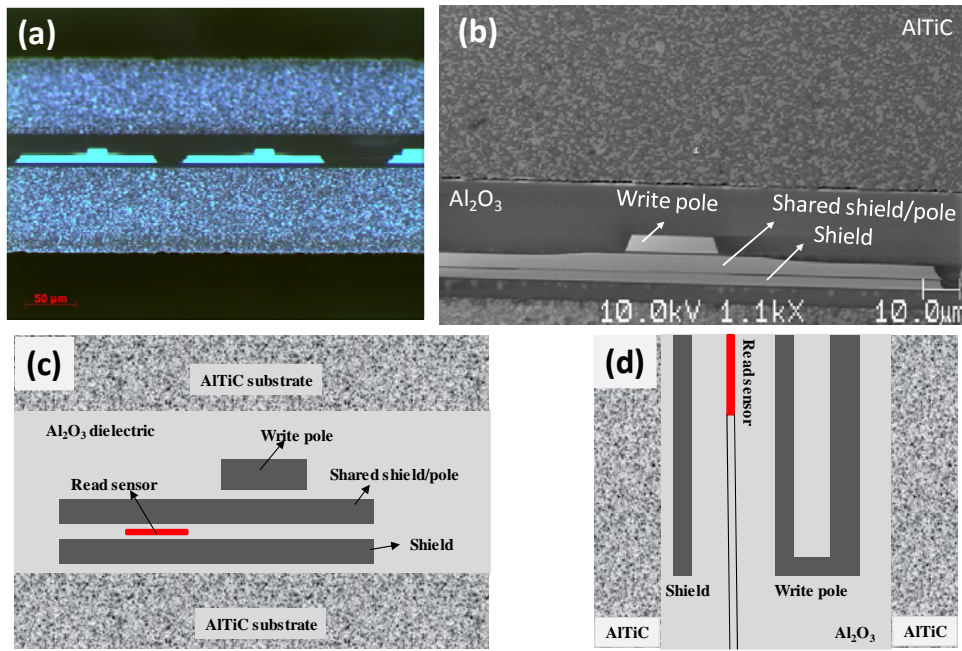
**Figure 2-7** (a) Optical microscope image and (b) SEM image of the read/write elements, schematic drawing of (b) top view and (c) cross-section of one of the head read/write channels
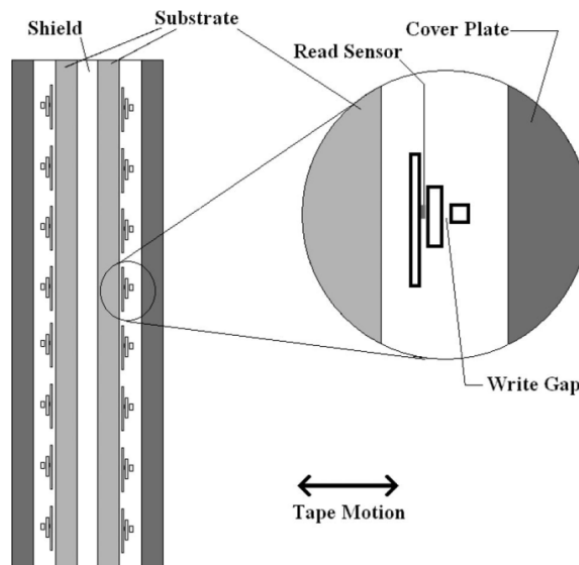


**Figure 2-8** Read/write head layout showing multiple elements for simultaneous bi-directional writing and reading

Today's tape drives use the shared shield read/write heads where the read and write heads are fabricated on top of one another to form a thin film structure similar to those used in magnetic disk drives (see Figure 2-8). They are fabricated in multi-channel arrays typically using two head modules to allow writing and reading in both directions of tape motion (Figure 2-8). Similar to HDDs, an AlTiC ceramic bearing

supports the magnetic sensing elements. Figure 2-7(b) shows the SEM image and schematic structure of a read/write element of the recording head.

## 2.3  Tribological problems at head/tape interface

For a number of decades, magnetic tape has been unparalleled in terms of price, performance and capacity, especially for back-up, archive and data protection applications. Since its invention, tape has seen an increase of almost six orders of magnitude in recording density [13]. The progression of tape reel/cartridge capacity is shown in Figure. 2-9 [6].
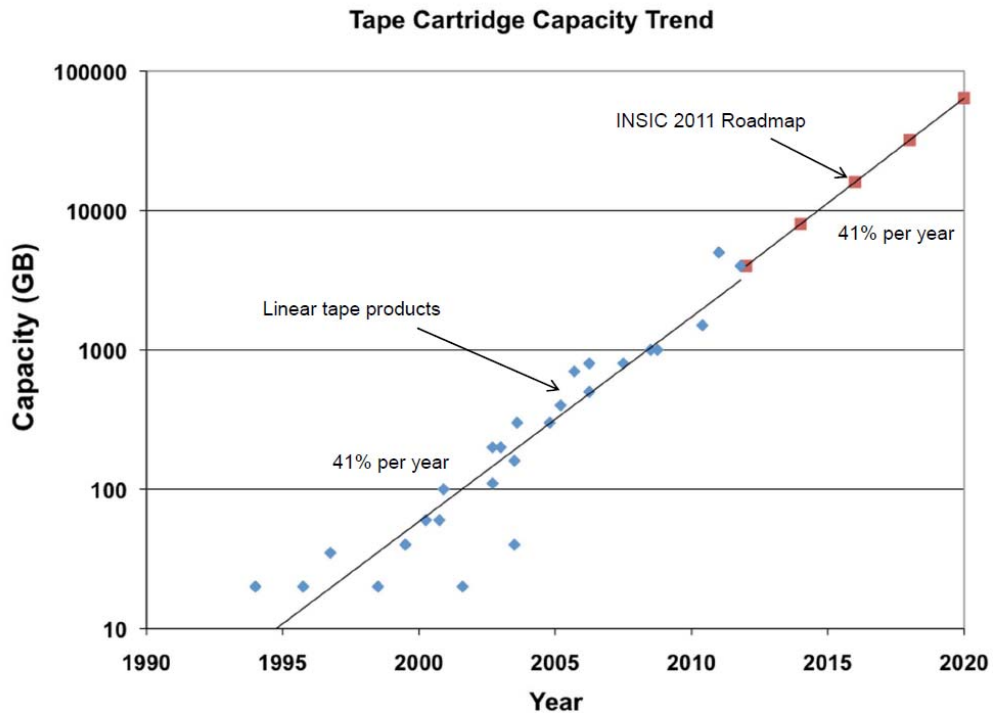


**Figure 2-9** Progression of magnetic tape reel/cartridge capacity over time [14]

Tape, however, has recently faced pressure from the introduction and growing use of low-cost magnetic hard disks. In order to retain its position over time, continued improvements in price, capacity, performance and reliability are necessary.

One of the most important factors for sustaining the present cost advantage of tape against hard disk storage is to advance its technology to enable storage of more data in

the same half-inch cartridge without a significant increase in its cost. This means being able to record more information in the same cartridge with 600-800 m length and 12.5 mm (half-inch) width of tape. In other words, this means increasing the areal density of the tape. Areal density is the raw number of data bits per square inch on the tape. This requires the recorded bit size on the tape media to be shrunk and the data transfer rate to be increased. In order to achieve this goal, many key technologies such as head, media, mechanical transport mechanisms and data read-write channels that make up a tape drive have to be improved. In most of these technologies, the surface science and tribology of head/media materials and lubricants as well as the tribology of very smooth surfaces are the technologies of high priority and importance for research [14]. A schematic view of a head-tape interface is shown in Figure 2-10. Similar to hard drives, in order to achieve good recording performance and high recording density, the recording head needs to be in closer proximity to the recording medium [2, 12], i.e. the magnetic layer in the tape.
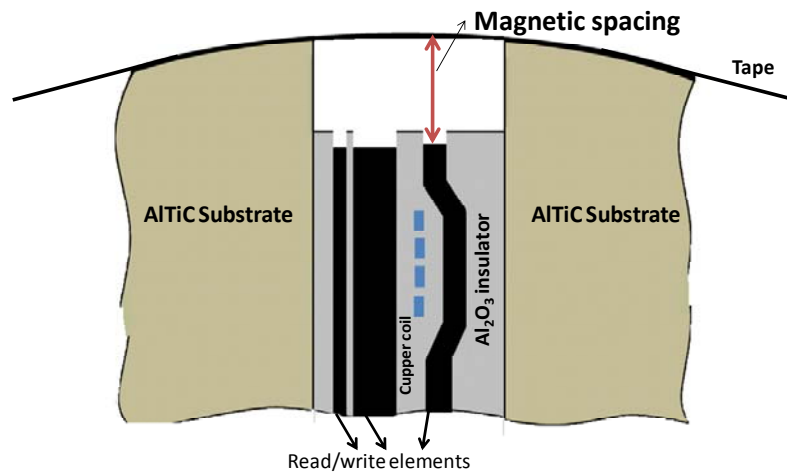


**Figure 2-10** Schematic cross-sectional view of a head/tape interface showing definitions of magnetic spacing and PTR

According to the Wallace equation [2], data storage density increases exponentially with a decrease in the physical spacing between the media and the head magnetic elements (pole tips). It should be noted that the spacing is the total head-media

magnetic separation, including the media magnetic layer finite thickness, any non-magnetic coating, as well as the surface roughness of the media and the head. Figure 2-11 shows how tape drive manufacturers should decrease this spacing in order to store more data in the same half-inch form factor cartridge [14].
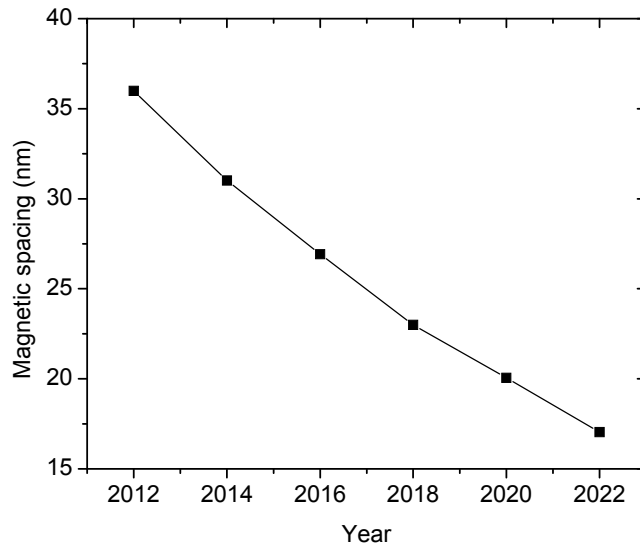


**Figure 2-11** Magnetic spacing trend based on INSIC tape technology roadmap [14]

Pole tip recession [15, 16] , tape roughness (due to surface asperities), stain build-up [17, 18], formation of an air film between head and tape (separation of tape from head), and mismatch between tape and head contour [19, 20] are some of the main sources of spacing loss (increasing the magnetic spacing) [21].

In addition to the smaller magnetic spacing, a further increase in the tape data storage density in the future requires more sensitive heads, higher tape speeds, smoother tape surfaces and many other improvements. However, these solutions will introduce greater tribological challenges in the performance of the future tape drives.

### 2.3.1   Pole tip recession (PTR)

When using a combination of different materials in the recording head, it is very difficult to match wear rates exactly. The head's read/write elements (consisting of the

poles and MR element) are made of mechanically soft and less wear resistant magnetic materials and have a greater wear rate than the surrounding hard AlTiC ceramic. This difference in the wear rates results in hollowing out the magnetic pole to a depth where the tape is no longer in contact with the active elements of the head (Figure 2-10). This process is called pole tip recession (PTR) and is the major contribution to the magnetic spacing between the active elements of the head and the media [10]. The major sources of PTR have not been well understood. In spite of extensive research work, the main source of PTR has yet to be well understood.

In a study by Bhushan et al., the main source of PTR was attributed to three-body abrasive wear modes [22, 23]. According to Sullivan et al., the major causes of this three-body abrasive mechanism are micro or nano particles sourcing from the ceramic tape-bearing surface of the head [16, 21, 24, 25]. They proposed that thin platelets of titanium oxide may form at the TiC phase of the head ceramic surface and then fragment into very hard three-body abrasive particles that are swept across the pole region, preferentially wearing the softer poles.

However, recent studies have shown a probable effect of tribo-electro-chemical reactions at the head tape interface as the main reason for recession of the recording element [26]. Understanding the exact mechanism of PTR is not within the scope of our current study; however, the most important fact that must be noted is that PTR occurs because of direct interaction (for a long time contact) between the running tape and recording head.

### 2.3.2  *Head stain and debris accumulation*

As mentioned earlier, the magnetic layer of tape is a combination of magnetic particles and a polymer binder. Thus, the surface which is in contact with the read-write heads has the tribological properties of a filled polymer [15]. Formation of chemical bonding

between the head surface and tape magnetic coating components leads to formation of strong adhesive junction between head and tape which my lead to material transfer from the media to the head. This phenomenon is known as "head stain" and may introduce unacceptable magnetic spacing. A function of the head-cleaning agent added to the magnetic layer is to remove or limit the thickness of this stain and to reduce spacing losses.

### 2.3.3    More sensitive heads

To achieve higher data recording density, tape heads must have increased sensitivity to recover the signal from the smaller bits. A change of reader sensor design from anisotropic magnetoresistive (AMR) technology, which has been used for the past 20 years [6], to Giant Magnetoresistance (GMR) as used in HDDs [27] could increase reader output by as much as one order of magnitude. However, GMR sensors have different materials and thinner films that might corrode or degrade over time because of chemical or electrochemical processes in the tape environment.

### 2.3.4    Smoother tape surface

Decreasing the magnetic spacing (and at the same time having a uniform magnetic spacing), and increasing the bit resolution and signal-to-noise ratio (SNR) require a roughness (AFM $R_a$) reduction from about 2.0-2.5 nm in current tapes [7] to about 1.0 nm in future products by 2022 [14]. The ongoing pursuit of extreme smoothness in the recording side of the tape tends to create tribological challenges. Significant reduction in roughness of the media naturally causes static friction (stiction) and dynamic friction issues at the head-tape interface.

## 2.3.5   *Stiction and dynamic friction*

A relatively strong adhesive junction between the head and very smooth media results in a high stiction force (which occurs at the beginning of tape motion) at the head-tape interface (HTI). This stiction force will place greater initial tension and stress on the tape magnetic coating and its surface integrity. This can enhance media delamination and debris formation, which results in loss of bits of information. Severe stiction may even lead to tape tearing.

In addition, achieving a higher data transfer rate requires higher tape speeds and many channels in the future heads. The friction force has a non-linear dependence on the tape velocity. High tape speeds (of about 6 m/s) and high dynamic friction at the HTI can potentially lead to longitudinal mechanical resonances (vibrations) [28] of the moving magnetic tape, which can cause tension and velocity variation at the HTI. These oscillations and/or transients can result in information recovery errors and affect the integrity of the tape elements.

## 2.3.6   *Head cleaning agents as defects*

In the past, debris from the tape needed to be removed from the head by some cleaning or wear particles included in the tape coating. In order to be effective as cleaners, these abrasive additives need to be present at the surface of the tape and be tightly held by the binder matrix. They are, however, essentially considered as defects in the magnetic layer and further hamper the effort to maintain smooth and uniform head to tape spacing.

## 2.3.7   *Lubricant and electrochemical reactions*

Introducing a boundary lubricant between the opposing surfaces of the head and media reduces the polar molecule content of the binder and therefore weakens the adhesive

forces at the HTI. This reduces the wear of the media, head stain build-up, as well as the head-tape stiction to a large extent.

An Information Storage Industry Consortium (INSIC) funded research [26, 29] suggested that fatty acid esters, which have been used extensively as lubricants in tape formulations for decades, participate in contamination or corrosion (an electrochemical reaction) of the head magnetic elements. There is evidence that in these electrochemical reactions, the tape serves as a conductor between different head elements. Consequently, replacement of the existing lubricants seems to be inevitable in the next generation of magnetic tape.

PFPE lubricants are widely used to reduce friction and wear of the head–disk interface in HDDs. Because of their desirable tribological properties [30-33], these lubricants have the potential of being superior to fatty acid lubricants in the next generation of magnetic tapes. Although the application of these lubricants is likely to solve the problem of tribo-chemical corrosion of the metallic elements in the head, it has been shown that some catalytic reactions on the $Al_2O_3/TiC$ surface of the head can rapidly decompose PFPE lubricant molecules at the HTI [32-36].

## 2.4 Proposed remedy to address tribological issues at head-tape interface

Most of the tribological problems at the HTI arise from its contact recording nature and existence of materials with different mechanical and/or chemical properties at the head surface. Tribo-chemical (tribological induced electrochemical) reactions between different materials (e.g. different phases of the head substrate, read and write elements, and tape components like lubricant, etc.) available at the HTI spoils the read/write elements of the head. In addition, high friction and different wear rates of the material may lead to differential wear of the head components.

One approach that can correct this situation, as a remedy for tribological problems of future tape drives, is to provide a coating on the head surface to give all phases the same surface (chemical and mechanical) properties and reduce the interactions of head materials with media components. It is likely that coating the head surfaces with a thin, long and durable protective film which is atomically dense, chemically inert, and mechanically hard with good adhesion to the head surface, can solve or eliminate the aforementioned tribological issues. This option will introduce almost no major changes in the head material stack and circuitry design and therefore imposes minimum extra charge in fabrication, which is an important factor in maintaining the position of magnetic tape as the lowest cost solution for mass data recording.

However, by coating the head surface with such a protective film, a trade-off between coating thickness and increasing the magnetic spacing must be made. The head technology roadmap predicts that magnetic spacing will reach 20 nm in 2020 [14]. This still allows the use of a coating on the head with a thickness of 10-15 nm, which is almost equal to half of the total allowable magnetic spacing between the head and media.

Unlike hard disk drives (with a head coating of 2-3 nm), the potential head coatings in present tape drives can be as thick as about 10-15 nm, which is the maximum in order to maintain the magnetic spacing. Since the tape is always in contact with the head surface, adhesion of the coating to the head substrate is very critical; otherwise, the coating may delaminate (peel off) from the head surface, which could lead to catastrophic (abrupt) failure of the coating. In order to survive under the severe wear condition at the head tape interface, the coatings should have an extremely high hardness. Since the head magnetic elements (especially the MR read element) are very

sensitive to elevated temperatures, the coating deposition should not be conducted at very high temperatures (higher than ~100°C).

Among many different types of hard protective coatings films, DLC films have shown promising results to be used as a candidate for coating magnetic tape recording heads. Among different types of DLC films, an ultra-thin tetrahedral amorphous carbon (ta-C) film with thickness of a few nanometers is continuous, dense and hard enough to be used for this purpose. Further details about the properties and deposition techniques of amorphous carbon films, and the application of these films (as well as other hard coatings) as a protective layer on the magnetic tape heads are provided in Chapter 3.

# Chapter 3: Amorphous Carbon and its Application in Magnetic Recording Industry

This chapter will first give a short introduction on carbon and its different allotropes. This is followed by a discussion of amorphous carbon films and different methods of deposition. Finally, key applications of DLC films in hard disk drives and their potential application as a protective coating on the heads of magnetic tape drives will be discussed.

## 3.1 Diamond-like carbon (definition and fundamentals)

Carbon is a very versatile element that can be found in crystalline (diamond and graphite) or amorphous forms. Carbon atoms are able to form three different types of hybrid orbitals ($sp^1$, $sp^2$ and $sp^3$) and therefore they can bond to each other or to other atoms in different ways.

### 3.1.1 Allotropes of carbon

Carbon atoms in different forms may have different configurations or allotropes. In cubic (natural) diamond, each carbon atom forms four identical $sp^3$ hybridized orbitals arranged tetrahedrally around the atom (Figure 3-1(b)). Carbon atoms are connected to their neighboring atoms by means of overlapping these similar $sp^3$ orbitals to form a three-dimensional lattice of carbon atoms bonded together with very strong covalent bonds (Figure 3-1(a)). This makes diamond the hardest material known so far.

In ordered graphite, one *s* and two *p* orbitals are mixed to form three identical $sp^2$ hybrid orbitals with a trigonal planar configuration (Figure 3-2(a)). In the structure of graphite, each atom is connected to its three neighbors (σ bond) to form a hexagonal network of carbon atoms (graphene plane) in extended layers (Figure 3-2(b)). The

bonds between the carbons within the layer are stronger than those in diamond. The un-hybridized remaining electron orbital, which is perpendicular to this plane, forms a $\pi$ bond with a similar orbital of the above or underlying layer. This $\pi$ bond is not as strong as the $\sigma$ bonds. Therefore, graphene layers can slip one on another and this makes graphite a soft and a lubricious material. In addition, this electron is de-localized (mobile) and allows graphite to conduct electricity.
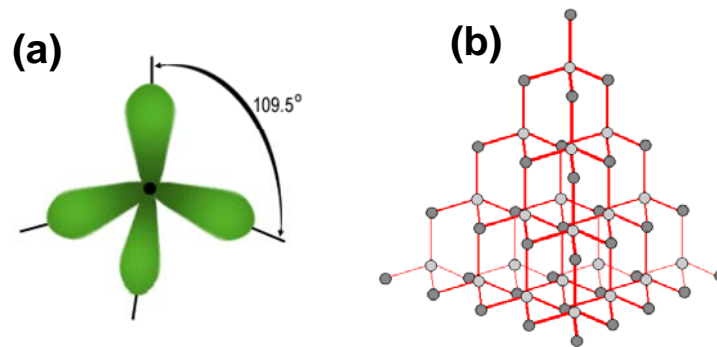


**Figure 3-1** (a) sp$^3$ hybridization of a carbon atom (b) carbon atoms making a giant macromolecular array (lattice) in diamond
(Figure from http://www.uwgb.edu/dutchs/Petrology/Diamond%20Structure.HTM)
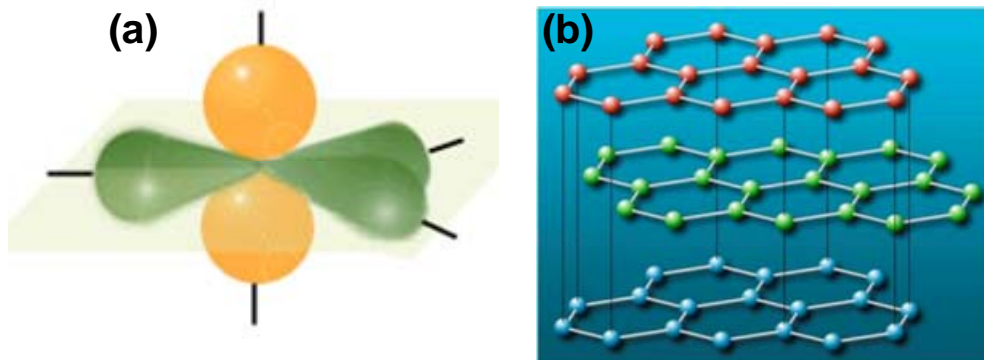


**Figure 3-2** (a) sp$^2$ hybridization of a carbon atom (b) configuration of carbon atoms in graphite (Figure from http://invsee.asu.edu/nmodules/carbonmod/hybrid.html)

Amorphous carbon (a-C) is an allotrope of carbon which is not crystalline and the atoms are connected to each other with a disordered combination of sp$^2$ and sp$^3$ bonds to form clusters, rings or chain network configurations (Figure 3-3). Depending on their deposition methods, the structure of a-C films may contain some other elements

such as H or N. Based on the various fractions of $sp^2$ and $sp^3$ bonds (C-C $sp^3$, C-C $sp^2$, C-H $sp^3$, etc.) this material may exhibit completely different chemical and physical behaviors.
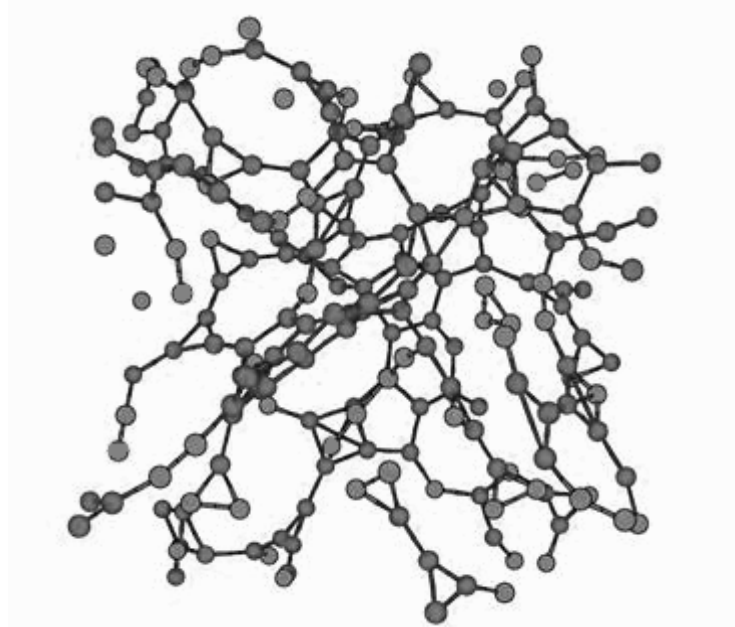


**Figure 3-3** Typical structure of C-C bonds in amorphous carbon
(Figure from http://kypros.physics.uoc.gr/resproj.htm)

Amorphous carbon containing a higher portion of C-C $sp^3$ bonds like those which connect carbon atoms in the lattice of diamond shows desired mechanical and chemical properties such as high hardness and Young's modulus, smoothness, chemical inertness and high atomic density. Because of the similarity of its properties to those of diamond, this type of amorphous carbon is called "*Diamond-Like Carbon*" or "*DLC*".

Unlike synthetic (laboratory-created) diamond which has a high growth temperature, DLC thin films can usually be manufactured at near the room temperature. The first hard amorphous carbon (a-C) films were grown by Aisenberg, Chabot and Holland in the 1970's by using a plasma deposition method [37, 38]. This work was continued by Meyerson and coworkers in the 1980's to produce hydrogenated amorphous carbons (a-C:H) [39, 40]. Meanwhile, the first [41, 42] systems were invented and a graphite

source was used to grow a new generation of DLC films (containing no hydrogen or nitrogen atoms) with a considerably high fraction of tetrahedrally bonded ($sp^3$) carbon atoms . Because of its structure, this type of DLC is usually referred to as tetrahedral amorphous carbon or ta-C [43-45].

A higher fraction of $sp^3$ oriented C-C bonds leads to desired mechanical and chemical properties such as high hardness, high Young's modulus, low roughness, chemical inertness, and high atomic density [46, 47]. Raman spectroscopy [48], X-Ray photoelectron spectroscopy (XPS), electron energy loss spectroscopy (EELS), and electron and neutron diffraction are some of the most important non-destructive characterization methods [47] used to determine the $sp^3$ content of a DLC film.

The properties of DLC films can be carefully adjusted by controlling the carbon $sp^1$, $sp^2$ and $sp^3$ hybridizations, and the amount of hydrogen and nitrogen atoms in the film as well as the deposition method. Due to their outstanding and versatile chemical and physical properties, DLC films have been extensively used in a broad range of applications in many different scientific and engineering fields such as tribology [49, 50], magnetic data storage [43, 51-53], food storage[54-56], auto industries [57, 58], optics [59, 60], and bio engineering [61, 62].

## 3.2 Different types of DLCs and their properties

DLC films can be categorized into three major groups: hydrogenated amorphous carbon (a-C:H), nitrogenated (a-C:N or $CN_x$) and hydrogen-free amorphous carbon. Other types of DLCs that are available can be categorized as doped or alloyed DLCs.

### 3.2.1 Hydrogenated DLC

Compositions of carbon films (without nitrogen) are usually shown on a ternary phase diagram of hydrogen, $sp^2$ and $sp^3$ hybridization, as illustrated in Figure 3-4 [63].
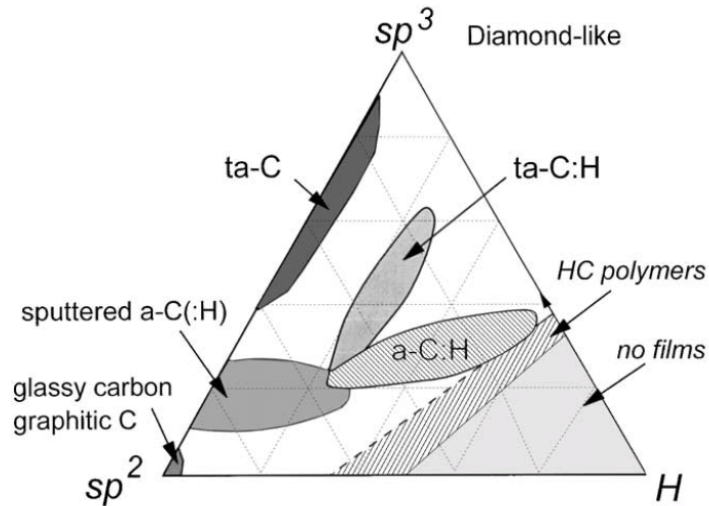
**Figure 3-4** Ternary phase diagram of the amorphous carbon hydrogen system [63]

Amorphous carbons such as soot, chars and glassy carbons with a disordered graphitic structure lie in the lower left-hand corner of this diagram. These materials mostly present properties similar to that of graphite. The bottom right-hand corner of the triangle (with H content greater than 70%) area corresponds to hydrocarbon molecules or soft polymers rather than a hard solid continuous carbon film. Although they have more than 70% sp$^3$, most of these positions are terminated by H-C bonds.

Amorphous carbon with intermediate hydrogen content (20-40%) is called amorphous hydrogenated carbon (a-C:H). This group lies at the center of the ternary diagram and because it has a considerable amount of C-C sp$^3$, it is categorized as DLC. a-C:H films can be grown by the sputtering of carbon in the presence of hydrogen gas (reactive sputtering) or by plasma enhanced chemical vapor deposition [1] techniques.

By keeping the hydrogen content in the range of 25-30 atomic % and using deposition methods with a high density plasma source, the C-C sp$^3$ bonds can be increased up to 70%. Because of the existence of H and a covalent network of tetrahedrally (sp$^3$) connected carbon atoms, these films are called tetrahedral hydrogenated amorphous carbon or ta-C:H. These films show better mechanical properties than a-C:H films.

### 3.2.2  *Hydrogen-Free DLC*

Simple sputtering of graphite forms an amorphous carbon (a-C) film with very low C-C $sp^3$ content which contains no hydrogen. This material is soft but still dense enough to be used as a corrosion-resistant layer.

Hydrogen-free amorphous carbon with a very high fraction of C-C $sp^3$ (tetrahedral) bonds is called tetrahedral amorphous carbon (ta-C). These films can be grown by deposition methods which contain highly ionized plasma of almost equal ion energy such as filtered cathodic vacuum arc (FCVA), mass selected ion beam (MSIB) or pulsed laser deposition (PLD) [44, 63].

A number of properties of ta-C films vary as a function of $C^+$ ion energy [47]. Many research groups have shown that the highest $sp^3$ fraction is obtainable at ion energy of ~100 eV [47, 52, 64, 65]. The $sp^3$ content of a film can be measured by methods such as EELS, XPS or Raman spectroscopy. At this ion energy, ta-C films have shown the maximum $sp^3$ content (up to 85%) which directly results in their stronger mechanical and chemical properties in comparison with sputtered or other types of amorphous carbon films. This is much higher than the $sp^3$ content of sputter-deposited hydrogenated carbon films (15-30%). Other properties of the film such as mass density, hardness, elastic modulus and internal compressive stress are directly correlated with the $sp^3$ content. Hardness and elastic modulus of thin films are measured by the nanoindentation method. At ~100 eV, FCVA ta-C films show maximum hardness and elastic modulus. At this condition, the hardness of the film ranged up to ~80 GPa compared with ~20 GPa of hydrogenated, sputtered carbon films [47]. In addition to the high hardness, these films have a remarkably high elastic modulus.

The film stress can be measured by the deposition of a film on a thin wafer and measuring the curvature of the wafer before and after deposition. The highest stress also occurs at ion energy of ~100 eV. High stress can impair the adhesion of the FCVA films to the substrate. In order to improve the adhesion of the carbon film to the substrate, materials such as Si, Cr, Ti, W or Mo can be used as the underlayer. In addition, a multilayer film with alternative hard and soft layers of carbon and other materials, or carbon layers with different $sp^3/sp^2$ fractions, can decrease the stress levels in the film. This facilitates the deposition of thicker films with better durability [66].

The thermal stability of ta-C films is very important in most applications. Deposition of carbon overcoats at higher temperatures leads to graphitization and deterioration of the film properties [63, 67].While hydrogenated carbon films begin to soften at temperatures as low as 350-400°C [68], FCVA ta-C films show high hardness and $sp^3$ content even at elevated temperatures up to 600°C [69-73].

The surface roughness of the FCVA films produced at ~100 eV is very small (~0.1 nm) [52, 74], and finally, the mass density of FCVA ta-C films measured by Rutherford backscattering spectroscopy (RBS) or EELS is at a maximum of 3g/cm$^3$, which is close to that of diamond (3.52 g/cm$^3$) [47, 55]. This makes the coating act as a barrier against corrosion and wear in many fields with very low dimensional tolerances such as micro electromechanical systems (MEMS) [75] and hard disk drives[55].

### 3.2.3   *Nitrogenated amorphous carbon*

The incorporation of nitrogen into amorphous carbon films has many considerably beneficial effects on their properties. Introducing $N_2$ gas into a-C deposited by sputtering of graphite at a temperature of 200 °C causes the formation of a nanostructured film in which graphite planes are strongly crosslinked together [76].

Although the $sp^2$ content in this film is still high, because of the increase in the disorder, the mechanical properties of the film (elastic recovery and hardness) are improved.

The deposition of carbon by methods which produce highly ionized plasma such as FCVA, MSIB and PLD in a very low pressure $N_2$ atmosphere will form tetrahedral nitrogenated amorphous carbon (ta-C:$N_x$) films with high $sp^3$ content of 80%. Because of their unique mechanical and chemical properties, nitrogenated amorphous carbon films can be used as protective layers against corrosion and wear on the surface of magnetic hard disks [77].

### 3.2.4   Doped or alloyed DLC

It has been shown that compressive internal stress has a key role in the formation of $sp^3$ bonds and the DLC's mechanical properties (hardness and elastic modulus) [63]. However, this stress makes DLC films, especially thicker ones, very easy to delaminate. This causes failure of the coating under high loads and impacts. Therefore, the formation of DLC films with high compressive stress requires excellent adhesion between the film and substrate; otherwise, by increasing the film thickness (internal stress increases by the thickness of the film) or by applying external loads, the film will be delaminated or peeled off the surface.

Alloying the carbon films with some metals or non-metallic elements may improve some of these limitations and enhance the mechanical properties of carbon films. For example, alloying of DLC films with Si facilitates the formation of $sp^3$ bonding in the absence of high compressive stress [78, 79]. Hydrogenated carbon films tend to be graphitized at high temperatures. Alloying these films by Si not only increases their thermal stability, it also improves their frictional behavior at higher relative humidity.

Metal alloying (Cu, Ni or Ag) is also used to improve the hardness and toughness of the carbon films in a similar manner [63].

## 3.3 DLC thin film deposition methods

Amorphous carbon films can be grown by completely different physical or chemical deposition methods. The deposition method directly affects the properties and behaviors of the deposited films. Among the many available methods, sputtering, the filtered cathodic vacuum arc and plasma enhanced chemical deposition methods are briefly explained below.

### *3.3.1 Sputtering*

Sputtering is one of the basic methods for the deposition of thin films of different materials such as metals, ceramics and carbon. In this method, the surface of the source material, which is called the target, is bombarded by energetic particles such as $Ar^+$ ions. If the plasma ($Ar^+$) particles which are colliding with the target have enough energy to overcome the surface binding energy of the target, the surface atoms of the target (for the case of a-C deposition, the target is high purity graphite) will be ejected into the environment of the sputtering chamber. These particles which may contain a combination of atoms and ions will deposit (condense) on the surface of the substrate. The pressure, energy and the angle of the bombarding plasma are key parameters to control during the sputtering process.

In sputter deposition of carbon, most of the produced particles (atoms) are electrically neutral and this mixture has a low energy of about 5 eV. For this reason, the deposited particles cannot penetrate into the outer surface of the substrate and overcome the coating nucleation obstacles; therefore, the particles landing on the substrate surface move toward each other to form separate islands in order to lower the surface energy.

This process causes the formation of a discontinuous and rough overcoat for thicknesses less than 2 nm. However, by continuing the deposition, these islands merge together to form a continuous overcoat. Because of the low energy of the sputtered particles, sputtered a-C films have very low content of $sp^3$ (15-30%) and are not very hard [51].

By sputtering graphite in an atmosphere of argon and hydrogen plasma, a-C:H will form. Similarly, the formation of a-$CN_x$ can be carried out in a nitrogen-argon plasma environment.

### 3.3.2  *Plasma enhanced chemical vapor deposition*

Chemical vapor deposition (CVD) is a method in which a solid thin film is formed from a chemical reaction between one or more chemical precursors in the vapor or gas phase. The required energy to initiate the reaction (to chemically decompose the reactive gases) is provided by heating the entire reaction chamber up to 600°C. This is the main disadvantage of this method to deposit carbon films, as this high temperature leads to graphitization and overall deterioration of film properties [80]. Thin films can be deposited by other CVD methods working at a lower temperature. Plasma Enhanced Chemical Vapor Deposition (PECVD) is one of the CVD methods in which the chemical reaction is initiated by the creation of plasma of the precursor gases. The plasma is formed by means of an electrical discharge between two electrodes between which is filled with the reacting gases. The existence of energetic electrons in the plasma provides extra energy to facilitate the initialization of dissociation of precursor molecules and formation of ions and radicals, which in turn lowers the deposition temperature.

For depositing a-C:H, the reactor chamber is filled with hydrocarbon precursors such as $C_2H_2$ or $CH_4$. Plasma is formed by the decomposition of the hydrocarbon molecules

between two parallel plates (electrodes) when a radio frequency (RF) voltage is applied to the plates. The sample is bombarded by the resulting ions and radicals, and the coating is formed by the condensation of these ionized particles on the surface followed by the formation of chemical bonds between these species on the surface and the other radicals from the plasma.

In this method, the fraction of ionized particles in the plasma is not much (< 10%). This cannot lead to the formation of carbon films with a high fraction of C-C $sp^3$ bonds and desired mechanical properties. These drawbacks can be overcome by exploiting high density plasma sources such as electron cyclotron wave resonance (ECWR), inductively coupled plasma (ICP), plasma beam source (PBS) or helicon sources, which create more ionised plasmas [55]. Some of these methods which work at low pressures (PBS or ECWR) are able to produce DLC films with a high fraction of tetrahedral C-C bonds (ta-C:H) with enhanced properties as compared to a-C:H films.

### 3.3.3   *Filtered cathodic vacuum arc (FCVA)*

Filtered cathodic vacuum arc (FCVA) is an established technique for producing metallurgical and hard coatings. It was first noted in the 1970's that carbon films deposited by this method exhibited diamond-like properties [81]. The plasma is produced by striking a low voltage, high current electric arc on the surface of the graphite source (target or cathode) in a vacuum chamber. This arc can be made using pulsed or DC current. In comparison with a pulsed arc, a DC current arc has shown higher deposition rates [34]. The generated plasma is highly ionized but initially contains many nano- and/or micro-particles which are considered defects in most of the cases where a very thin carbon coating is required. The quality of the plasma can be improved dramatically by using magnetic filters [35].
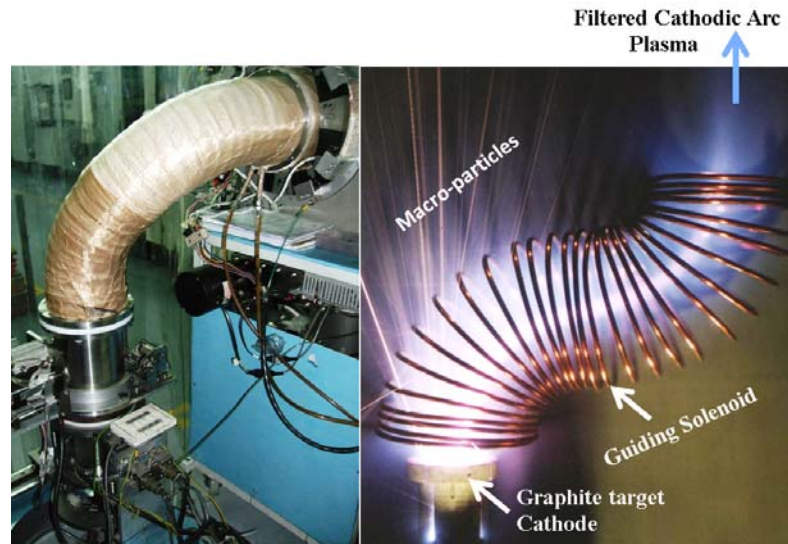
**Figure 3-5** Configuration of a Filtered Cathodic Vacuum Arc with an S-shaped filter (Figure from http://www-ibt.lbl.gov/)

These filters are magnetic ducts (magnetic solenoid) bent at an angle of 90-degrees from the arc source and the plasma is guided out of the duct (Figure 3-5). The magnetic field forces electrons to follow the filter shape. Because of the electrostatic potential of the electrons, the positive carbon ions follow the same path. However, clusters and unionized macroparticles are not affected by this field due to their higher momentum or lack of electric charge, and hence they continue their motion in a straight line and get trapped on the duct surface. Although most of these macroparticles are filtered by this method, some of them may return to the plasma by bouncing back from the walls. These bounced particles can be removed by adding another 90-degree bent filter in series (either in plane or out of plane) with the first filter to make a so-called "S-bent filter" (Figure 3-5).

This filtered plasma is approximately fully ionized with a kinetic energy of about 20 eV. The properties of the cathodic arc carbon films can be controlled by varying the energy of the $C^+$ ions. The energy of the ions leaving the S-bent filter can be increased by accelerating the ions to the substrate surface. This is carried out by applying a negative bias voltage (either by DC or pulsed biasing) to the substrate.

In the FCVA deposition method, if reactive gases such as nitrogen are introduced during the plasma formation process, films such as ta-CN$_x$ may be deposited due to interaction between the ion flux and the gas compounds.

## 3.4 *Application of carbon overcoat in magnetic recording industry*

### 3.4.1 *Hard disk drives*

As mentioned in Chapter 2, in order to prevent the magnetic medium and the head read-write elements from oxidation and wear, the surfaces of the media and head are coated with a thin protective overcoat and a thin layer of lubricant. An ideal overcoat should be able to protect the magnetic surface against corrosion and wear while its thickness is as low as a few nanometers. This requires the coating to cover the surface completely without any defects or pin holes. The film should also be very dense to act as a diffusion barrier. This material should be compatible with the lubricant and provide good adhesion sites for the lubricant molecules. This coating should be as smooth as possible and extremely hard, tough and have a low coefficient of friction to protect the surface against wear. Because of their unique properties, DLC films have been the only candidate for coating the surface of the magnetic layers in hard disk drives for decades.

As explained in Chapter 2, the read-write elements of the head (magnetic sensor and poles) are made of mechanically soft magnetic materials which have a greater wear rate than the surrounding hard Al$_2$O$_3$ dielectric insulator. This difference in the wear rates results in a recession of the magnetic poles. This process is called pole tip recession (PTR) and increases the magnetic spacing between the active elements of the head and the media. PTR can be reduced by coating the head with an ultrathin hard DLC film.

Head overcoats not only prevent wear and corrosion of the head elements, but are also necessary as a barrier against lubricant degradation. Using uncoated $Al_2O_3/TiC$ sliders could lead to the rapid decomposition of PFPE molecules. Frictional effects can lead to a decomposition of the PFPE molecule and emission of fluorine. Fluorine can react with a-C:H films and form HF and $CF_2O$ [82, 83]. HF and $CF_2O$ react with aluminum oxide in the slider and form $AlF_3$, which is a Lewis acid (able to accept electron pair from other atoms or molecules). Lewis acid catalytic reactions on the $AlF_3$ surface can rapidly decompose PFPE lubricant molecules. Coating the sliders with DLC films can be a remedy to reduce chemical interaction between the lubricant molecules and $Al_2O_3$ phase of AlTiC or dielectric of the head. In addition, because of its low friction, the DLC coating remarkably decreases the decomposition rate of the lubricant [84, 85].

In the earlier generations of hard disks, sputtered amorphous carbon (a-C) films (with a high fraction of $sp^2$ bonds) were used to mostly act as a corrosion barrier. In the next generations of hard disks, amorphous hydrogenated carbon films with higher $sp^3$ content were used to further protect the media against wear and mechanical damage. These films were generally deposited by magnetron sputtering.

Due to their desirable tribological performance (higher wear resistance, low coefficient of friction, toughness and strong adhesion on the surface), nitrogenated carbon ($CN_x$) films were introduced as an advanced protective overcoat option for disk media. $CN_x$ films presented better compatibility with existing lubricants. The above-mentioned catalytic reactions are prevented due to less hydrogen evolution from the $CN_x$ overcoat, resulting in better tribological performance for the $CN_x$ film as compared to that of the $CH_x$ film [85].

In traditional hard disks with an areal density of 10 Gbit/in$^2$, the magnetic spacing was approximately 25 nm, which allowed a protective carbon layer on the head and media

not thicker than 5 nm. In modern hard disks of 1 Tbit/in$^2$ areal density, the DLC coating should not be thicker than ~2 nm. However, these films should still be atomically smooth, continuous, dense and also hard to be able to protect the magnetic layer against wear and corrosion.

Although hydrogenated and nitrogenated carbon overcoats (mostly sputtered films) have been widely used, their durability drops off markedly at thicknesses below 5 nm. Moreover, these films are not able to form continuous films thinner than 2 nm. This requires researchers to find an alternative overcoat material. Among many different types of DLC films, an ultra-thin ta-C film (deposited by the FCVA technique) with thickness of less than 5 nm is still continuous, dense and hard enough to be used as a potential option for tribology of the new generation of hard disks.

In this research work, FCVA ta-C overcoats as thin as 1 nm have been applied on the surfaces of magnetic films. It has been shown that these thin films can still provide adequate protection on the substrate and show good corrosion and oxidation resistance. In addition, new attempts have been made to investigate surface modification of the magnetic medium of hard disks by energetic C$^+$ ion bombardment under controlled FCVA conditions, in order to produce surface modification, prevent corrosion resistance and provide strong tribological protection. This could help to produce 'overcoat-free' magnetic media and heads that exhibit superior mechanical strength and good oxidation resistance. The above strategy, if achieved successfully, can create the required magnetic spacing (~2 nm) needed for 10 Tbit/in$^2$ disk drives in the future.

### 3.4.2   *Magnetic tape drives*

Unlike HDDs in which the recording head flies over the media and both surfaces are coated with a DLC film and lubricant layer, the head and media in magnetic tape drives are in direct contact and do not have any overcoats. For this reason, tape drives

suffer from friction at the head-tape interface, wear of the head, and PTR [10, 16] over the lifetime of the drive.

With the invention of advanced magnetic tape drives, tribological and corrosion problems at the heads were also manifested. Most of these problems were solved largely by a combination of good design, lower contact pressures, better lubricants as well as better materials for heads and media. However, the problem of PTR and head corrosion continued to persist.

Coating the head surface in magnetic tape drives has been one of the ideas to mitigate wear, PTR and corrosion in magnetic heads. Zieren and his co-workers applied a 50 nm to 100 nm thick CrN coating deposited by RF sputtering of chromium in an Ar-$N_2$ atmosphere on multi-track thin-film inductive tape heads for digital compact disk cassette (DCC) recorders as a safeguard against head wear, corrosion, and severe PTR [86]. In 1995, DLC films of about 1 μm thick produced by the high frequency PECVD technique were deposited on video cassette recorder (VCR) head drums to alleviate the tribological problems between the head drum and VCR tape [87]. Although this DLC coating showed promising tribological results (50% lower wear rate and 30% less friction as compared with the bare head [88]), it suffered from lack of durability because of its poor adhesion to the head surface.

In order to improve the adhesion of the DLC films to the surface of the VCR heads, Trakhtenberg et al. [89] proposed a surface pretreatment method. In this method, the head surface was initially cleaned using $Ar^+$ and $O^+$ sputter-etching and a thin titanium interlayer was deposited on the surface prior to deposition of a 10-80 nm sputtered a-C coating. This surface treatment improved the film adhesion to ferrite and provided a smoother DLC surface.

Bhushan et al. studied the wear resistance of different hard films deposited by various deposition techniques as a potential coating for the magnetic tape heads [90]. In their studies, they deposited 20 nm thick films of a-C, $Al_2O_3$ and SiC on Ni-Zn ferrite and $Al_2O_3$-TiC flat substrates of magnetic heads as well as on dummy heads using various deposition techniques such as sputtering, filtered cathodic arc and ion beam deposition (IBD). Among the developed coatings, 20 nm carbon films deposited by cathodic arc and ion beam showed the best tribological performance. By conducting functional accelerated wear tests against metal particle (MP) tapes in a real tape drive, the wear performance and effect of these carbon coatings on PTR were evaluated and compared with that of the bare heads [91]. Their results showed that the performance of the cathodic arc carbon coated head in preventing PTR was better than the other coatings and uncoated head, but was still not enough to eliminate the PTR.

In 2000, Scott et al. further studied the wear progression and failure mechanism of 5, 10, and 20 nm DLC films deposited on $Al_2O_3$–TiC recording heads [92]. Based on their findings, wear of the DLC coatings was more severe on the AlTiC substrate as compared with that of the read/write elements. In addition, the DLC film deposited by the FCVA technique showed better durability and adhesion to the substrate as compared to similar films subjected to direct ion beam deposition [91]. Although these coatings could postpone the initiation of PTR, as the coating on the substrate was worn off, PTR began to increase. From these studies, it can be concluded that coating the head surface can be a durable remedy for PTR, provided that the coating has a good adhesion to all the components of the head (substrate, magnetic elements and poles and dielectric).

Conducting a multi-component flowing mixed gas test, Scott et al. studied the effect of DLC coatings deposited by an ion beam on the corrosion of head materials. The 20 nm

DLC coating was shown to increase the corrosion resistance of the heads while the 5 or 10 nm thick coating exhibited about the same weak performance [5].

In recent years, hard ceramic coatings were also examined as a potential candidate for coating magnetic tape drive heads. The application of chromium oxide as a protective coating for magnetic heads was studied by Bijker and Sullivan [93, 94]. The films were deposited by RF sputtering of a chromium target in an argon/oxygen atmosphere. In this study, the effect of bias voltage and thickness of chromium interlayer on the stress, hardness and wear resistance of the coating was explored. Sourty and Sullivan [95] investigated the wear performance of 20 and 40 nm thick chromium oxide protective films in different test environmental conditions [96]. In this work, the role of the coating and environmental effects on debris and stain formation were studied.

In their more recent work, Shi and Sullivan [97] investigated the tribological behavior of 20–50 nm thick $Cr_2O_3$ hard coatings, that were deposited on linear tape open (LTO) recording heads using an unbalanced magnetron sputtering technique. According to their results, the coating of the head read/write elements was less durable than that of the AlTiC surface and was removed from the surface of the poles much faster due to the lack of adhesion.

Even though many different coatings (mostly thicker than 20 nm) such as chromium oxide and different types of DLC have been applied to magnetic heads [94, 95, 97, 98], most of these coating materials and methods were not successful in producing a commercially viable solution for tapes because most of these films were very thick (up to 50 nm), which introduced a large magnetic spacing, hence resulting in a decrease in the areal density. Moreover, none of the head coatings survived when it ran in contact against the tape for the 30,000 to 50,000 hours required for the life of the tape head [14]. Among many well-known hard materials used as protective coatings such as

oxides [95, 99], nitrides [100], carbides [101], or DLC deposited by different techniques [98, 101], the most promising candidate for such applications is DLC and, more specifically, ta-C coatings.

However, one of the most serious drawbacks of ta-C coatings, like the other types of DLC films, is their poor adhesion to AlTiC substrates [98, 102]. This has significantly delayed commercial applications of DLCs as protective coatings on tape drive heads. The adhesion of the coating to the head materials (AlTiC substrate and poles material) is very critical. An ideal coating for low thickness (less than 10 nm by 2020) should have excellent adhesion to the substrate and magnetic elements.

In this study, various strategies surface treatment techniques have been developed by exploiting different surface techniques to improve the adhesion and durability of the ta-C head overcoats with thickness of less than 10 nm. In these techniques, while keeping the desirable properties of ta-C films (as mentioned earlier in Section 3-2-2), it was sought to modify the properties of the head/ta-C interface in order to strongly bond the overcoat to the surface of the head components. These proposed methods will be elaborated upon in the subsequent chapters, and they can be summarized as follows:

(i) Surface modification of the AlTiC substrate by energetic $C^+$ ions (Chapter 5).

(ii) Surface modification of the head with application of Si and Al-Si-C composite layer as interlayer (Chapter 6).

(iii) Surface modification of the head by developing an Al-TiN$_x$C$_y$ composite interlayer (Chapter 7).

# Chapter 4: Experimental Procedures

In the present chapter, various common experimental methods used for fundamental physical, chemical, mechanical and tribological characterizations of ultrathin films developed in this research are described. Details of the materials used, film deposition and sample preparation are given in respective chapters for easy reference.

## 4.1   Specimens and sample preparation

In this study two different types of substrates have been used:

1- AlTiC flat wafers

2- Real Linear Open Tape (LTO) recording heads

Commercially available AlTiC wafers consisting of ~70% $Al_2O_3$ and ~30% TiC (by weight) were used as substrate specimens. AlTiC wafers with a thickness of 1 mm were cut into dimensions of $10 \times 10$ mm$^2$. The root-mean-square roughness of the samples was measured as ~2 nm using an AFM (Innova Scanning Probe Microscope, Bruker) in the tapping mode with a scan size of $20 \times 20$ μm$^2$ and scanning rate of 1 Hz. Before conducting any surface treatment, the samples were ultrasonically cleaned by isopropyl alcohol (IPA) and acetone respectively for 20 minutes and then dried by blowing pure nitrogen gas.

Generation 4 of the LTO-4 recording heads manufactured by Oracle America Inc., Broomfield, CO, USA were used as the specimens. A recording head consists of 32 read-write elements located in two parallel rows of 16 at both sides of the head. Each read-write element consists of write poles and shield made of cobalt-zirconium-tantalum (CZT) and the read sensor is made of NiFe. Read-write elements are electrically insulated from each other and also from the substrate by a sputtered $Al_2O_3$

film. These elements are sandwiched and supported by a hard composite ceramic (AlTiC) consisting of about 70% $Al_2O_3$ and 30% TiC by weight (Figure 4-1).
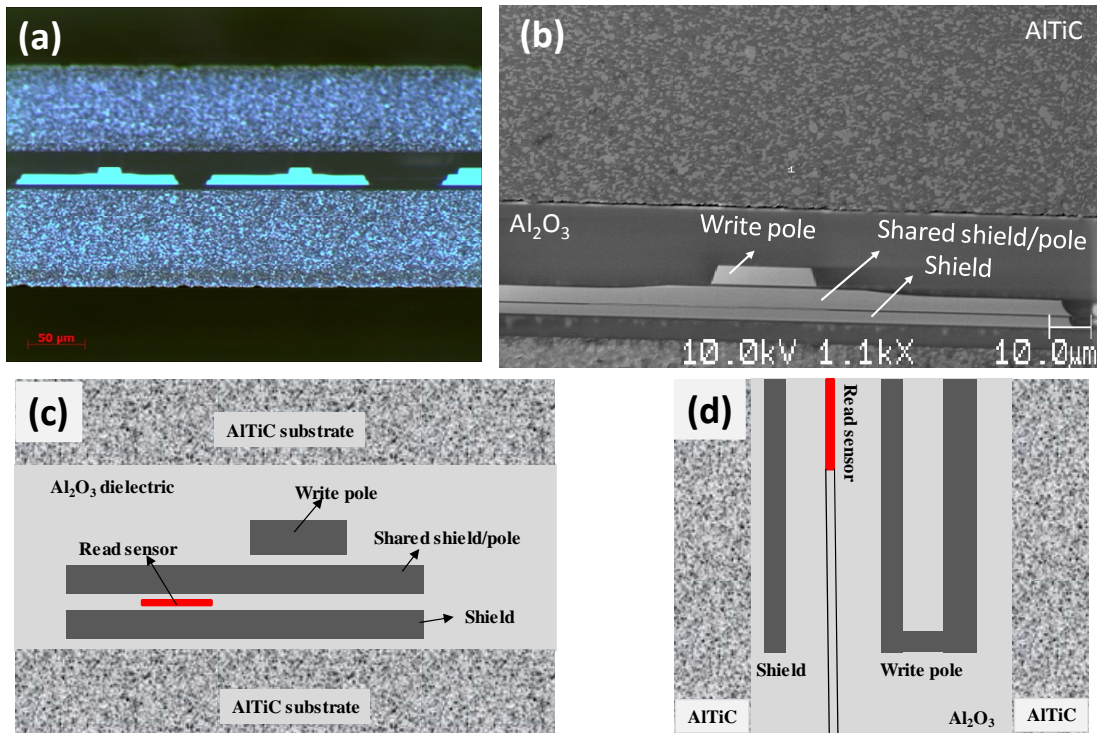


**Figure 4-1** Optical microscope image of the read/write elements, schematic drawing of (b) top view and (c) cross-section of one of the head read/write channels

Since the cleanness of the surface is of great importance for proper adhesion of the coatings to the surfaces, prior to the deposition of the coatings, the heads were ultrasonically cleaned with acetone and isopropanol IPA for 20 minutes, rinsed with deionized water and dried with pure nitrogen. In order to decrease the out-gassing in the deposition chamber due to the release of the adsorbed moisture or other chemicals from the heads, the cleaned heads were baked at 50 °C for 20 minutes.

To ensure good adhesion between the protective coating and substrates, the surface of the substrates (head or AlTiC flat samples) was cleaned by $Ar^+$ plasma sputter-etching. In this process, the surface was exposed to strong ion bombardment with ion energies of a few hundreds to thousands of eV. Interaction of $Ar^+$ ions with the surface led to removal (sputtering/etching) of the material (contaminants) from the top layers of the

surface. In a sputtering tool, $Ar^+$ plasma cleaning is done by applying a potential difference (an additional voltage higher than the floating voltage) between the plasma and the substrate to be cleaned. This potential difference accelerates the $Ar^+$ ions towards the surface and gives them enough energy to overcome the surface binding energy of the atoms on the top layer and remove them from the surface. This process may affect the topography of the surface and change the roughness. In order to minimize this effect while obtaining the benefit of $Ar^+$ plasma etching for cleaning the surface, the plasma parameters were optimized. To determine the optimum etching parameters, a number of samples were etched with various plasma parameters, and the topography and quality of the adhesion of the coatings on the etched surfaces were examined. From the findings, $Ar^+$ plasma with ion energy of 230 eV, beam current of 45 mA, incident angle of 45 degrees and etching time of 8 seconds showed the optimum results.

## 4.2   Surface pre-treatment and deposition of protective coating

Surface pre-treatment techniques consist of deposition of different interlayers and/or bombarding the surface of the substrate (with or without interlayer) with energetic carbon ions. Bombarding the surface with energetic carbon ions and deposition of tetrahedral amorphous carbon (ta-C) films were conducted using the filtered cathodic vacuum arc (FCVA) technique. Other metallic or ceramic materials (Si, Ti, TiN, SiN, etc.) were deposited using the sputtering technique.

### *4.2.1   Application of FCVA technique for bombardment of the surface of the samples with energetic $C^+$ ions and deposition of ta-C thin film*

Deposition of the ta-C overcoat and bombardment of the surface with energetic $C^+$ ions prior to deposition of the overcoat was performed using FCVA (Nanofilm

Technologies International Pte. Ltd., Singapore). The deposition mechanism of this system has been extensively described in Chapter 2. As mentioned earlier, this system is able to develop a highly ionized mono-energetic plasma, which enables precise control of the chemical properties of the ta-C overcoat (for example $sp^3/sp^2$ content) as well as the embedment depth of the bombarding ions into the substrate surface.

The samples with the cleaned surface were subjected to pure $C^+$ ion flux produced by the FCVA technique. $C^+$ plasma was produced by striking an electric arc between a mechanical trigger and a highly pure (99.999%) graphite target with a continuous direct current (DC) current of 40 A and voltage of 20 V. In comparison with the pulsed arc, the DC current arc has shown higher deposition rates [103]. The generated plasma initially contains many nano- and/or micro-particles which are considered as defects in most of the cases where a very thin carbon coating is required. The quality of the plasma can be improved dramatically by using magnetic filters [104]. In this work, an out of plane S-shape filter (consisting of two 90° bent magnetic ducts connected to each other in series and in out-of-plane orientation) was used to minimize the presence of the nano- or micro-particles in the coating (Figure 4-2).

The plasma leaving the filter was approximately fully ionized (~100% $C^+$ ions) [105] with kinetic energy of about 20 eV [51]. Previous work has shown that the ion energy of about 100 eV can lead to the highest fraction of $sp^3$ bonds with the maximum density and hardness [47, 52]. The energy of the ions can be increased by accelerating the ions to the substrate surface by applying a negative bias voltage (Figure 4-3) to the substrate based on Eq. 4.1.

$E_2-E_1=-Q(V_2-V_1)$  <span style="float:right">Eq. 4.1</span>
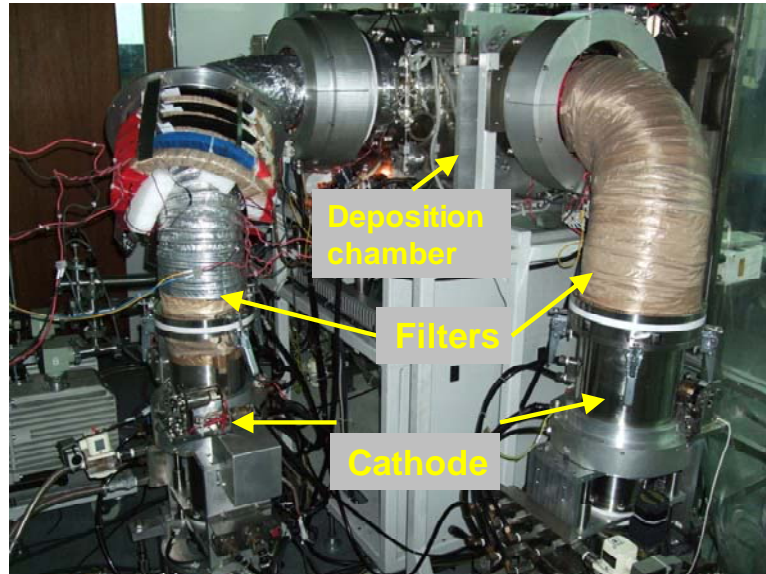
**Figure 4-2** Outer view of the FCVA system with two sources and out-of-plane S-shape filters

In this equation $E_2$ is energy at the substrate, $E_1$ is the ion energy at the exit of the filter (~20 eV), $V_1$ is the potential of the filter exit which is considered as zero, and $V_2$ is the bias voltage of the substrate holder. Q in this specific problem is the electric charge of a $C^+$ ion which is $+1e$ $(1.6\times10^{-19}$ C).
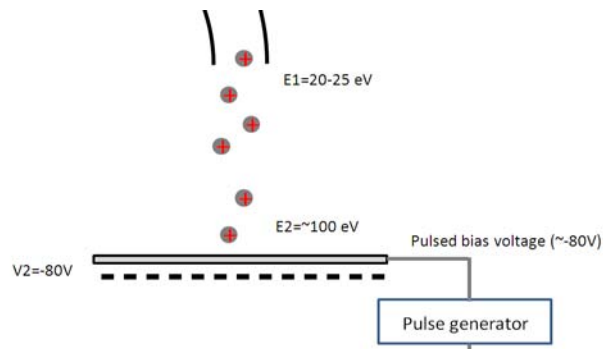


**Figure 4-3** Schematic structure of the $C^+$ ions accelerated towards the substrate by proper biasing of the substrate holder.

Based on this equation, in order to obtain the ion energies of 100 eV and 350 eV, a potential of -80 V and -330 V should be respectively applied to the sample surface.

It has been shown that pulsed biasing the substrates can lead to better ion mixing and adhesion between the ta-C film and its underlying layer [106, 107]. In all depositions,

a negative pulsed bias voltage of 20 kHz with a duty cycle of 60% was applied to the substrates. Figure 4-4 shows a schematic block diagram of the pulsed biasing scheme.
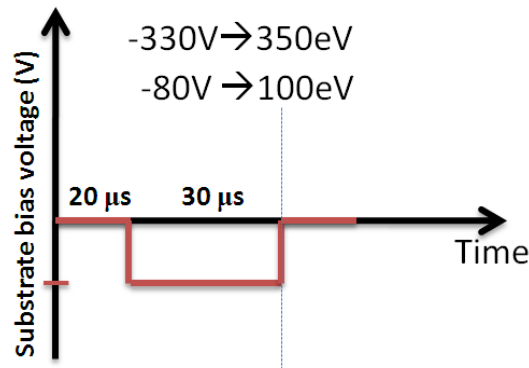


**Figure 4-4** Schematic block diagram showing the repetitive pulse biasing of the substrate during one period of biasing

### 4.2.2   *Deposition of interlayers (adhesion layers) using magnetron sputtering*

All depositions other than the deposition of ta-C films were conducted in a magnetron sputtering tool (*AJA international Inc, MA, USA*). Sputtering is a coating process which involves the transport of almost any material from a source, called a target, to a substrate of almost any other material (i.e., metals on plastic, plastic on metal, plastic on paper, ceramic on metal, etc.). The ejection of the source material is accomplished by the bombardment of the surface of the target with gas ions (usually an inert gas like Ar) accelerated by a high voltage. Particles of atomic dimension from the target are ejected as a result of momentum transfer between the incident ions and the target atoms. The mechanism of momentum transfer was first proposed by F. Stark in 1908. The target-ejected particles traverse the vacuum chamber and are subsequently deposited on the substrate as a thin film.

In this work, different materials (ceramic compounds or pure elements) such as Si, SiC, Ti, and TiN were used for pretreatment of the substrate surface (as an interlayer between the substrate and the ta-C overcoat). In addition, Co was deposited on the Si wafer as the magnetic layer of the magnetic media in the hard disk related studies.

The sputtering tool consists of a deposition chamber with eleven magnetron sources (Figure 4-5) which enables us to deposit different materials separately or at the same time (co-sputtering) on the substrate without breaking the vacuum.

The power supply for sputtering may be of two varieties: Direct Current (DC) or Radio Frequency (RF). The selection mainly depends on the type of the material to be deposited. In either case, the purpose of using the power supply is to generate the plasma and to induce sputtering by setting up a negative surface charge on the target. DC biasing is usually used for metals and other conductors, while RF biasing applies when the depositing film is a non-conductor. In this work, a DC power of 60 W was used for the deposition of conductive materials (Ti and Co) whereas, for ceramics or dielectric materials (Si, SiC, SiN, TiN), an RF power of 150 W was used. The base pressure of the chamber was always lower than $1.0 \times 10^{-8}$ Torr and the working pressure and argon flow rate were 3.0 mTorr and 15 sccm for all depositions. The deposition rates of all materials were measured by the deposition of a relatively thick film (about 20 nm thick) and measuring the height of a sharp step on the surface (made by photolithography) using scanning probe microscopy (SPM).
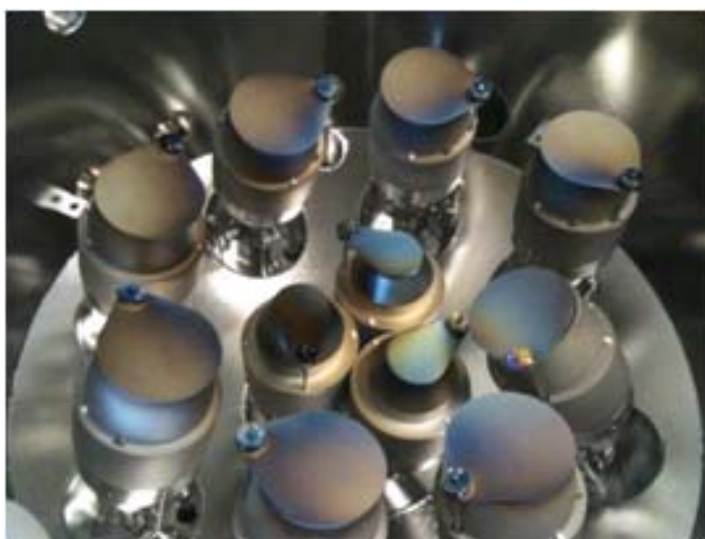


**Figure 4-5** Magnetron sources of the AJA sputtering tool enable us to deposit different elements or compounds on the substrate at the same time

## 4.3   SRIM simulation

As the surface of a material (target) is bombarded by energetic ions, the bombarding ions may embed themselves into a certain depth of the target surface. This process is called direct implantation. On the other hand, the bombarding ions may transfer significant energy to the target surface (recoil) atoms, and these can move long distances and create significant collision cascades. The process of moving (diffusing) the recoil atoms from one layer of the target to the other layers is called recoil intermixing. In special cases where recoil intermixing may be used to modify the properties of the surface, this process may be referred to as "*recoil implantation*".

During the process of sputter-etching to remove the top oxide layer of the thin films (interlayers) or surface pre-treatment of the samples (with or without interlayers) with $C^+$ ions, the surface of the substrates was bombarded by energetic $Ar^+$ (at 500 eV) or $C^+$ ions (at 350 eV) respectively. To have a better understanding of the possible effects of this bombardment on the distribution of the ions on the surface of the substrate (bare AlTiC or Co film) or in the structure of the interlayers, the SRIM (Stopping and Range of ions in Matter) or TRIM (Transport of Ions in Matter) code [108] was used to simulate implantation (direct and recoil) distribution of the existing species in the interface of the interlayer(s) and the AlTiC substrate or on the outermost layer of the bare AlTiC or bare Co surfaces.

TRIM or SRIM is a Monte Carlo computer program that calculates the interactions of energetic ions with amorphous targets. This program has been called TRIM for more than 30 years. The program uses several physical approximations to obtain high computing efficiency, while still maintaining the accuracy. The two most important approximations are: (a) using an analytic formula for determining atom-atom collisions, and (b) using the concept of a Free-Flight-Path between collisions, so that

only significant collisions are evaluated. This program is primarily concerned with the quantitative evaluation of how ions lose energy into matter and the final distribution of these ions after they stop within the target.

In this simulation, ion flux of $Ar^+$ or $C^+$ was perpendicular to the surface of a semi-infinite medium of the substrate (e.g. $Al_2O_3$ phase of the AlTiC substrate which might be coated with a thin layer ($\leq$ 2nm) of Si or TiN). The simulation was performed for ion energies of 500 eV for $Ar^+$, and 100 eV and 350 eV for $C^+$. In this simulation, the interface between the layers (for example $Si/Al_2O_3$) was perfectly smooth and free from defects. This method assumes that no chemical reaction would take place during the implantation of ions. It does not consider the deposition of ions on the surface of the substrate. In addition, it is assumed that the ion implantation takes place in a perfect (absolute) vacuum. In this simulation, the controllable parameters are:

- Ion type ($C^+$, $Ar^+$)

- Ion energy (350 or 100 for C, and 500 eV for Ar ions)

- Direction of ions (perpendicular to the substrate)

- Substrate material, thickness, and arrangement of layers

## 4.4 Thin film characterization techniques

### 4.4.1 *Transmission Electron Microscopy (TEM)*

Transmission electron microscopy (TEM) is a microscopy technique whereby a beam of electrons is transmitted through an ultra thin specimen, interacting with the specimen as it passes through. An image is formed from the interaction of the electrons transmitted through the specimen; the image is magnified and focused onto an imaging device, such as a CCD camera. TEMs are capable of imaging at a significantly higher resolution than light microscopes. This enables the instrument's user to examine fine

detail even as small as a single column of atoms, which is tens of thousands times smaller than the tiniest resolvable object in a light microscope.

In our work, in order to precisely measure the film thickness as well as to study the structural characteristics of the substrate/interlayer/coating interface, the cross-sectional structure of the ta-C overcoat with Si (without pre-treatment) and with composite interlayer was observed by TEM (JEM, 3200FS, JEOL Ltd). The TEM samples were prepared by cutting the specimens and bonding the treated surfaces face-to-face by epoxy and thinning the specimens transversely by grinding and polishing. The resulting thin samples (thinner than 50 μm) were ion milled until a hole appeared in the film-epoxy area.

Due to their similar structures, it is usually very difficult to tell the distinction between the ta-C overcoat and the epoxy adhesive used for TEM sample preparation. In order to distinguish between the epoxy and the ta-C overcoat, a thin layer of a crystalline material (e.g. a metal film) can be deposited on the ta-C surface before application of the epoxy to the surface. Because of their good adhesion to the substrate, a thin film of Ta or Ti was used in this work.

### 4.4.2   *X-ray Photo-electron Spectroscopy (XPS)*

X-ray Photo-electron Spectroscopy (XPS), also known as Electron Spectroscopy for Chemical Analysis (ESCA), is the most widely used surface analysis technique because of its relative simplicity in use and data interpretation. XPS utilizes the photoelectric effect[1]. In this phenomenon, the sample surface is irradiated with x-ray photons of a known energy. This energy is absorbed by the atoms in the material, leading to the ejection of photoelectrons from either the core levels of the atom or one

---

[1] Albert Einstein received the Nobel Prize in Physics in 1921 for explaining the photoelectric effect.

of the valence levels. The emitted photoelectron has a characteristic binding energy (BE) which is characteristic of the element that it originates from. XPS spectra are able to provide information about the chemical state of the surface based on these characteristic binding energies. Different chemical state are identified by measuring the deviation of a peak relative to the known elemental or core level binding energy (chemical shifts).

Most of the mechanical properties of the DLC films are directly related to the amount of $sp^3$ oriented C-C bonds in the structure of the film [46, 47]. The surface chemical composition of the ta-C films can be interpreted in terms of the XPS results. Surface chemical analysis of the treated surfaces was carried out in an XPS system (VG ESCALAB 220I-XL). An Al-$K_\alpha$ X-ray source with a spot size of 400 μm and pass energy of 40 eV was used for this measurement. Chemical composition analysis of the ta-C films and depth profiles of the existing elements in the coating, interlayer and substrate were performed by the XPS depth profiling technique. In depth profiling of thicker (10 nm) films, the surface of the sample was sputter-etched by $Ar^+$ ions of 500 eV. In order to obtain enough information about the chemical state of the AlTiC/interlayer/ta-C interface, a depth profile with high spatial resolution in depth was required. To achieve this goal, the surface was etched in very small depth steps from the overcoat surface down to the substrate with an etching time of 10 seconds. The chemical state of each level was precisely measured by acquiring a high resolution XPS spectrum ($Si_{2p}$ and $C_{1s}$) with energy step of 0.1 eV. Each spectrum was obtained as an average of 10 scans.

Angle-Resolved XPS (AR-XPS) technique [109] was used to study the chemical state of the films or modified surfaces with thickness (depth) of about 1 nm. It has been demonstrated that the XPS information depth (the depth from which the XPS data can

be acquired) decreases by decreasing the photoelectron take-off angle (collection angle); and therefore, more surface sensitive analysis can be done at grazing take-off angles.
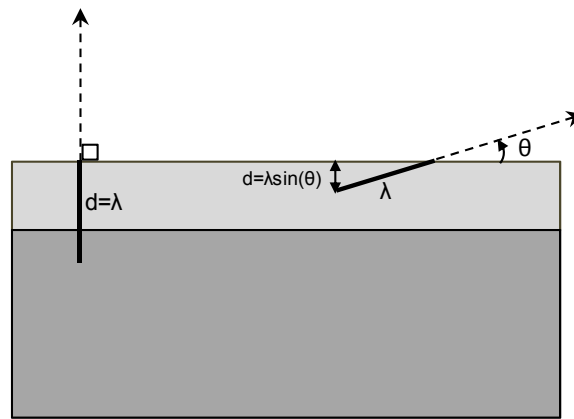


**Figure 4-6** schematic drawing of the ARXPS concept

Due to the reduced thickness of the layers we are working with (1 nm Si/C mixed layer for protecting the hard disk media surface as will be described in chapter 10), which is below the information depth of XPS, ARXPS analyses was preferred over XPS sputtering depth profiling. In ARXPS, the acquisition of x-ray photo-electron spectra at different emission angles allows the characterization of the sample with different surface sensitivities in a non-destructive manner. In this work, the photoelectron take-off angle was varied from 15° to 75° (measured with respect to sample surface) with intervals of 5°. Figure 4-6 schematically shows how escape depth of photo electrons changes by the take off angle.

### 4.4.3 Auger Electron Spectroscopy (AES)

Another important form of electron spectroscopy used in surface science is Auger electron spectroscopy (AES) [110]. Auger electrons are named after their discoverer, Pierre Auger. If the surface is being excited by highly energetic photons or an incident high energy electron, an electron can be ejected from a core level of an atom. This core

hole will be filled by another electron from a higher energy level. The energy lost by this electron (difference between the initial energy of the electron and the energy level of the core hole) may be released in the form of an X-ray photon or the quantum of energy may be transferred to another electron in the atom, which is referred to as the Auger electron. That electron (the Auger electron) is thus released from the atom. The kinetic energy of the Auger electron, unlike that of a photoelectron, is not dependent on the energy of the incident radiation (or electron) that produced the initial core hole. Thus, Auger electrons have energies that are characteristic of the atom from which they arose and may be used for elemental identification. Generally, AES is carried out using an electron gun to produce relatively high energy electrons (in the 2 to 25 keV range) for initial core-level excitation.

When the surface of the sample is excited by a highly energetic electron beam (2-25 keV), the Auger electrons can only escape from a depth of 0.5-2 nm below the surface. This behavior makes AES a surface-sensitive method with very fine depth resolution. When used in combination with a controlled sputter-etching process, AES is able to conduct depth profiling with a high depth and lateral resolution, which makes it useful for analyzing the composition of ultrathin films. In addition, a finely focused electron beam can be used to scan very small features of the surface and create Auger elemental mapping images [111].

Because of the thinness of the coating (less than 10 nm) used in this study and the small size of the features (head read/write elements), AES was considered as the most suitable tool for investigating the head surface. In this work, the coated surfaces (AlTiC flat samples or heads) were examined using Auger electron spectroscopy (AES:JEOL model JAMP-10SX ).

For all the samples, in order to eliminate or minimize the effect of airborne contamination, the surface of each sample was lightly cleaned by $Ar^+$ sputter-etchings with low ion energy of ~500 eV. Next, the interested area was first scanned with an electron beam to acquire a wide spectrum to check which elements existed on the surface.

In the AES spectrum, the Auger peaks are superimposed onto the secondary electron background and are generally quite weak. To address this problem, the Auger spectrum is usually electronically – and sometimes numerically – differentiated to highlight the Auger peaks. Conducting the wide AES scans, Auger elemental mapping with a resolution of 128×128 pixels was performed to determine the distribution of the available elements on the surfaces. The thickness of the coatings after the wear tests as well as the composition of the coatings and their underlayer (if any) was analyzed by AES depth profiling. By comparing the time needed to etch the ta-C coating and reach the substrate, and also by knowing the actual thickness of the unworn overcoat (measured by TEM), the thickness of the coatings after the wear test was calculated.

### 4.4.4 *Secondary Ion Mass Spectroscopy (SIMS)*

Secondary ion mass spectrometry (SIMS) is used to analyze the composition of solid surfaces and thin films by sputtering the surface of the specimen with a focused primary ion beam, and collecting and analyzing ejected secondary ions. These secondary ions are measured with a mass spectrometer to determine the elemental, isotopic, or molecular compositions of the surface. SIMS is the most sensitive surface analysis technique, with the ability to detect elements present in the parts per billion ranges.

Elemental composition analysis of the ta-C films and depth profiles of the embedded $C^+$ ions into the substrate surface were performed by the TOF-SIMS (ion-TOF GmbH)

technique. TOF-SIMS in imaging mode was used for surface analytical studies of the top surface of the samples. In depth profiling, the surface of the samples was sputter etched by $Ar^+$ ions of 3 keV. The sputtering area was 450×450 $\mu m^2$. In order to prevent the effect of slanted sputtered crater walls on the results, the analyzed area was selected to be nine times smaller (150×150 $\mu m^2$). Bismuth (Bi) ions were used as the primary ion source for analysis.

### 4.4.5   *Atomic force microscopy (AFM)*

Atomic force microscopy (AFM) is a very high-resolution type of scanning probe microscopy (SPM), with a resolution in the order of fractions of a nanometer. The AFM is one of the most advanced tools for imaging, measuring, and manipulating matter at the nanoscale. The information is gathered by "feeling" the surface with a mechanical probe (AFM tip). The AFM consists of a cantilever with a sharp tip (probe) at its end which is used to scan the specimen surface. The cantilever is typically silicon or silicon nitride, with a tip radius of curvature on the order of nanometers. When the tip is brought into proximity of a sample surface, forces between the tip and the sample lead to a deflection of the cantilever according to Hooke's law. Typically, the deflection is measured using a laser spot reflected from the top surface of the cantilever into an array of photodiodes.

The AFM can be operated in a static (also called contact) or dynamic (non-contact or "tapping") mode. In the static mode, the cantilever is "dragged" across the surface of the sample and the contours of the surface are measured directly using the deflection of the cantilever. In the dynamic mode, the cantilever is externally oscillated at, or close to, its fundamental resonance frequency or a harmonic frequency. The oscillation amplitude, phase and resonance frequency are modified by tip-sample interaction forces. These changes in oscillation with respect to the external reference oscillation

provide information about the sample's characteristics. Non-contact mode AFM does not suffer from tip or sample degradation effects which are sometimes observed after taking numerous scans with contact AFM. AFM provides a three-dimensional surface profile which enables it to be used as the best tool for studying the topography of the surface. In this work, the surface topography of the samples was studied by imaging the surface using an AFM (Bruker, Innova Scanning Probe microscope) working in tapping mode. The drive frequency and scan rate were set at 259.332 kHz and 1 Hz respectively for the $10\times10$ $\mu m^2$ scan area. The AFM in contact mode with a special cantilever and with a natural diamond tip was used to carry out nano-wear and nano-scratch tests.

## 4.5 Characterization of nano-tribological properties of the coatings

### 4.5.1 *Nano-scratch test*

The adhesion strength of different overcoats to their substrates can be qualitatively compared using a single asperity contact scratch test. This experiment was conducted using an AFM probe with a sharp natural diamond tip with a tip radius of 40 nm mounted on a stainless steel cantilever, which had a spring constant of 277 N/m and contact sensitivity of 189 nm/V working in contact mode (Figure 4-7).
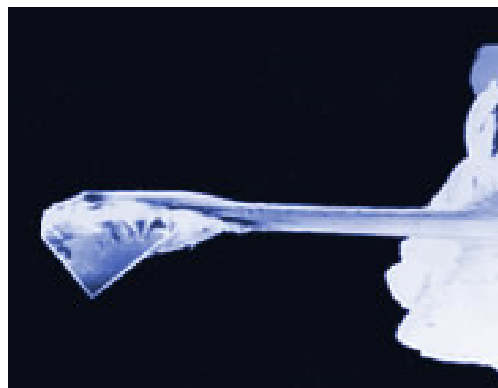


**Figure 4-7** SEM image of the diamond probe used for nano-scratch tests (Figure from
http://www.brukerafmprobes.com/p-3253-dnisp.aspx)

### *4.5.2   Ball-on-flat wear tests*

The fundamental friction and wear tests were performed using a ball-on-disc tribometer (CSM Instruments, Swiss) in rotating mode. Sapphire or silicon nitride balls of 2 mm diameter were used as the counterparts. In this test, the ball was kept in fixed contact with the surface of the sample, and the sample was rotating at a constant speed. The ball was also connected to a sensitive cantilever. The normal force was adjusted by pushing the ball to the surface and applying proper deflection to the cantilever. Normal and lateral (friction) forces were recorded by measuring the deflection of the cantilever using two optical sensors (Figure 4-8).
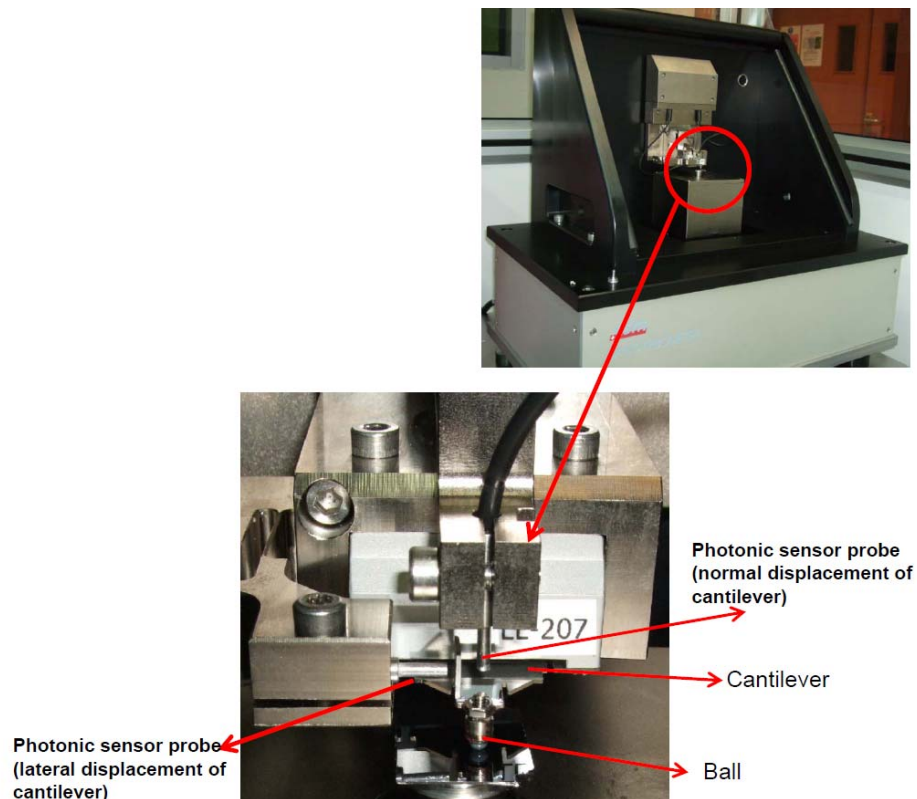


**Figure 4-8** Nano-tribometer and the ball on flat assembly

The tests were performed at a sliding linear velocity of 10 mm/s (track radius of 1.2 mm), a normal load of 20 mN, and for 10,000 sliding cycles. For each set of samples, the test was repeated at least three times to ascertain the reproducibility of the data. Taking the elastic moduli of the ball and coated substrate as 310 GPa and 365 GPa

respectively, the static contact pressure calculated by the Hertz contact theory was approximately 350 MPa. In this calculation, the Poisson's ratio of sapphire and AlTiC were considered to be 0.29 and 0.22 respectively.

### 4.5.3   *In-situ sliding wear tests on the coated magnetic heads*

The sliding wear tests on the coated heads were conducted using a SDS tape transport system provided by Imation Corp., Oakdale, MN, USA. This system consists of a deck and a controller. The deck has two motors to run the supply and take-up reels with Linear Tape Open (LTO) clutches sized to handle an LTO tape cartridge reel (Figure 4-9).
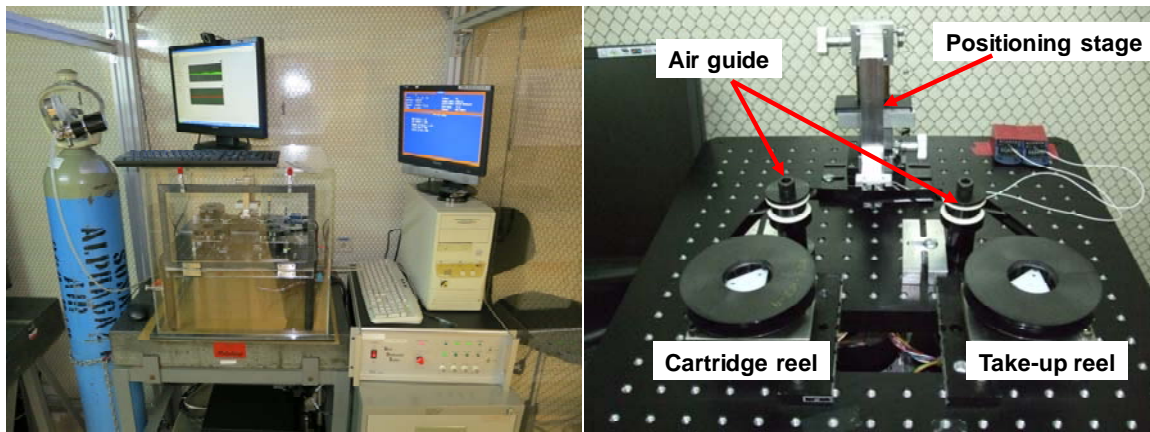


**Figure 4-9** SDS tape transport system for the in-situ head/tape interface wear test

In order to control the wear test environment (primarily relative humidity), the tape drive was enclosed with a chamber properly sealed from the outside ambient (Figure 4-9). Humidity of the chamber was controlled by purging the chamber with pure dry air (mixture of $21.0\pm1.0\%$ $O_2$ and $79\pm1.0\%$ N2 with water content of <3.0 ppm and total hydrocarbon content of < 5 ppm).

Communication between the user and the controller was done through the SDS software or a Matlab program provided by Imation. In order to maintain a head/tape interface with a fixed orientation, the tape passed through two fixed hydrodynamic

guides with a micro-textured surface and ceramic flanges. These guides did not rotate, but the speed of the tape pulled in enough air to create an air bearing between the tape and the guide surface. This provided an almost frictionless bearing for the tape while it was running; however, at the beginning of the tape motion, the tape experienced considerable start-up friction.

This system is completely programmable with several built-in routines to precisely control and record the tape position, speed, and tension. This enabled us to conduct different kinds of tape cycling such as shoe-shine for a short length of tape, or winding/rewinding cycles from beginning to the end of the tape for a desired number of cycles.
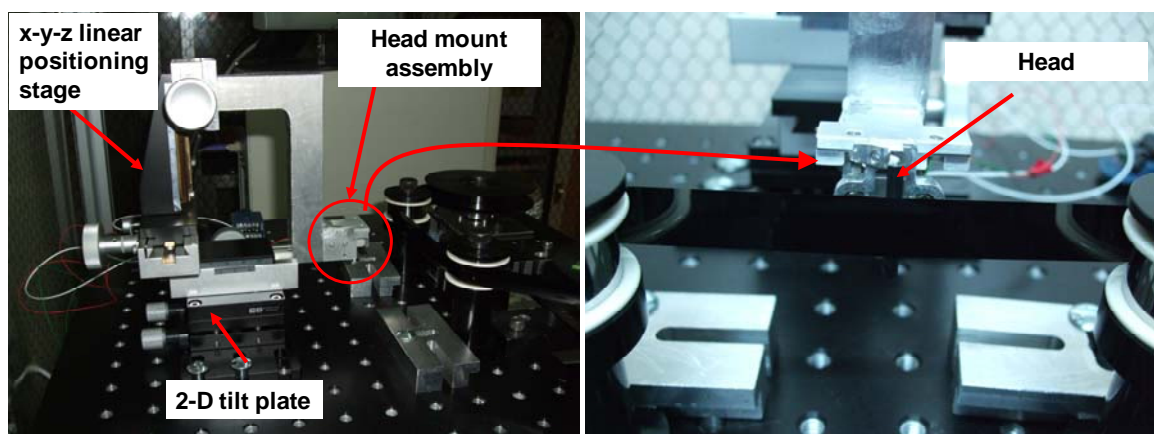


**Figure 4-10** Structure of the head positioning stage and head mount assembly

To control the head orientation and tape wrap angle, heads were loaded on a custom-built positioning stage. This positioning stage consists of a 3D (x-y-z) linear stage mounted on a 2D tilt plate. This enables us to adjust the alignment of the head with respect to the tape path as well as to control the protrusion of the head into the tape path to maintain the proper wrap angle (Figure 4-10).

In order to measure the normal and lateral (friction) forces at the interface of the head and the running magnetic tape during the test, a custom-built load cell was designed, fabricated and installed on the head mount assembly. This load cell was fixed to the

head positioning stage and the head was connected to the load cell by using an adapter plate and a set of screws (Figure 4-11(a)).
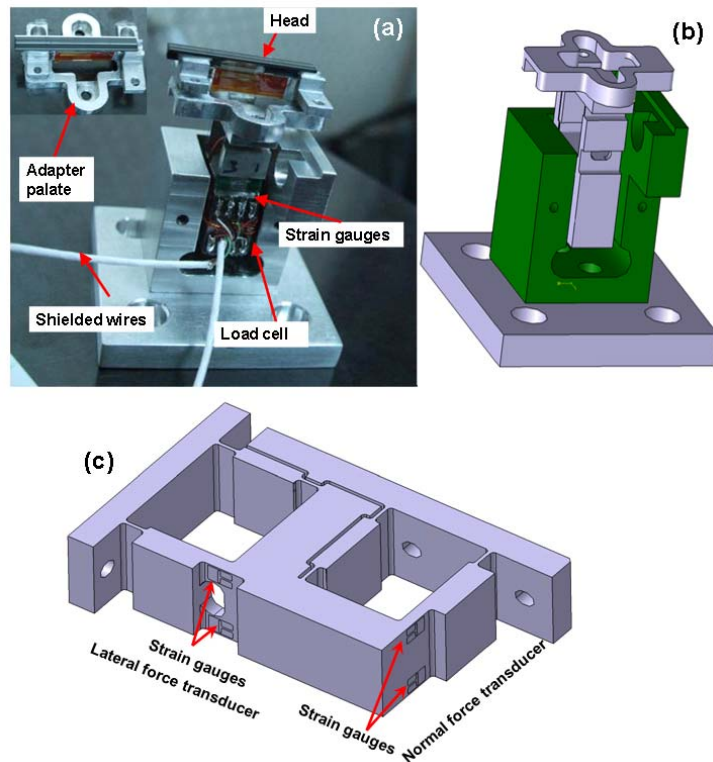


**Figure 4-11** Head mount assembly and structure of the load cell

The structure of the load cell is shown in Figures 4-11(b) and (c). The load cell consisted of two independent thin cantilevers to measure the normal and lateral forces independently. Four pieces of wire-type strain gauges were attached to both sides of the cantilever in a Wheatstone bridge configuration. Keeping the thickness of the bending beams (where the strain gauges are mounted) the same is critical because all strain gauges should sense the same strain. In order to meet this requirement, the load cell was fabricated using EDM (electro-discharge machining) with a narrow tolerance of ±0.025 mm.

The electrical output signal of the strain gauges setup is typically on the order of a few millivolts. This signal was amplified by an instrumentation amplifier and converted into digital signals using an analog to digital converter, all embedded in a data

acquisition (DAQ) card (National Instruments). The analog output of the strain gauges would always be subjected to noise. In order to eliminate this noise, the strain gauges were connected to the data acquisition card using properly shielded wires.

Because of the spring-like behavior of load cells, they would always be subjected to ringing or resonance when an abrupt load change is applied to them or the frequency of the applied force is near to their natural frequency. To address this problem, the current load cell was designed in such a way so as to maximize its natural frequency. To further increase the natural frequency of the transducer, it was made of aluminum, which has high elastic modulus to density ratio (to have a high stiffness and a low mass). Using finite element analysis, the natural frequency of the load cell was estimated to be 1 kHz. The maximum sampling rate of the selected DAQ card was 5 kHz, which was much higher than 2X of the natural frequency (the Nyquist frequency). Using such a stable and sensitive load cell assembly, one can capture almost any small force interactions (dynamic friction, static friction peaks, stick-slip forces, etc.) at the head tape interface. The friction and normal force were separately captured in different data files using LabView program.

In this work, Imation LTO Ultrium Generation 3 (LTO3) tape cartridges were employed for the sliding wear tests. 660 meters out of the total length of 680 meters of the tape cartridge were used for the wear test. In order to keep the tape condition consistent for all the heads, the usable length of the tape was divided into four equal sections whereby each section was slid back and forth against only one head. To study the durability of the coatings, the heads of each batch were tested for three different tape lengths of 170 km, 340 km, and 1000 km. During the experiment, the tape speed and tape tension were fixed at 5 m/s and 0.7 N respectively. The test parameters used for these experiments are summarized in Table 4-1.

**Table 4-1** Parameters of the tape used for sliding wear on the coated heads

| Tape speed | Tape tension | Tape total length | No. of cycles |
|:---:|:---:|:---:|:---:|
|  |  | 170 km | 515 |
| 5 m/s | 0.7 N | 340 km | 1030 |
|  |  | 1000 km | 3030 |

# Chapter 5: Surface modification of the AlTiC ceramic substrate by energetic C⁺ ions to improve tribological properties of the ta-C coating

Depositing an ultra-thin tetrahedral amorphous carbon (ta-C) protective coating on the surface of the recording heads in magnetic tape drives can improve the tribological performance of the head/tape interface. In this chapter the effect of pre-treatment of the surface of AlTiC flat substrate (material of the main bearing surface of head in contact with tape) by C⁺ ions of moderate energy (~350 eV) on the structural and tribo-mechanical behaviors of the coated surfaces is studied. Sample preparation consisted of two separate stages of surface pre-treatment and deposition of the protective film, and was done by means of filtered cathodic vacuum arc (FCVA).

## 5.1 Introduction

As mentioned in chapters 1 and 2, decreasing the magnetic spacing and maintaining it to narrow tolerances is very challenging in tape technology. One way to overcome the tribological problems at the head surface is to provide an ultra-thin protective coating on the head surface in order to reduce direct interactions of the head materials with the tape media components hence, protecting the head and its components against wear and corrosion. An ideal material for this application should be able to form a continuous (pinhole free), hard, dense, and inert thin overcoat.

Since an ideal coating should be able to protect the head throughout the life of the drive, it is expected to have a very low wear rate. This requires the coating material to be hard, but not brittle (tough), and to demonstrate excellent adhesion to its substrate. In order to protect the head elements from corrosion, the coating should also be

continuous and dense (with high atomic density) to act as a diffusion barrier against chemical (corrosive) species existing on the tape surface. Moreover, the coating material is required to be inert and chemically compatible with the tape environment (e.g. tape lubricant).

So far, many different types of wear resistant oxides [95, 99], nitrides [100], carbides [101], or diamond-like-carbons (DLC) [98, 101] deposited by different techniques have been applied to magnetic heads. However, because of their poor durability and/or unacceptable thicknesses, most of these coating materials and methods have not been successful in producing a commercially viable solution.

Tetrahedral amorphous carbon (ta-C), which is a type of DLC with a high fraction of C-C $sp^3$ bonds (up to ~80%) [43, 51], has shown promising tribo-mechanical properties such as high hardness (slightly less than that of diamond) [47], low roughness [52, 74], high inertness, and low mass diffusivity [55]. The outstanding and versatile chemical and physical properties of ta-C coatings have made them a potential material of choice for protecting magnetic heads in tape drives.

However, the serious drawback of ta-C coatings, like all other DLC films, is their poor adhesion to the AlTiC substrate of the head [98, 102], which may cause delamination of the coating off the substrate and hence, abrupt failure of the coating.

Various strategies have been used to enhance the adhesion and durability of carbon coatings to different types of substrates. Application of very high ion energy at the first stage of deposition was shown to improve the adhesion of the DLC coatings to the metallic substrates [112, 113]. This strategy which is referred to as "surface pre-treatment" was usually performed on metallic substrates by using very high ion energies of about 10 keV. This technique has also been used to improve the adhesion of the DLC film on the AlTiC substrate of the recording heads [102]. Ion energies of

1-2 keV were used for pre-treatment of whole surface of the head. However, this high energy can cause destruction or alteration of the magnetic behavior of the read-write elements to a depth of up to 10 nm which is considered as a magnetic dead layer and increases the effective magnetic spacing between the head and media [114]. In order to maximize the benefit of this method, proper optimizations in terms of ion energy and treatment time must be performed to develop a thin ta-C film with good tribo-mechanical properties while minimizing the side effects of the method on the magnetic performance of the head elements. In this surface treatment method, having a fundamental understanding about the chemical, physical and structural changes at the bombarded surface of the AlTiC ceramic is of great importance and can provide valuable information in order to optimize the surface treatment parameters for the real heads.

The main objective of this chapter is to investigate the effect of pre-treatment of the AlTiC substrate by $C^+$ ions with moderate energy (E = ~ 350 eV) on the structural and nano-tribological behaviors of the coated surface.

## 5.2   Experimental procedure

Surface treatment and protective film growth on the flat AlTiC samples (10 mm × 10 mm × 5 mm) was performed by FCVA deposition method. Before loading onto the substrate stage of the FCVA system, samples were ultrasonically cleaned with IPA and acetone respectively for 20 minutes and then dried by blowing pure nitrogen gas. To ensure a good adhesion between the protective coating and the substrate, the top surface of the substrate was cleaned by $Ar^+$ sputter etching with ion energy of 1 keV, and incident angle of 45° for 420 second in a working pressure of 100 mPa in the same chamber that FCVA treatment would be conducted.

In order to study the effect of bombardment of the sample surface by higher energetic $C^+$ ions on the structure and nano-tribological properties of the ta-C protective overcoats, two sets of samples were prepared. For the first set (sample A), 10 nm ta-C film was grown under a pulsed bias voltage of -80 V which resulted in an ion energy of 100 eV. A second set of samples (sample B) was synthesized in two steps: firstly, the surface of the substrate was bombarded with $C^+$ ions with higher energy of 350 eV (bias voltage of -330 V) for 25 seconds. This stage is referred to as "pre-treatment". In the second step, the bias voltage was reduced to -80V and the 10 nm overcoat was grown using an ion energy of 100 eV. A summary of the deposition stages is depicted in Table 5-1.

**Table 5-1** Deposition conditions of deposited ta-C films

|  | Pre-treatment | | Thin film deposition | |
|---|---|---|---|---|
|  | Ion energy (eV) | Time (s) | Ion energy (eV) | Time (s) |
| Sample A (Not pre-treated) | --- | --- | 100 | 275 |
| Sample B (Pre-treated) | 350 | 25 | 100 | 250 |

$C^+$ ion range and embedment depth were estimated by trajectory of ions in matter (TRIM) simulation [115]. Before setting the deposition parameters, the TRIM code [115] was used to simulate implantation distribution of the energetic $C^+$ into different phases ($Al_2O_3$ and TiC) of the substrate surface. In this simulation, ion flux is perpendicular to a surface of a semi-infinite medium of $Al_2O_3$ and TiC. The simulation was performed for two constant ion energies of 100 and 350 eV.

Atomic force microscopy (AFM) was used to study the topography of the surfaces. TEM and TOF-SIMS were used to study the structure of the ta-C film and its interface with the substrate. Chemical characterization of thin ta-C coatings were conducted by

means of X-ray photoelectron spectroscopy (XPS). High resolution XPS spectra (C$_{1s}$ peak) were obtained with energy steps of 0.1 eV. Each spectrum was obtained as an average of 13 scans.

Nano-tribological properties of treated flat AlTiC surfaces were examined using ball-on-flat wear test. After the wear test, the surface of the wear track was studied using Auger electron spectroscopy (AES) technique to check whether or not the surface is still covered with ta-C coating. AES depth profiling was performed on a point on the wear track and a reference point (not-worn area). Knowing the initial thickness of the ta-C film (on the reference point), by comparing the required time for etching the ta-C film to reach the substrate for both points, the thickness of the coating left on the wear track was measured. Detailed information about the experimental procedures has been presented in chapter 4.

## 5.3 Results and discussion

### 5.3.1 *Embedment of C$^+$ ions into the outermost surface of the AlTiC substrate*

Before depositing the 10 nm ta-C overcoat, the outermost surfaces of the substrates were bombarded by C$^+$ ions. The distribution of the C$^+$ ions with ion energies of 100 and 350 eV on the bare AlTiC as well as distribution of the Al and Ti atom were studied by TRIM simulation. The depth profiles of embedded and recoiled ions are shown in Figure 5-1.

The simulation results predict the formation of a mixed layer of a few nanometers (about 1-2 nm) thick inside the substrate surface. According to these results, the intensity of Al and Ti atoms within this layer is higher than that of the bulk material. The maximum penetration depth of ions into the Al$_2$O$_3$ and TiC phases of the AlTiC surface at two ion energies of 100 and 350 eV are summarized in Table 5-2.

**Table 5-2** Maximum penetration depth of ions into Al$_2$O$_3$ and TiC phases of the AlTiC surface at two ion energies of 100 and 350 eV obtained from the TRIM simulations.

| Ion energy | 100 eV | | 350 eV | |
|---|---|---|---|---|
| Phase | Al$_2$O$_3$ | TiC | Al$_2$O$_3$ | TiC |
| Subplantation depth (nm) | 0.9 | 1.1 | 1.4 | 2.2 |
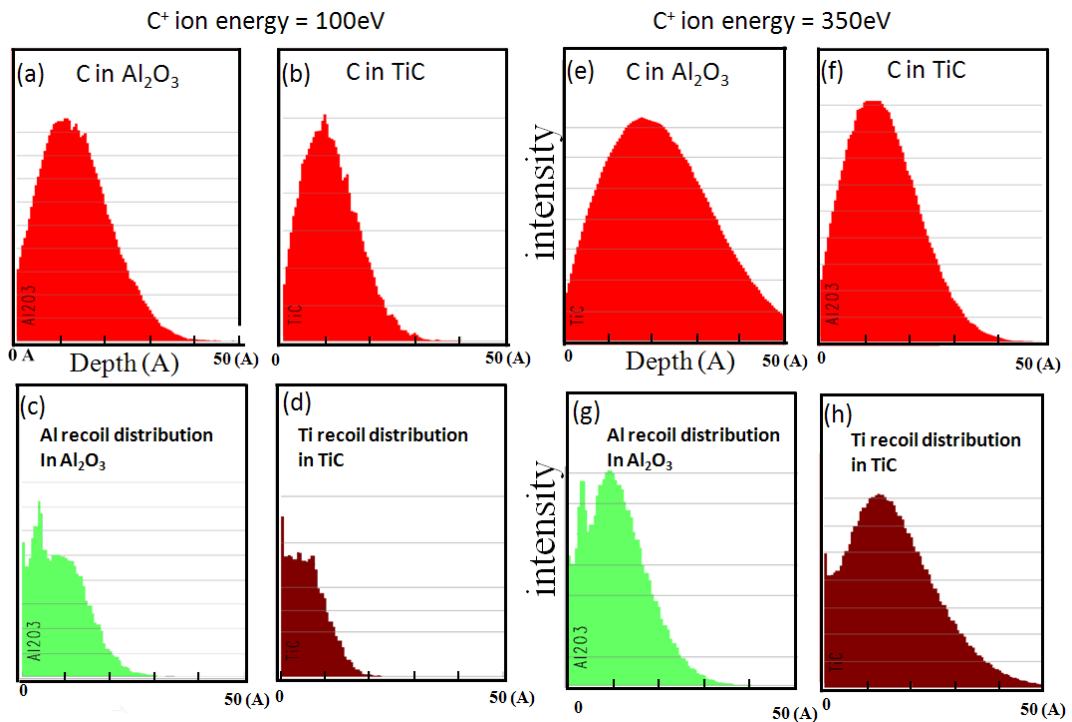


**Figure 5-1** Depth profiles of ions in substrate surface calculated by TRIM simulation program. Distribution of embedded carbon ion in (a) Al$_2$O$_3$ and (b) TiC phases and recoil distribution of (c) Al ions in Al$_2$O$_3$ and (d) Ti ions in TiC phases of AlTiC substrate when the surface is bombarded with C$^+$ ions of 350 eV

The data indicates that the larger penetration depth happens with higher ion energy (350 eV) and in the TiC phase of the surface. In addition, by using higher C$^+$ ion energy, ion embedment affects a deeper area inside the substrate and the mixed layer becomes broader.

TEM images and TOF-SIMS depth profiling measurements confirmed the formation of an atomic mixing layer at the interface of the ta-C film and the substrate. Cross-

section images of the samples observed by TEM are shown in Figure 5-2. The exact thickness of the ta-C films was measured as 9 nm for sample A and 10 nm for sample B (according to Table 5-1). The TEM results provided qualitative evidence of the formation of a dense thin mixing layer at the film interface of both samples. This layer is visible in dark color between the crystalline structure of substrate and the amorphous ta-C overcoat. The thicker mixed layer of sample B in Figure 5-2(b) is the effect of pre-treatment with higher ion energy and indicates the higher depth of penetration for C$^+$ ions into the substrate. The formation of this dense layer near the film and substrate boundary can be explained in terms of penetration of bombarding ions into the surface and entering the subsurface interstitial site [116], which increases the local atomic density.

In addition, because of the direct and recoil collision cascade of the ions at the boundary between the substrate and ta-C film, the surface of the substrate has become amorphized. The amount of amorphization is increasing by the energy of bombarding ions. Figure 5-3 shows the depth profile of C and Al extending from top surface of the ta-C film to the bulk AlTiC substrate. For impinging ions of 100 and 350 eV energy, the thicknesses of the mixed layer measured by SIMS depth profiling were 1.4 and 2.2 nm, respectively. As can be seen, the concentration of Al and Ti atoms at the interface of the film and the substrate is higher than that of the bulk substrate. This behavior is in agreement with the results of TRIM simulations and can be explained by the recoil implantation of the substrate material into the thin film due to collision between the high energetic C$^+$ ions and Ti/Al atoms.
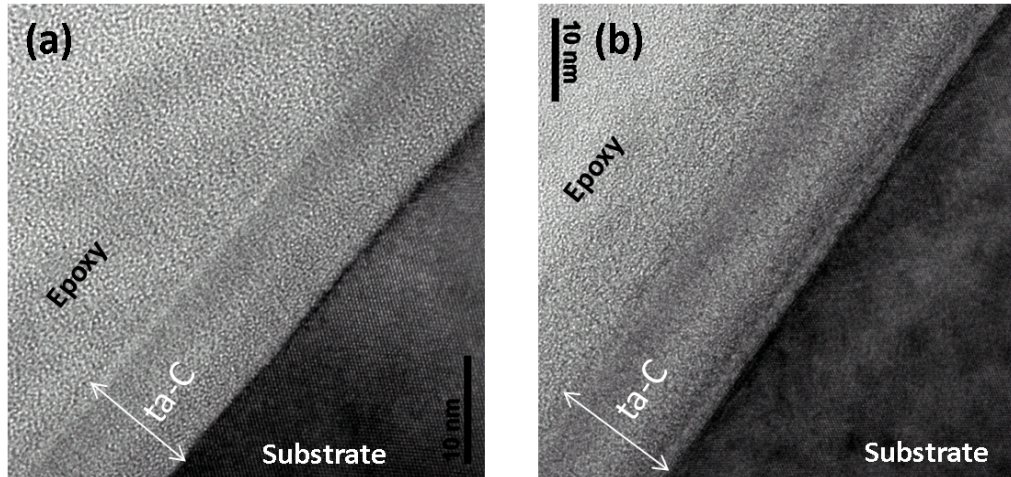
**Figure 5-2** Cross-section TEM image of ta-C coated substrate, (a) without pre-treatment, (b) with pre-treatment with ion energy of 350 eV and treatment time of 25 seconds.
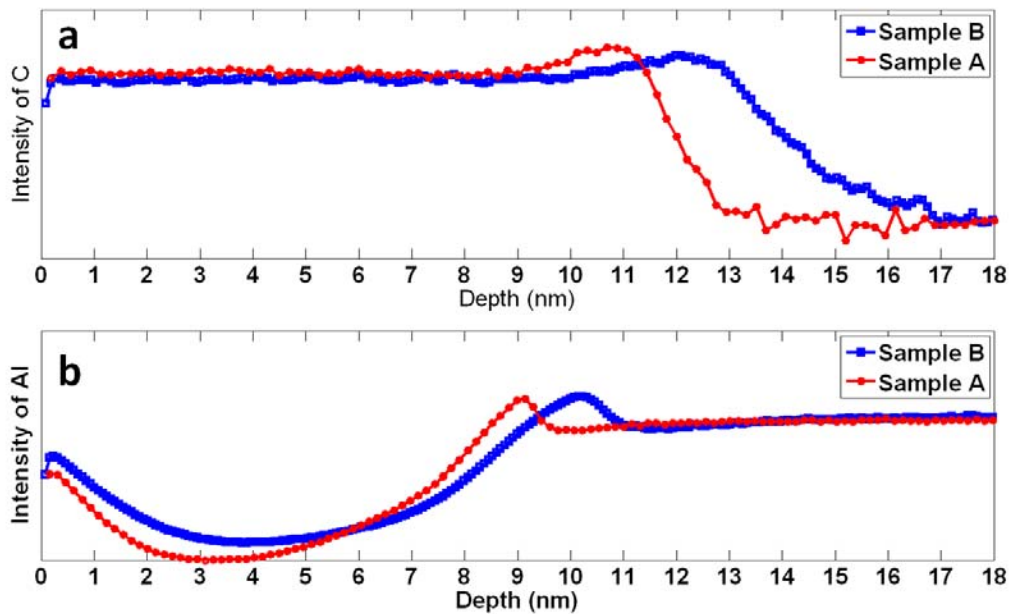


**Figure 5-3** Depth profile of (a) C and (b) Al extending from top surface of the ta-C film to the bulk AlTiC substrate for samples without and with pre-treatment.

In addition, bombardment of the surface with highly energetic species (ions or atoms) leads to implantation of the atoms into the top surface of the substrate, and alteration of the surface structure and crystallinity (amorphization) of the surface. This structural change together with the formation of a mixed layer at the ta-C film-substrate interface can greatly enhance the film adhesion and reduce stresses due to lattice mismatches.

Moreover, Figure 5-3 shows traces of existence of Al at the top surface of the film. This is because of the condensation of the sputtered species on the top surface of the film at the end of the FCVA deposition. These particles are generated due to the sputtering of the AlTiC surface by the energetic carbon ions, especially under deposition conditions of 350 eV ion energy.

### 5.3.2 Chemical state of the ta-C film

Most of the mechanical properties of the DLC films are directly related to amount of the sp$^3$ oriented C-C bonds in the structure of the film [46, 47]. The surface chemical composition of the ta-C films can be interpreted in terms of the XPS results. The high resolution XPS spectrum of the C$_{1s}$ peak of the films (sample A and B) is shown in Figure 5-4 and it can be used to determine the fraction of sp$^2$ and sp$^3$ bonding.
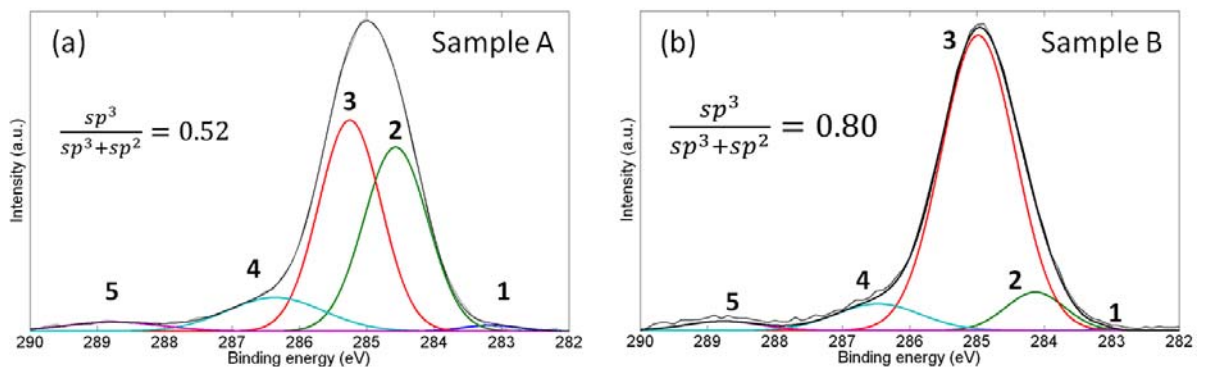


**Figure 5-4** C$_{1s}$ XPS spectra with Gaussian fits of ta-C films (a) without pre-treatment, and (b) with pre-treatment with 350 eV for 25 seconds

The C$_{1s}$ spectra of the samples were adjusted by subtracting the Shirley Background as reported in reference [117], and the adjusted spectra were subsequently deconvoluted with a set of Gaussian distribution. Each Gaussian curve is located at a certain binding energy which corresponds to one of the chemical states (C-C sp$^1$, C-C sp$^2$, C-C sp$^3$, C-O, and C=O) existing in the structure of the film [118, 119]. The atomic fraction of each component is determined by integrating the associated Gaussian curve. The

atomic percentage as well as the binding energy of each film constituent is presented in Table 5-3.

**Table 5-3** Binding energies (BE) of characteristic Gaussian profiles and corresponding atomic percentages in XPS spectra of ta-C films

| Constituents in ta-C film | | $C_{1s}(1)$ C-C $sp^1$ | $C_{1s}(2)$ C-C $sp^2$ | $C_{1s}(3)$ C-C $sp^3$ | $C_{1s}(4)$ C-O | $C_{1s}(5)$ O=C-O |
|---|---|---|---|---|---|---|
| **Sample A** | **BE (eV)** | 283.15 | 284.57 | 285.25 | 286.36 | 288.76 |
| | **at%** | 1.18 | 40 | 45.2 | 11.16 | 3.0 |
| **Sample B** | **BE (eV)** | 283.14 | 284.13 | 285.0 | 286.46 | 288.76 |
| | **at%** | 0.2 | 8.4 | 80.4 | 8.4 | 2.56 |

It can be seen from Table 5-3 that only 52% of the carbon constituents of ta-C film without pre-treatment (sample A) is pure $sp^3$ carbon and the remainder is pure $sp^2$ carbon or carbon containing surface contaminants. In contrast, sample B which is pretreated with 350 eV C⁺ for 25 seconds contained more than 80% $sp^3$ C-C bonds. In the microstructure of this film most of the $sp^2$ bonded C-C atoms in graphite like rings have been converted to tetrahedral diamond like C-C chains which are directly responsible for the enhanced mechanical properties of this film.

Subplantation (shallow implantation) of impinging ions [115] is an accepted concept to explain the growth mechanism of DLC films. It is proposed by Robertson [120] that subplantation can increase the density of the outermost layer of the substrate in a metastable manner. In addition, the hybridization of carbon atoms can be tuned with respect to the local density of the bombarded surface, and the C-C atomic bonding in the dense regions tends to change from $sp^2$ hybridization to $sp^3$. Therefore, in the conditions of ion bombardment existing during the growth of the films in our

experiments, more $sp^3$ bonds are generated in sample B (bombarded with higher energy) in which the atomic density is higher than that of sample A.

But this may not imply that increasing the pre-treatment ion energy always favors $sp^3$ content of the film. With an increase in the ion range and the ion energy above an optimum value, the penetration depth of ions into the surface increases. But only a small part of the ion energy is used for embedding into the surface, while the rest of the ion energy is dissipated as thermal energy (phonons) [121]. According to Robertson[106], this released thermal energy at the film-substrate area is able to cause relaxation of the excess density to zero, and a decrease in $sp^3$ portion [106].

### 5.3.3   Nano-tribological tests

Figure 5-5 shows the frictional behavior of the bare substrate as well as that for the ta-C films without and with pre-treatment with 350eV C⁺ ions for 25 seconds. The obvious difference in the friction coefficients of the bare and coated substrates demonstrates the effectiveness of the 10 nm ta-C film to attain very low friction and wear on the surface of the substrate.

The wear life of the samples without and with pre-treatment is shown in Figure 5-6. As can be seen, sample A (without pre-treatment) has failed (coefficient of friction has suddenly increased) only after about 1200 cycles rubbing against silicon nitride ball with a contact pressure of about 350 MPa. However, sample B (with pre-treatment) survived even after 10,000 cycles without failure (the tests was terminated due to long duration of the tests). It should be emphasized that the contact pressure in this experiment is about 3,000 times greater than that of the head-tape interface (0.1 MPa) in actual tape drives. And since the wear life increases by decreasing the contact

pressure, application of this method in order to provide a durable protective coating on the head surface may be feasible.
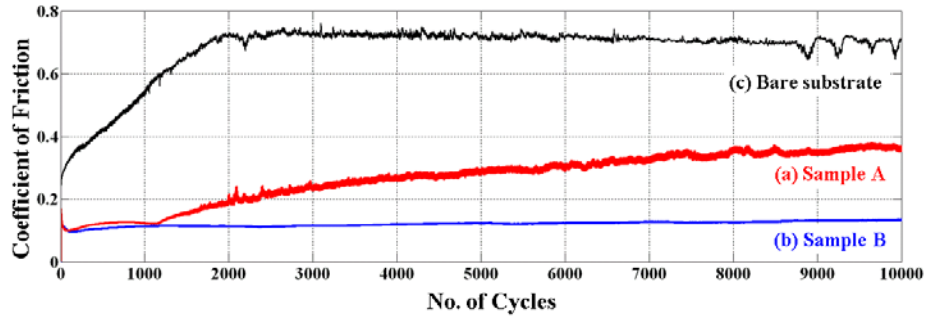


**Figure 5-5** Comparison of the friction coefficient of (a) ta-C coated AlTiC substrate without pre-treatment, (b) ta-C coated AlTiC substrate with pre-treatment, and (c) bare AlTiC substrate in ball on flat rotary wear test against silicon nitride ball
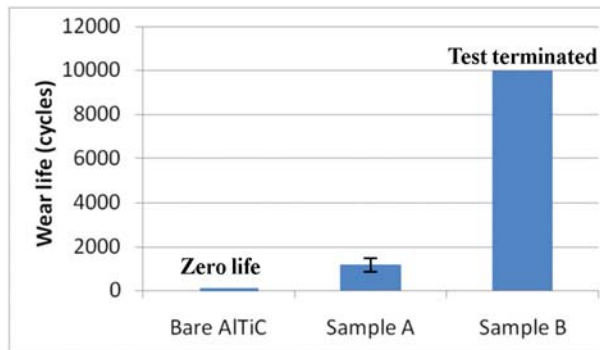


**Figure 5-6** Comparison between wear life of bare AlTiC and ta-C coated samples with and without pre-treatment
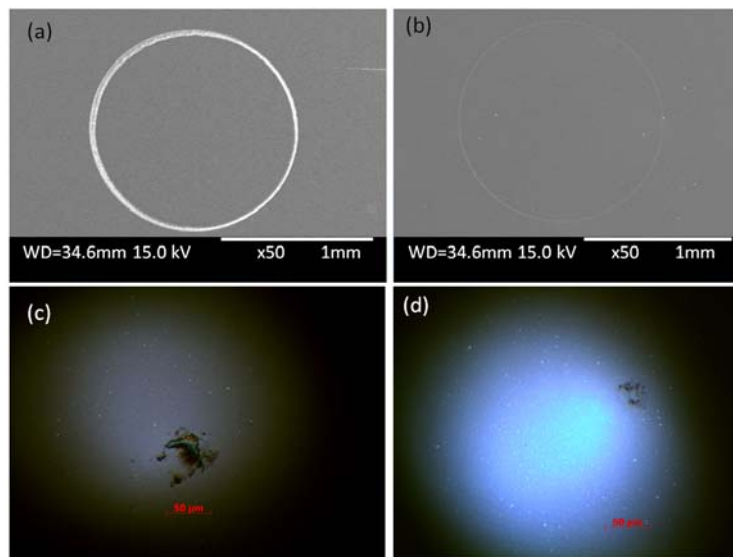


**Figure 5-7** SEM images of wear track formed on ta-C coated AlTiC substrate, (a) without pre-treatment and, (b) with pre-treatment with 350ev C⁺ ion energy for 25 seconds. Optical image of the silicon nitride ball counterpart (c) rubbed against ta-C coated surface without pre-treatment and (d) with pre-treatment

The micrographs of the wear tracks on the substrates and wear scars on the silicon nitride balls are presented in Figure 5-7. A wider wear track on the substrate (Figure 5-7(a)) and higher amount of tribo-film transferred to the ball surface of sample A (Figure 5-7(c)) (without pre-treatment) compared with a very narrow wear track (Figure 5-7(b)) and less transferred tribo-film of sample B (Figure 5-7(d)) indicate the effect of surface pre-treatment on the wear life of the protective film. The higher amount of transferred tribofilm on the counterface of sample A is evident of the poor adhesion of the film to the substrate and its lower sp$^3$ content, while sample B with about 80% sp$^3$ (diamond like) bonds and a thicker mixing layer at the film-substrate interface presents excellent adhesion to its substrate coupled with good wear resistance behavior.

In order to verify the existence of the ta-C film on the surface of the wear track of sample B after 10,000 cycles, the surface of the wear track was observed by SIMS surface imaging (Figure 5-8). In this figure, brighter regions in each window correspond to a higher concentration of a specific element or compound, while darker regions correspond to lower concentrations of the same element or compound. Figure 5-8 shows no evidence of Al, Ti, O, or TiC from the substrate on the surface of the wear track. In addition, the distribution of C on the whole surface is almost the same and is slightly higher at the wear track (appeared as a more shiny area in Figure 5-8(a)). All of these confirm that even after 10,000 cycles of dry sliding, the ta-C film is still intact on the surface and is able to protect the substrate. Moreover, this result indicates that the traces of Al and Ti that condensed on the top surface of the ta-C film as explained earlier have been wiped off the surface during the wear tests.

Field of view: 200.0x200.0 µm²
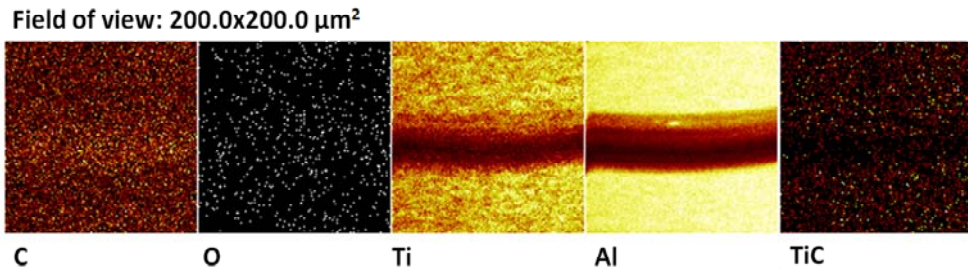


**Figure 5-8** (a) carbon, (b) oxygen, (c) titanium, (d) aluminum, and (e) TiC TOF-SIMS images of wear track formed on pre-treated ta-C coated AlTiC surface after 10,000 cycles.

In order to measure the thickness of the ta-C coating on the wear track after the wear test, AES depth profiling tests were conducted on the wear track and also on the not-worn region of the surface (Figure 5-9). In the depth profiling process the surface of sample B was etched until the substrate was reached (atomic concentration of C approached to zero). By knowing the initial thickness of the ta-C overcoat (~10 nm) and the elapsed etching time to remove the ta-C overcoat, the thickness of the ta-C overcoat after the wear test was estimated. The results revealed that the carbon coating on the wear track is still thick and the thickness is high enough (~ 5nm) to prevent the ball from coming into contact with the mixed layer or the substrate.
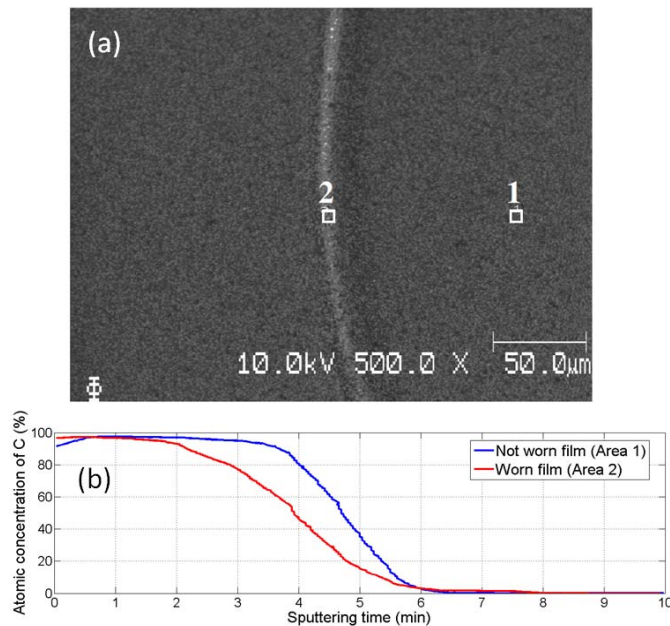


**Figure 5-9** AES depth profile of carbon on the worn and not worn regions of the sample B after the wear test

## 5.4   Conclusion

Simulation and experimental tests were conducted to study the surface pre-treatment of the AlTiC substrate prior to deposition of 10 nm ta-C film on the surface by FCVA treatment. The top surface of the AlTiC substrate was sputter-etched to remove the surface contaminations and oxide layers and was pre-treated by energetic C$^+$ ion bombardment under the condition of 350 eV for 25 seconds. Thin ta-C films with a thickness of 10 nm were deposited on the pre-treated and non-pre-treated surfaces using an ion energy of 100 eV.

The effects of FCVA pre-treatment conditions on the distribution of elements in the ta-C films and substrates, the formation of a mixing layer at the film-substrate interface, structure of the films, carbon atom hybridization, and nanotribological properties of the ta-C coated AlTiC substrate were studied by conducting TRIM simulations, TEM, TOF-SIMS, XPS, and ball on flat wear tests. Pre-treatment of the surface with a C$^+$ ion energy of 350 eV and a treatment time of 25 seconds caused the formation of a thicker mixing layer at the film-substrate interface, higher fraction of C-C sp$^3$ bonding, and an enhancement of the wear resistance of the surface.

The results revealed that FCVA pre-treatment of the surface with moderate ion energies (~350 eV) is an efficient method to enhance the adhesion of the ta-C film to the substrate and greatly improves the nano-tribological properties of AlTiC substrates when coated with ta-C.

These findings are promising and provide insights for further investigations of FCVA plasma treatment in order to produce coated magnetic tape recording heads that can solve the tribological problems at the head-tape interface in magnetic tape drives for ultra high-density magnetic recording. Moreover, this method can be potentially exploited in improving the surface properties of the ultrathin DLC coatings on the

surface of the magnetic disks and recording heads in the next generation of hard drives

with extremely high recording density.

# Chapter 6: Application of Si and Al-Si-C composite layer as interlayer to improve nano-tribological properties of ta-C overcoat

In the previous chapter (chapter 5), the effect of pre-treatment of the AlTiC surface with energetic $C^+$ ions on the tribological properties of the 10 nm ta-C films was studied. In this chapter, surface modification of the AlTiC by developing a mixed layer containing Si and C atoms is investigated as another method to improve the durability of the ta-C coating. A thin layer of silicon has been used to improve the adhesion between amorphous carbon coatings and different substrates. However, the mechanism responsible for this improved adhesion to ceramic substrates, especially the $Al_2O_3$-TiC (AlTiC) substrate of magnetic recording heads, has not been well studied. In this chapter, this mechanism is investigated by conducting simulations and experimental tests. The chemical state of the ta-C overcoats and interlayers as well as the nanotribological properties of the ta-C coated AlTiC substrate were studied by means of XPS analysis, nano-scratch and ball-on-flat tests. Prior to deposition of the ta-C overcoat, the surface of the Si interlayer was bombarded (pre-treated) by $C^+$ ions with an ion energy of 350 eV. The effect of this pre-treatment on the structure and tribological properties of the coated surfaces is also studied in this chapter.

## 6.1 Introduction

As mentioned in the earlier chapters, in order to improve the durability and adhesion of the DLC coatings to different substrates, various methods have been proposed including pre-treatment of the surface with highly energetic $C^+$ ions [112, 122, 123] or deposition of carbide-forming intermediate layers (such as a Si, Cr, or W adhesion

layer) before the deposition of the main carbon overcoat [124-126]. Among these different interlayer materials, silicon has shown good adhesion to the AlTiC substrate and an interlayer thinner than 2 nm has been working well for the hard disk drive heads [114, 127, 128].

The Si interlayer has a finite thickness which imposes an undesirable magnetic spacing, while on the other hand if the interlayer is too thin, it may not function properly as an adhesion layer. In order to derive the benefits of this method and apply it to tape drive heads, proper optimization in terms of ion energy, treatment time, and structure of the interlayer must be taken into account to minimize the side effects on the magnetic properties while increasing the durability of the coating.

In order to have good adhesion between the coating and the substrate, the interlayer should not only have strong bonding to the overcoat, but should also form very strong bonds with its underlying substrate. It is well known that deposition of carbon coatings on a Si interlayer or metallic films forms strong carbide bonds, which enhance the adhesion between the coating and the interlayer or the metallic substrate [129-132]. In addition, it is known that when deposited on a metallic surface, Si can react with the surface and produce a silicide [130]. The formation of such chemical bond is responsible for the strong adhesion between Si and metallic surfaces.

However, the mechanism responsible for adhesion between the Si interlayer and ceramic surfaces (e.g. the AlTiC substrate in hard disk drive heads) has not been fully understood. The knowledge of this mechanism would enable us to engineer the interface between the interlayer and the substrate in order to increase the adhesion strength between the overcoat, interlayer, and the substrate, which is beneficial for tape drive heads.

The main goal of this study is to understand the mechanism and influencing factors responsible for the adhesion of Si to the AlTiC ceramic substrates. In addition, the effect of bombarding the interlayer with energetic $Ar^+$ and $C^+$ ions prior to deposition of the ta-C overcoat on the chemical state of the interlayer is studied by means of *Stopping and Range of Ions in Matter* (SRIM) simulation and X-ray photo-electron spectroscopy (XPS) analysis. The overall tribo-mechanical behaviors of the coatings were investigated using nano-scratch and ball-on-flat tests.

## 6.2   Experimental Procedure

### 6.2.1   *Specimens and sample preparation*

Before deposition of Si interlayer, the samples (AlTiC flat samples) were ultrasonically cleaned by isopropanol (IPA) and acetone respectively for 20 minutes each, and then dried by blowing pure nitrogen gas.

To ensure good adhesion between the protective coating and the substrate, the surface of the substrate was cleaned by $Ar^+$ sputter etching. However, this process may affect the topography of the surface and increase the roughness. In order to minimize this effect while obtaining the benefit of $Ar^+$ plasma etching for cleaning the surface, the plasma parameters were optimized. To determine the optimum etching parameters, a number of samples were etched with various plasma parameters and the topography and quality of the adhesion of the Si on the etched surfaces were examined. From the findings (Figure 6-1), $Ar^+$ plasma with ion energy of 230 eV, beam current of 45 mA, incident angle of 45 degrees and etching time of 8 seconds showed the minimum topography change.
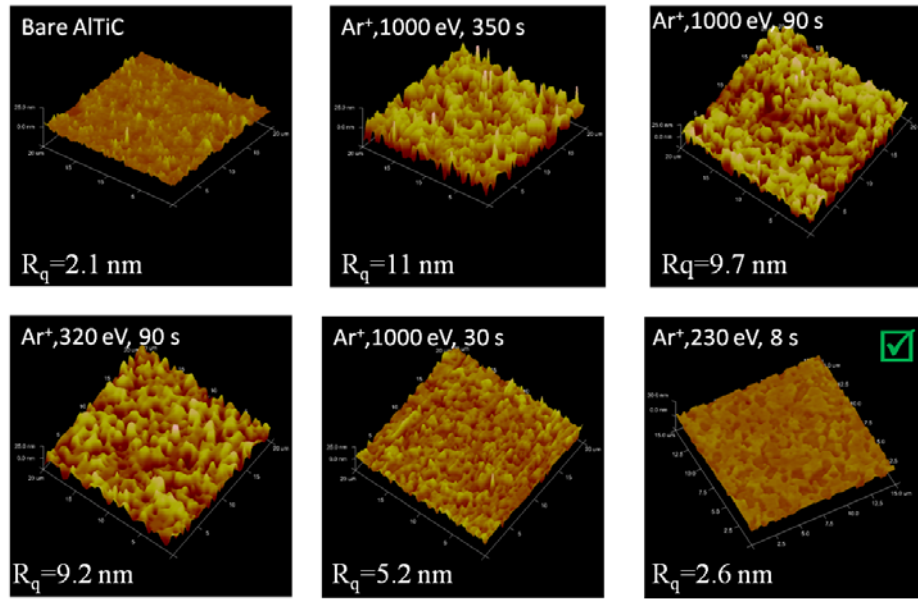
**Figure 6-1** Effect of $Ar^+$ plasma cleaning parameters (ion energy and etching time) on the topography of the AlTiC surface

After cleaning the surface, without breaking the vacuum of the deposition chamber, a 5 nm Si interlayer was deposited on the substrates using an RF-magnetron gun at an RF power of 150 W, with an Ar flow rate of 20 sccm and working pressure of 3 mTorr. Deposition of ta-C overcoats and bombardment of the surface with energetic $C^+$ or $Ar^+$ ions were carried out using a filtered cathodic vacuum arc (FCVA) deposition tool [133]. During the transportation of the samples from the Si deposition chamber to the FCVA chamber, the samples were exposed to ambient oxygen, which oxidized the outermost layer of the Si film. The thickness of the oxide on the sputtered Si film was estimated to be less than 2 nm [134]. In order to remove this oxide layer prior to bombardment of the pure Si interlayer with $C^+$ ions, the samples were again sputter-etched with $Ar^+$ plasma sputter etching with an ion energy of 1 keV and an incident angle of 45° for 20 seconds in a working pressure of 100 mPa in the same chamber that FCVA treatment would be conducted. The thickness of the remaining Si layer was approximately 2 nm.

In order to study the role of the thin Si interlayer and also the effect of pre-treatment of this interlayer with highly energetic $C^+$ ions on the interface structure and nano-tribological properties of the ta-C protective overcoats, three sets of samples (on flat AlTiC wafers) were prepared. For the first set (Sample A), a 5 nm overcoat was grown with an ion energy of 100 eV (substrate bias voltage of -80 V), without any pre-treatment and interlayer. For the second set (sample B), a 5 nm ta-C film was grown on the Si-coated substrates with ion energy of 100 eV. For the third set of samples (Sample C), the Si-coated AlTiC surfaces were pre-treated (as described in chapter 5) with $C^+$ ions with 350 eV energy (substrate bias voltage of -330 V) for 25 seconds followed by deposition of a 5 nm ta-C overcoat with ion energy of 100 eV.

**Table 6-1** Deposition conditions of ta-C films

| | Pre-treatment | | | Thin film deposition | | |
|---|---|---|---|---|---|---|
| | Underlayer | Ion energy (eV) | Time (s) | Ion energy (eV) | | Overcoat thickness (nm) |
| Sample A | --- | --- | --- | 100 | | 5 |
| Sample B | 2 nm Si | --- | --- | 100 | | 5 |
| Sample C | 2 nm Si | 350 | 25 | 100 | | 5 |

As mentioned in chapter 5, bombardment of the surface with ion energy of 350 eV for 25 seconds affects only the top region of the substrate up to a depth of 1-2 nm and also results in the best tribological properties of the coating. A summary of the deposition stages is depicted in Table 6-1. Further details of the deposition of the ta-C overcoats and surface pre-treatment have been extensively explained in chapters 4 and 5.

### 6.2.2 SRIM simulation

To have a better understanding of the prospective effect of bombarding the Si-coated surface with energetic $Ar^+$ ions (during the sputter etching of the oxide layer) and $C^+$ ions (during the pre-treatment and deposition), the SRIM code was used to simulate implantation (direct and recoil) distribution of the existing species (Si, O, Al, and C) in the interface of the Si interlayer and the $Al_2O_3$ phase of the AlTiC substrate. In this simulation, ion flux of $Ar^+$ or $C^+$ was perpendicular to the surface of a semi-infinite medium of $Al_2O_3$, which was coated with 2 nm Si layer. The simulation was performed for ion energies of 500 eV for $Ar^+$, and 100 eV and 350 eV for $C^+$.

### 6.2.3 Characterization procedure

Surface chemical analysis of the treated surfaces was carried out by an XPS system. An Al-$K_\alpha$ X-ray source with a spot size of 400 μm and pass energy of 40 eV was used for this measurement. Chemical composition analysis of the ta-C films and depth profiles of the existing elements in the coating, interlayer and substrate were performed by XPS depth profiling technique. In depth profiling, the surface of the samples was sputter-etched by $Ar^+$ ions of 500 eV. In order to obtain enough information about the chemical state of the AlTiC/Si/ta-C interface, a depth profile with high spatial resolution in depth was required. To achieve this goal, the surface was etched in very small depth steps from the overcoat surface down to the substrate with an etching time of 10 seconds. The chemical state of each level was precisely measured by acquiring a high resolution XPS spectrum ($Si_{2p}$ and $C_{1s}$) with energy step of 0.1 eV. Each spectrum was obtained as an average of 10 scans.

The effect of the aforementioned methods on the general tribological behaviour of the ta-C coatings on flat AlTiC surface was investigated using fundamental tribological tests such as ball-on-flat and scratch tests (for details refer to sections 4.5 and 5.2).

Scratch test was conducted using an AFM probe with a sharp natural diamond tip with a tip radius of 40 nm mounted on a stainless steel cantilever, with a spring constant of 277 N/m and contact sensitivity of 189 nm/V working in contact mode. To measure the scratch resistance (critical load) of the coated surfaces, a 4 μm × 4 μm area was scratched (scanned) with an ascending normal load ($F_{N, wear}$). Each one-fifth of this area (i.e. an area of $0.8 \times 4$ μm$^2$) is scanned with a constant normal load (i.e. 115, 125, 136 μN, etc.) after scratching an area of 0.8 μm × 4 μm, the normal load was increased. Therefore, the scanned area was scratched with five different normal loads as depicted in Figure 6-2. Finally, a clear image of the scratched region (4 μm × 4 μm) was acquired by scanning a larger area of the sample (8 μm × 8 μm) which includes the scratch region, using the same tip, in contact mode but with a much smaller normal load ($F_{N,scan}$= ~15 μN).
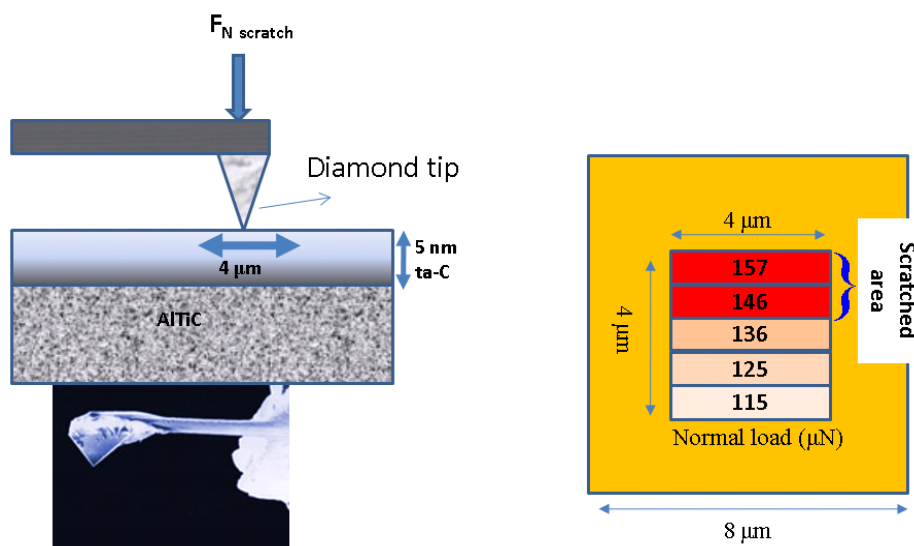


**Figure 6-2** Mechanism of the SPM based scratch test

In this test, since a sharp single asperity was in contact with the surface, conducting the test for a big scan size would lead to wear of the diamond probe tip. In addition, because of the high resolution of the AFM, this scanning range provides enough information about the depth and topography of the scratched region.

## 6.3   Results

### *6.3.1   Bombardment of the Si/AlTiC interface by energetic Ar$^+$ and C$^+$ ions*

Before depositing the ta-C overcoat, the outermost surfaces of the samples B and C were sputter-etched by Ar$^+$ ions of 500 eV (to sputter-etch the 3 nm excess SiO$_x$/Si layer) followed by C$^+$ bombardment with energies of either 100 eV (for sample A) or 350 eV (for sample B). The effects of these two processes on the distribution of the embedded C$^+$ ions, as well as on the recoiled distribution of the Si, Al and O atoms at the interface of the Si and Al$_2$O$_3$ phase of the AlTiC substrate were predicted by SRIM simulation. The distributions of the direct or recoil implanted ions/atoms in a region with a depth of 40 angstroms (including the Si/Al$_2$O$_3$ interface) are shown in Figure 6-3.
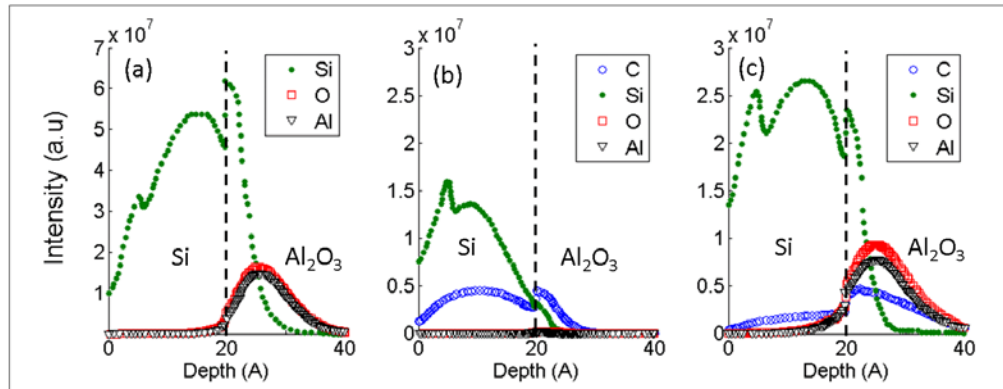


**Figure 6-3** Distribution of the implanted and recoiled ions/atoms at the Si/Al$_2$O$_3$ interface due to bombardment of the surface with (a) Ar$^+$ ions with energy of 500 eV, (b) C$^+$ ions with energy of 100 eV, and (c) C$^+$ ions with energy of 350 eV

As can be seen in Figure 6-3(a) and Figure 6-3(c), bombarding the surface with highly energetic Ar$^+$ and C$^+$ ions can lead to embedment of Si atoms from the interlayer into the Al$_2$O$_3$ phase of AlTiC substrate due to knock-on events [135]. At the same time, this bombardment created recoil cascades, which gave the substrate atoms near the interface enough energy to be driven away from the Al$_2$O$_3$ surface into the Si region. This atomic transport phenomenon gives rise to an interface mixing, which can be a

desirable effect when modification of the interface between the two layers is required. While $Ar^+$ ions are less likely to react with the species in this mixed layer, implanted $C^+$ ions can potentially react with the radicals and broken bonds available in the mixed interface and form new chemical bonds between the substrate, interlayer and overcoat elements. A comparison between Figure 6-3(b) and Figure 6-3(c) shows the effect of $C^+$ ion energy on the transport of species at the $Si/Al_2O_3$ interface. Most of the more highly energetic $C^+$ ions could pass through the Si layer and were stopped inside the $Al_2O_3$ region, which was already implanted by Si atoms due to the knock-on effects as explained above. However, the collision cascades due to bombardment of the surface with $C^+$ ions of lower energy were not strong enough to lead to considerable direct and recoil implantation of species. These $C^+$ ions with lower energy (100 eV) were mostly trapped in the Si interlayer and were not very effective in developing a mixed interface.

### 6.3.2   Chemical Characterization of the Overcoat and the AlTiC/Si/ta-C Interface

The possibility of the formation of an intermixing layer at the AlTiC/Si/ta-C interface due to bombardment by energetic ions was further examined by XPS depth profiling (Figure. 6-4).
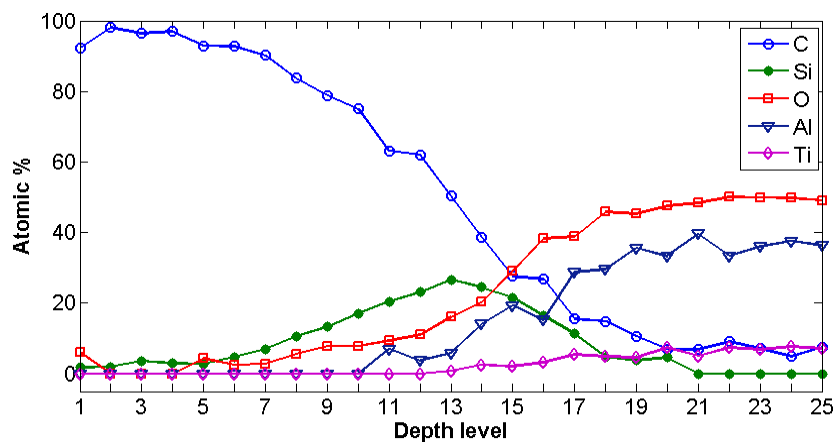


**Figure 6-4** Depth profile of the sample with 5 nm ta-C overcoat and 2 nm Si interlayer, pretreated with $C^+$ ions of 350 eV. The Si interlayer is considered as the point at which Si has the maximum concentration

In the XPS depth profile, the interlayer can be determined as a region with a higher atomic concentration of Si. As can be seen in Figure 6-4, there were no well-defined ta-C/Si or Si/AlTiC margins. In addition to Si, the interlayer region showed the presence of considerable amounts of C, Al, and O atoms. This result indicates the embedment of $C^+$ ions into the interface and confirms the formation of an atomic mixing layer at the AlTiC/Si/ta-C interface predicted by SRIM simulation. It also supported the idea of displacement of the Si atoms into the substrate as well as the diffusion of the substrate elements into the Si interlayer as a result of collision cascades.

Most of the mechanical properties of the DLC films are directly associated with the amount of $sp^3$ oriented C–C bonds in the structure of the ta-C overcoat [46, 47] and the nature of bonding between the overcoat and its underlying surface. In order to study the effect of pre-treatment of the AlTiC/Si interface by energetic $C^+$ ions on the chemical state of the ta-C overcoat and the AlTiC/Si/ta-C interface, the high resolution $C_{1s}$ and $Si_{2p}$ core level spectra of the overcoat and the interlayer were carefully investigated.

The high resolution $C_{1s}$ XPS peaks of the films deposited on the Si interlayer with and without pre-treatment (samples B and C) are shown in Figure 6-5. These spectra were adjusted by subtracting the Shirley Background as reported in reference [117], and subsequently deconvoluted with a set of Gaussian distributions. Each Gaussian curve was located at a certain binding energy which corresponded to one of the chemical states (C–C $sp^1$, C–C $sp^2$, C–C $sp^3$, C–O and C=O) existing in the structure of the film [118, 119]. The atomic fraction of each component was determined by integrating the associated Gaussian curve. The atomic percentage as well as the binding energy of each film constituent is presented in Table 6-2.

**Table 6-2** Binding energies (BE) of characteristic Gaussian profiles and corresponding atomic percentages in XPS $C_{1s}$ spectra of ta-C films with Si interlayer

| Constituents in ta-C film | | C–C sp[1] | C–C sp[2] | C–C sp[3] | C–O | C=O |
|---|---|---|---|---|---|---|
| Pre-treated with | BE (eV) | 282.80 | 284.36 | 285.05 | 286.90 | 288.76 |
| energetic C[+] | at% | 1.28 | 18.39 | 70.25 | 7.59 | 2.49 |
| Not pre-treated | BE (eV) | 282.9 | 284.48 | 285.16 | 286.85 | 288.52 |
| with energetic C[+] | at% | 0.88 | 24.60 | 60.85 | 9.17 | 4.49 |

According to the obtained results, pre-treatment of the Si-coated AlTiC surfaces with energetic carbon ions has increased the $sp^3$ content of the ta-C films. This behavior can be attributed to the fact that density of the outermost layer increases to a metastable state [120] due to subplantation [115, 136] of C[+] ions in the pre-treated surface. According to previous reports [106, 120], C–C bonding tends to form more $sp^3$ hybridization rather than $sp^2$ hybridization in the denser regions.
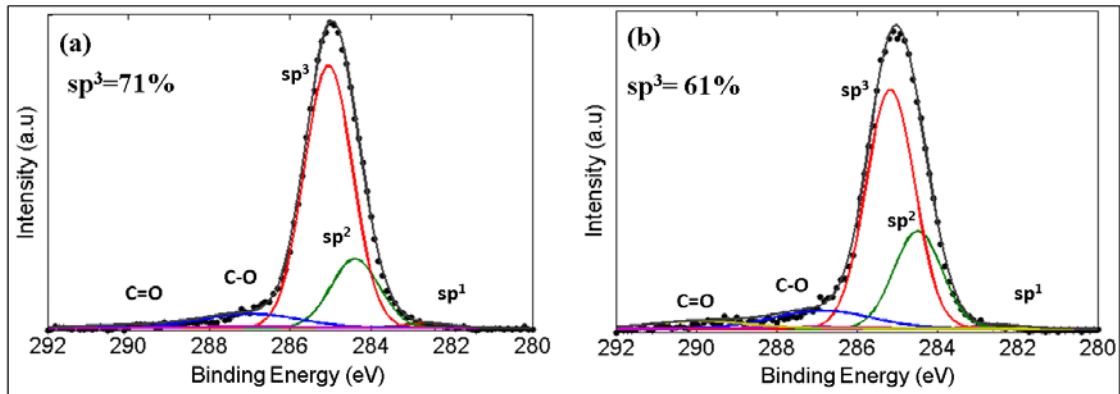


**Figure 6-5** $C_{1s}$ XPS spectra with Gaussian fits of ta-C films with Si interlayer (a) with pretreatment (sample C), and (b) without pretreatment with energetic C ions (sample B)

To acquire information about the chemical structure of the AlTiC/Si/ta-C interface bombarded by energetic C[+] ions, the depth profile of sample C was further studied. The $C_{1s}$ spectrum at each depth level of the coating is depicted in Figure 6-6.
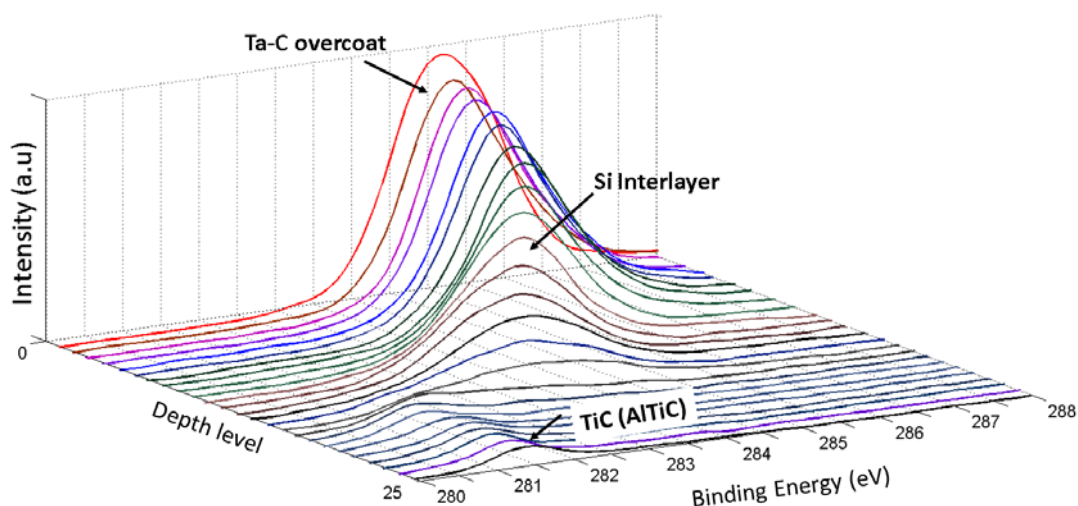
**Figure 6-6** XPS $C_{1s}$ spectrum of 5 nm ta-C coating with 2 nm Si interlayer pretreated with energetic C ions (sample C) as function of etch level

As can be seen from Figure 6-6, from the top surface to the bulk substrate, the intensity of the $C_{1s}$ peaks gradually decreased and its position steadily shifted from about 285 eV corresponding to the ta-C overcoat to about 283 eV near the ta-C/Si interface, which could be attributed to the formation of $sp^1$ carbide bonds [137-139]. Finally, peaks maxima position approached a constant binding energy of ~281.5 eV associated with existing TiC in the substrate [109]. A similar behavior was also observed in sample B with Si interlayer but without pre-treatment with energetic $C^+$ ions (the results are not shown). This finding is in agreement with other studies which reported the formation of Si–C bonds at the Si/carbon coating interface [114, 132, 140]. This phenomenon might be able to promote the formation of $sp^3$ bonding [106, 141]. In addition, the formation of Si–C networks at the Si/ta-C interface is able to bond the ta-C overcoat covalently to its underlying Si layer.

To examine the chemical state of the Si intermediate layer, the XPS high resolution scans of the $Si_{2p}$ spectra for the samples with and without pre-treatment were also studied in detail (Figure 6-7). The $Si_{2p}$ spectrum of each sample was deconvoluted with five Gaussian distributions corresponding to the potentially available bonds

existing in the interlayer region, i.e. Si–Si, Si–C, Si–O–C, Al–O–Si and $SiO_x$. The estimated atomic percentage as well as the binding energy position of each constituent is listed in Table 6-3.

**Table 6-3.** Binding energies (BE) of characteristic Gaussian profiles and corresponding atomic percentages in XPS $Si_{2p}$ spectra of the interlayer.

| Constituents in interlayer | | Si–Si | Si–C | Si–O–C | Al–O–Si | $SiO_x$ |
|---|---|---|---|---|---|---|
| Sample B | BE (eV) | 99.6 | 100.5 | 101.5 | 102.3 | 103.2 |
| (Not pretreated) | at% | 41.8 | 48.2 | 4.9 | 4.0 | 1.1 |
| Sample C | BE (eV) | 99.6 | 100.6 | 101.6 | 102.4 | 103.3 |
| (Pretreated) | at% | 14.6 | 58.2 | 13.1 | 12.1 | 2.0 |
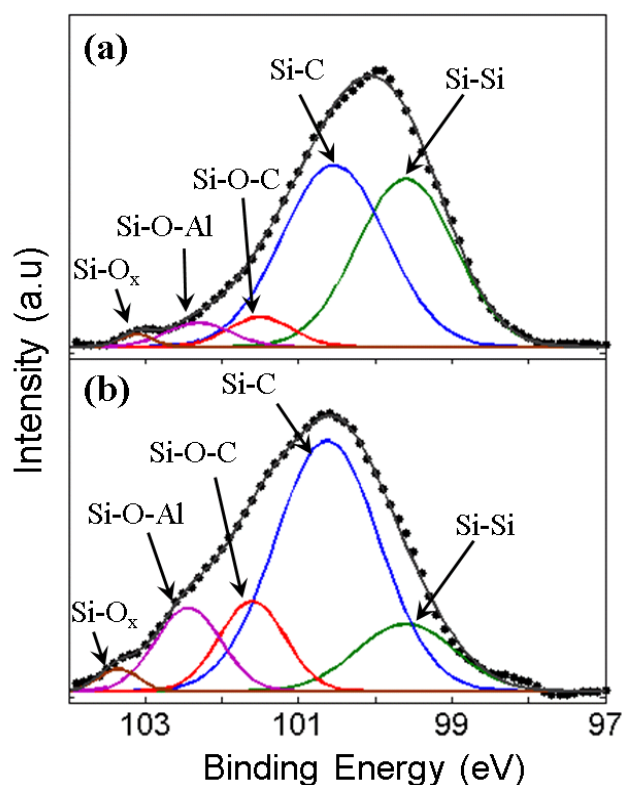


**Figure 6-7** High resolution $Si_{2p}$ XPS spectra with Gaussian fits of Si interlayer (a) without pretreatment (sample B), and (b) with pretreatment with highly energetic C ions (C)

According to Figure 6-7(a), the $Si_{2p}$ core level spectrum of sample B (without pre-treatment with energetic $C^+$ ions) consisted of two dominant peaks at 99.6 eV and

100.5 eV, which are attributed to Si–Si [139, 140] and Si–C bonds [137, 142-144]. It can be inferred that about half of the Si atoms in the interlayer film have reacted with the $C^+$ ions to form expected Si–C bonds. The $Si_{2p}$ spectrum of sample B also comprised three minor peaks at higher binding energies of about 101.5 eV, 102.3 eV, and 103.2 eV assigned to silicon-oxycarbide (Si–O–C) [137, 144-146], aluminum silicate (Al–O–Si) [147, 148], and Si–O bonds [109, 137, 142, 144], respectively.

The $Si_{2p}$ peak of the pre-treated sample (sample C), as shown in Fig. 6-7(b), was slightly broader and shifted about 0.5 eV to a higher binding energy, indicating higher Si–C and oxygen content within the probed region [143, 146]. Deconvolution of this spectrum led to a dominant Si–C peak and a weaker Si–Si peak, indicating that the interlayer of sample C consisted primarily of Si–C bonds. This result also showed stronger Si–O–C and Al–O–Si peaks in comparison with sample B (without pre-treatment), indicating a higher relative percentage of silicate and silicon oxycarbide bonds.

According to the SRIM simulation results, most of the $C^+$ ions with ion energy of 100 eV were not able to embed themselves in the Si interlayer beyond a depth of about 1 nm, and only a small portion of them were able to go deeper and/or pass through the interlayer to be implanted into the AlTiC substrate. Therefore, the top layer of the Si interlayer (about 1 nm) was expected to consist mostly of Si–C bonds while the rest of the Si atoms (about 40%) remained intact. In contrast, in sample C, the Si interlayer was bombarded with more highly energetic ions that had enough energy to penetrate deeper and pass through the interlayer to be implanted into the AlTiC substrate. In addition, because of their higher energy, these ions were more effective in knocking the Si atoms into the AlTiC substrate. Consequently, these $C^+$ ions were likely to react not only with the Si atoms in the deeper levels of the interlayer, but also with the

implanted Si atoms within the Si/AlTiC intermixing region. Furthermore, the deposition of a ta-C overcoat with ion energy of 100 eV on this pre-treated surface caused further embedment of $C^+$ ions and formation of Si–C bonds in the outermost part of the interlayer. This may explain the higher concentration of Si–C bonds in the interlayer of sample C (pre-treated with energetic $C^+$ ions) in comparison with sample B (without pre-treatment).

The formation of Al–O–Si (silicate) bonding units can be explained by the reaction at the interface between $Al_2O_3$ and the Si interlayer. The presence of $SiO_x$ bonds can be attributed to silicon oxide residuals remaining in the structure of the interlayer after sputter-etching the thicker interlayer and before deposition of the ta-C film. It can be speculated that $C^+$ radicals may react with these residuals and form Si–O–C bonds. It is also probable that the $SiO_x$ and Si–O–C bonds were formed due to the reaction between the implanted $C^+$ ions, Si interlayer, and the substrate.

A comparison between the narrow $Si_{2p}$ spectra of samples B and C (pre-treated with energetic $C^+$ ions) provides evidences which favor the latter hypothesis, i.e. a chemical reaction between Si and C with the O and Al containing species of the substrate. The process of deposition of the Si interlayer using magnetron sputtering as well as the sputter etching process of the oxide layer of the Si films within the FCVA chamber were exactly the same for both samples. Hence, the interlayers were expected to have almost the same content of residual silicon oxide in their structures before being treated by $C^+$ ions. The XPS data of the samples indicated a higher concentration of Si–O–C bonds in sample C. Provided that the formation of silicon oxycarbide bonds due to the reaction between these oxide residuals and $C^+$ ions is a correct assumption, sample B should contain much higher fraction of $SiO_x$ bonds in its structure. However, from Table 6-3, it can be seen that after deposition of ta-C overcoats, both samples had

almost the same amount of $SiO_x$ which is negligible in comparison to the content of the other bonds existing in the AlTiC/Si/ta-C interface. Therefore, the oxygen in the Si–O–C bond should be supplied by another source other than the silicon oxide residuals, which could only be the $Al_2O_3$ from the substrate.

It would be very likely that the sputter-etching of the substrate surface before deposition of Si as well as $C^+$ ions implanted into the substrate were able to destroy a number of Al–O bonds near the interface and form radicals containing O and Al. In addition, bombardment of the surface with these ions can lead to recoil implantation of Al and O atoms (radicals) into the Si interlayer. These resultant radicals are able to react with either existing C and/or Si atoms in the interlayer or with implanted C and/or Si ions within the $Al_2O_3$ substrate, and form Si–O, Si–O–C, and Al–O–Si bonds. The formation of Al–O–Si bonds between $Al_2O_3$ and silicon-containing films or surfaces such as SiC or Si have been reported elsewhere[147, 148]. In most of these cases, the films were either grown by means of chemical vapor deposition at relatively high temperatures or annealed at high temperatures after deposition. The mechanism governing the formation of Al–O–Si bonds in such cases was mostly thermal diffusion, rather than atomic intermixing due to ion implantation and its consequent collision cascades.

The existence of stronger Si–O–C and Al–O–Si components (peaks) within the $Si_{2p}$ peak of sample C shows the effective role of pre-treatment of the interlayer by energetic carbon ions in the formation of strong (covalent) bonds between the substrate, interlayer, and overcoat. As mentioned before, most of the $C^+$ ions with higher energy were implanted into the interlayer and substrate, and caused stronger collision cascades. This phenomenon enhances the development of a mixed layer between the interlayer and the substrate due to more effective direct and recoil

implantation of the species, and promotes formation of chemical bonds between the existing radicals at the intermixing layer. These chemical bonds strongly attach the interlayer to the substrate.

### 6.3.3 Tribological tests

#### 6.3.3.1 Nano-scratch

$sp^3$ content is one of the important factors which control the mechanical properties of the ta-C thin films. In addition to the $sp^3$ content, another important factor which determines the durability and wear resistance of these coatings is the adhesion strength of the films to their substrates.
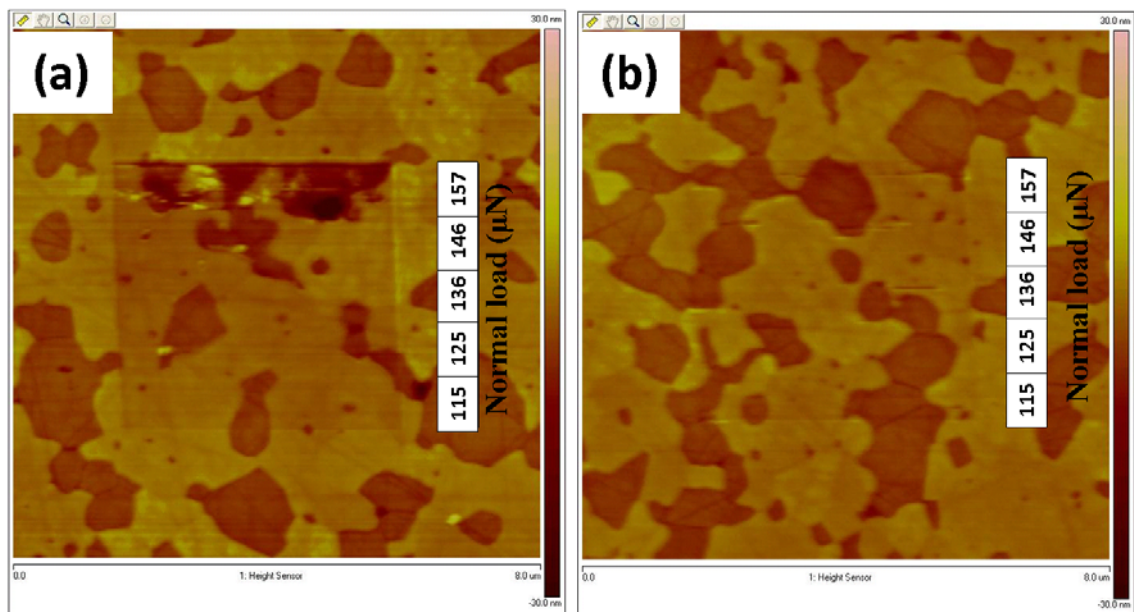


**Figure 6-8** Scratch profiles of the ta-C coated substrates with Si interlayer (a) without pretreatment (sample B), and (b) with pretreatment using highly energetic C ions (sample C)

Figure 6-8 shows the effect of pre-treatment of the Si interlayer with energetic $C^+$ ions on the scratch resistance and adhesion of the ta-C films to the substrate. In this experiment, the surfaces of the samples were scratched with a sharp diamond tip. The normal load was incrementally increased from 115 µN to 157 µN. As can be seen in Figure 6-8(a), the surface of sample B (without pre-treatment) was damaged (scratches

deeper than the thickness of the coating appeared on the surface) at a critical normal load of about 157 µN. In contrast, the surface of sample C (Figure 6-8(b)) did not show any significant scratch or wear scar under this normal load. By increasing the applied force, the scratch resistance of sample C was measured as 209 µN (the result is not shown), which was about 30% higher than that of sample B. This result clearly affirmed the role of pre-treatment on the improvement of the adhesion of the ta-C film to the substrate.

As explained in the previous section, the formation of Si–C bonds between the ta-C overcoat and Si interlayer together with the formation of Si–O–C and Al–O–Si bonds between the Si interlayer and the substrate strongly bond the ta-C overcoat to the AlTiC substrate. This phenomenon can account for the mechanism by which a thin Si interlayer improves the adhesion of carbon coatings to their ceramic substrates. According to the XPS results, bombardment of the Si interlayer caused the formation of a larger amount of chemical bonds between the ta-C film and the interlayer and also between the interlayer and the substrate in sample C. Formation of such strong covalent bonds can directly enhance the adhesion of the ta-C to the AlTiC substrate and increase its scratch resistance.

### 6.3.3.2   *Ball on flat wear tests*

Tetrahedral amorphous carbon overcoats are able to maintain a very low coefficient of friction between the substrate surface and the counterface. As long as the coating is still on the surface, friction remains low. The failure mechanism of the DLC-coated AlTiC substrates was reported as delamination due to the lack of adhesion to the substrate [98]. At the onset of failure of the coating, the friction suddenly increases to higher values and then keeps increasing with considerable fluctuations to a stable higher value. This behaviour can be used as a scale to compare the wear lives of the

tested samples. Figure 6-9 shows the frictional (ball-on-flat wear test) behavior of the AlTiC substrate coated with a 5 nm ta-C overcoat without the Si interlayer as well as that for the ta-C films with the Si interlayer, with and without pre-treatment with $C^+$ ions. The wear lives of the samples with and without pretreatment are shown in Figure 6-10.
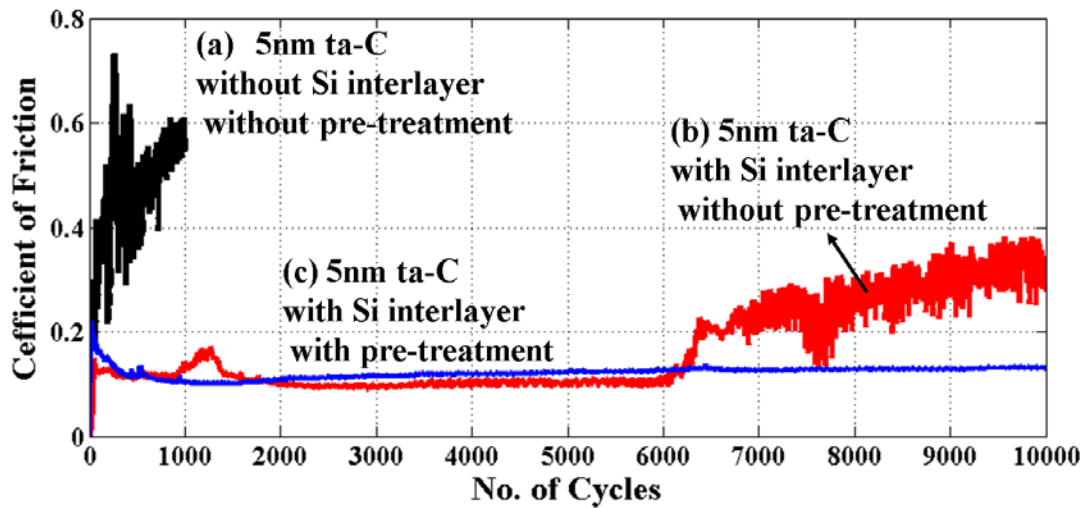


**Figure 6-9** Comparison of the friction coefficient of (a) ta-C coated AlTiC substrate without Si interlayer (sample A), (b) ta-C coated AlTiC substrate with Si interlayer and without pretreatment (sample B), and (c) ta-C coated AlTiC substrate with Si interlayer
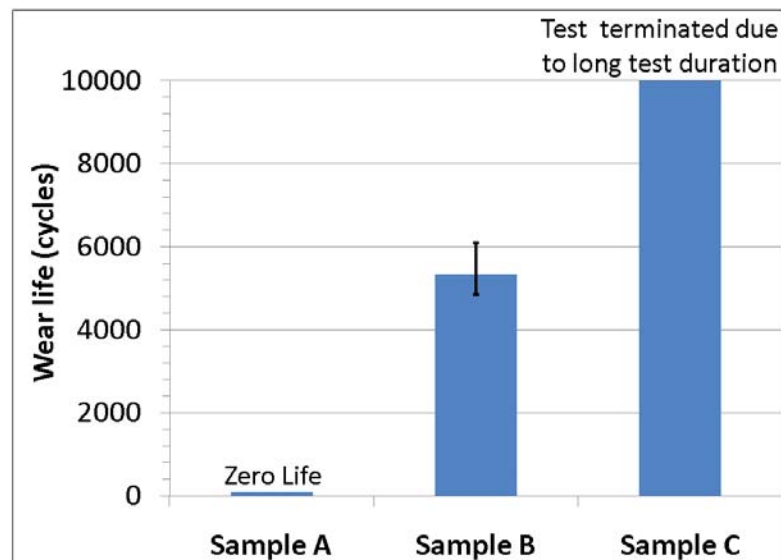


**Figure 6-10** Comparison between wear lives of AlTiC surfaces coated with 5 nm ta-C overcoats: sample A without Si interlayer, sample B with Si interlayer but without pretreatment, and sample C with pretreated Si interlayer. (Note that in the case of sample C, the test was terminated at 10,000 cycles due to its long duration.

As can be seen in Figure 6-10, sample A (without silicon interlayer) failed immediately (coefficient of friction suddenly increased and remained high) after rubbing against the sapphire ball with a contact pressure of about 350 MPa. Sample B (with no pre-treated Si interlayer) survived for a longer time while maintaining a low and constant friction. This sample eventually failed (coefficient of friction suddenly increased to 0.2) after approximately 6,000 cycles. In contrast, sample C (with pre-treated Si interlayer) survived up to 10,000 cycles (the test was terminated due to the long duration of the test) without failure. The obvious difference in the wear lives of the samples with and without the Si interlayer underlined the role of the Si adhesion layer between the ta-C film and AlTiC substrate in attaining higher durability and wear resistance. In addition, the difference between the wear lives of samples B and C demonstrated the effectiveness of pre-treatment of the interlayer with energetic $C^+$ ions in improving the durability (more than 60%) of the ta-C coating.

In order to verify the removal or existence of the ta-C film on the wear tracks of the samples (B and C) after 10,000 cycles, surface of the wear tracks and the not-worn film in their vicinity were observed by SIMS surface imaging (Figure 6-11). The brighter region in each window corresponds to a higher concentration of a specific element or compound, while the darker region corresponds to a lower concentration of that element or compound.

As can be seen in Figure 6-11(a), the Al and Ti windows showed shinier wear tracks compared to their unworn neighborhood. This result confirms the exposure of the Al- and Ti-containing substrate due to the removal of the ta-C overcoat. The wear track of sample C (with pre-treated Si interlayer) is depicted in Figure 6-11(b). As shown in the Al window of Figure 6-11(b), the intensity of the Al signal on the wear track is much lesser (the wear track appears darker) than that of the intact region at its vicinity which

has a uniform ta-C overcoat. This result implies that the wear track is still covered with carbon which does not let the Al from the substrate be exposed. Ti image of sample C also shows no evidence of the existence of Ti on the wear track, indicating that the AlTiC surface is still covered with a continuous ta-C overcoat. According to the depth profile of sample C as shown in Figure 6-4, small traces of Si exist within the bulk of the ta-C coating. In the Si window of Figure 6-11(b), the distribution of Si on the entire probed surface is almost uniform but slightly higher at the wear track (appearing as a shinier area), implying the existence of more Si atoms on this region. This behaviour could be due to the removal of a very thin top layer of the ta-C overcoat during the wear test, which led to exposure of the lower layers of the film containing minor amounts of Si in their structure.
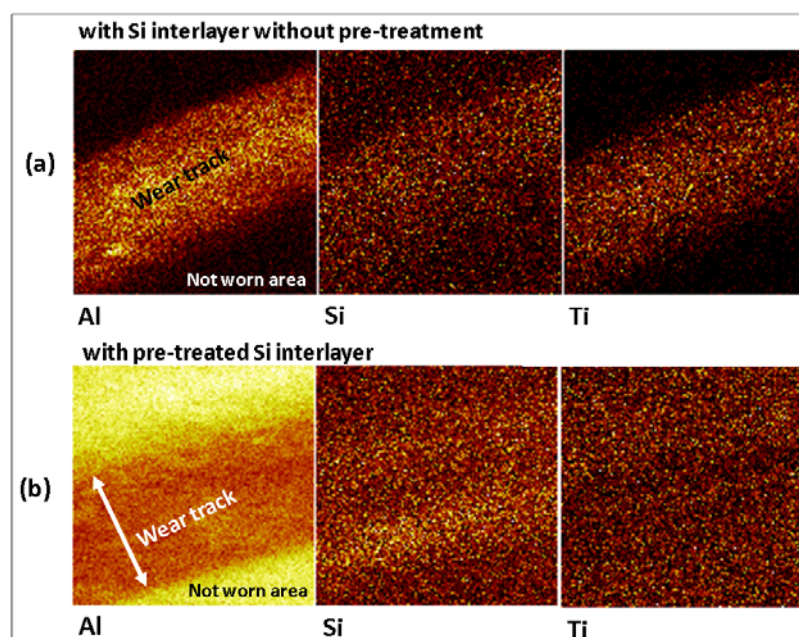


**Figure 6-11** Aluminum, silicon, and titanium SIMS surface images of wear tracks formed on ta-C coated AlTiC substrates (a) with Si interlayer without pretreatment and (b) with pretreated Si interlayer after 10 000 wear cycles

A comparison between the wear behaviour of samples with and without the pre-treated Si interlayer implied that the shorter wear life of sample B constitutes evidence of its weaker adhesion to the substrate and also its lower $sp^3$ content. In contrast, sample C

with about 10% more sp$^3$ content, as well as a considerably higher amount of chemical bonds between the interlayer, overcoat, and substrate exhibited much improved adhesion to its substrate, resulting in enhanced wear resistance.

## 6.4   Conclusion

The results of this investigation shed light on the mechanism by which the Si interlayer improves the durability of amorphous carbon films on the AlTiC ceramic. In addition, this study shows the potential of bombarding the interlayer with energetic Ar$^+$ and C$^+$ ions as a novel surface treatment method for improving the adhesion and durability of the carbon coating on the head substrate.

Simulation and experimental tests were conducted to study the adhesion mechanisms between the Si interlayer and AlTiC ceramic surfaces when the surface was coated with FCVA-deposited ta-C coating. In addition, this study also investigated the effect of pre-treatment of the Si interlayer by bombarding the surface with more highly energetic C$^+$ ions prior to deposition of the ta-C overcoat, on the chemical structure and tribo-mechanical behaviour of the coated surfaces. The effect of bombardment of the Si interlayer with ions of different energies on the distribution of elements in the Si/AlTiC interface was studied by SRIM simulation. The chemical states of the ta-C films and their interlayers were investigated by means of XPS analysis. Nanotribological properties of the ta-C coated AlTiC substrate were studied by nano-scratch and ball-on-flat tests.

The results showed a remarkable improvement in wear life and durability of the ta-C coating when deposited on the AlTiC surface with a Si interlayer. The formation of a Si–C network between the Si interlayer and ta-C overcoat as well as the formation of strong Al–O–Si and Si–O–C covalent bonds between the interlayer and the substrate

were found to be the two main phenomena responsible for the adhesion of the ta-C films to their substrates. Understanding this mechanism enabled us to engineer the interface between the overcoat, interlayer, and substrate to achieve better adhesion by enhancing the formation of such strong bonds. The results revealed that bombarding the interlayer with energetic $C^+$ ions prior to deposition of the ta-C coating, was an effective way to form a mixed interface and enhance the formation of a larger number of chemical bonds between the substrate and the overcoat. This phenomenon improved the adhesion of the overcoat to the substrate and enhanced its wear life by more than 60%. In addition, pre-treatment of the Si-coated AlTiC surfaces led to increase of the $sp^3$ content of the ta-C films due to the densification of the interlayer which may have further contributed to the improved wear resistance of the film.

These findings are promising and provide insights for further investigations of FCVA plasma treatment in order to produce coated magnetic tape recording heads that can solve or reduce the tribological problems at the head-tape interface in magnetic tape drives for ultra-high density magnetic recording. Moreover, this pre-treatment method can be potentially exploited in the surface modification of recording heads and media as well as the development of overcoat free magnetic disks in the next generation of hard drives with extremely high recording density which is extensively studied in chapter 10

.

# Chapter 7: Developing AlTiN$_x$C$_y$ interlayer to improve the durability of the ta-C coating on the recording heads

## 7.1 Introduction

Hard materials such as nitride and carbide films have been used as interlayers (as thick as a few microns) to improve the durability of DLC films on metallic substrates [149, 150]. Nitrides, particularly TiN films, have a high load capacity and can form Ti-C bonds with DLC films, which could improve the adherence of the DLC films to the substrate [151-154]. Avelar-Batista *et al.* fabricated DLC, TiN/DLC, CrN/DLC, and CrAlN/DLC films on different metallic surfaces and proved that the DLC/TiN film had the best wear resistance [155]. Application of TiN or functional graded layers of TiN$_x$C$_y$ was shown to improve the wear durability of DLC coatings on metallic substrates such as Al-based alloys or steel. [154, 156, 157]. However, the application of such hard materials as an interlayer for DLC films on ceramic substrates has not been studied so far. In this work, an ultrathin TiN film was used as an interlayer between the AlTiC substrate (ceramic) and ta-C overcoat. In addition, the effect of pre-treatment of the TiN-coated AlTiC substrate by bombarding the surface with energetic C$^+$ and Ar$^+$ ions prior to deposition of the ta-C film was studied.

## 7.2 Experimental Procedure

### 7.2.1 *Specimens and sample preparation*

The preparation procedure for TiN/ta-C samples was very similar to the procedure explained in Section 6-2. Before deposition of the TiN interlayer, the samples (AlTiC flat samples) were ultrasonically cleaned by IPA and acetone respectively for 20 minutes and followed by Ar$^+$ sputter etch cleaning. After cleaning the surface without

breaking the vacuum of the deposition chamber, a 5 nm TiN interlayer was deposited on the cleaned substrates using an RF-magnetron gun at an RF power of 150 W, Ar flow rate of 20 sccm and working pressure of 3 mTorr. The deposition rate of TiN was measured earlier by deposition of a thicker TiN film on a masked Si wafer and measuring the pattern height using AFM.

The deposition of ta-C overcoats and bombardment of the surface with energetic C$^+$ or Ar$^+$ ions were carried out using an FCVA deposition tool [133]. During the transportation of the samples from the sputtering chamber to the FCVA chamber, the samples were exposed to ambient oxygen, which could oxidize the outermost layer of the TiN film [158]. In order to remove this oxide (oxygen rich) layer prior to bombardment of the TiN interlayer with C$^+$ ions, the samples were again treated with Ar$^+$ plasma sputter etching with ion energy of 500 eV, at a normal incident angle for 45 seconds in a working pressure of 100 mPa, in the same chamber that the FCVA treatment would be conducted. The thickness of the remaining TiN layer was approximately 2.0 nm. The TiN-coated AlTiC surfaces were pre-treated (as described in Section 5-2) with C$^+$ ions of 350 eV (substrate bias voltage of -330 V) for 25 seconds followed by the deposition of a 7-8 nm ta-C overcoat with ion energy of 100 eV. As mentioned in Section 5-2-1, bombardment of the surface with ion energy of 350 eV for 25 seconds affects only the top region of the substrate up to a depth of 1-2 nm. Further details of deposition of the ta-C overcoats and surface pre-treatment have been extensively explained in Sections 4-2-1 and 5-2. The sample preparation procedure is schematically depicted in Figure 7-1.
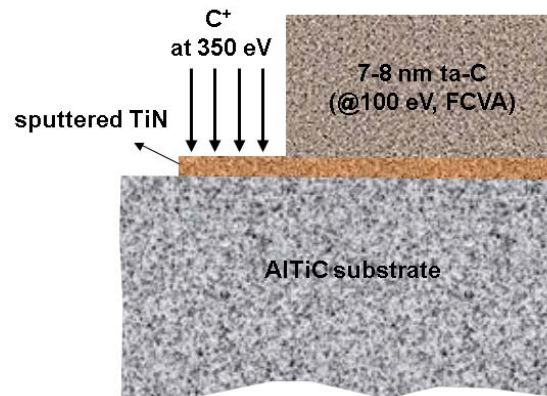
**Figure 7-1** Schematic structure of the ta-C film with ultrathin TiN interlayer

To have a better understanding of the possible effect of bombarding the TiN-coated surface with energetic Ar$^+$ ions (during the sputter etching of the oxide layer) and C$^+$ ions (during the pre-treatment and deposition), the Stopping and Range of Ions in Matter (SRIM) code was used to simulate the implantation (direct and recoil) distribution of the existing species (Ti, N, O, Al, and C) in the interface of the TiN interlayer and the Al$_2$O$_3$ phase of the AlTiC substrate. In this simulation, the ion flux of Ar$^+$ or C$^+$ was perpendicular to the surface of a semi-infinite medium of Al$_2$O$_3$, which was coated with a 2.0 nm TiN layer. The simulation was performed for ion energies of 500 eV for Ar$^+$, followed by bombardment of the surface with C$^+$ ions of 350 and 100 eV respectively.

### 7.2.2    *Characterization procedure*

TEM cross-sectional imaging was used to measure the thickness of the head coating and also to study the structural characteristics of the substrate, interlayer, and coating interface. The chemical composition analysis of the ta-C films and depth profiles of the existing elements in the coating, interlayer and substrate were performed by the AES depth profiling technique. Surface chemical analysis of the treated surfaces was carried out in an XPS system. Chemical composition analysis of the ta-C films and

depth profiles of the existing elements in the coating, interlayer and substrate were performed by the XPS depth profiling technique. The details of this process have been explained in Section 4-4-2. The chemical structure of the ta-C/TiN/AlTiC interface was precisely measured by acquiring high resolution XPS spectra with energy steps of 0.1 eV. Each spectrum was obtained as an average of 10 scans. The effect of the aforementioned methods on the general tribological behavior of ta-C coatings on flat AlTiC surfaces was investigated using ball-on-flat test (for details, please refer to Section 4.5). Following the wear tests, the surfaces of the coated heads were examined using Auger electron spectroscopy.

## 7.3 Results

A cross-section of the sample observed by TEM is shown in Figure 7-2. The exact thicknesses of the TiN interlayer and ta-C film were measured as 2.0 nm and 8 nm, respectively. TEM results provided qualitative evidence of the formation of a dense thin mixing layer at the film interface of both samples. This layer was visible in dark color between the crystalline structure of the substrate and the amorphous ta-C overcoat.
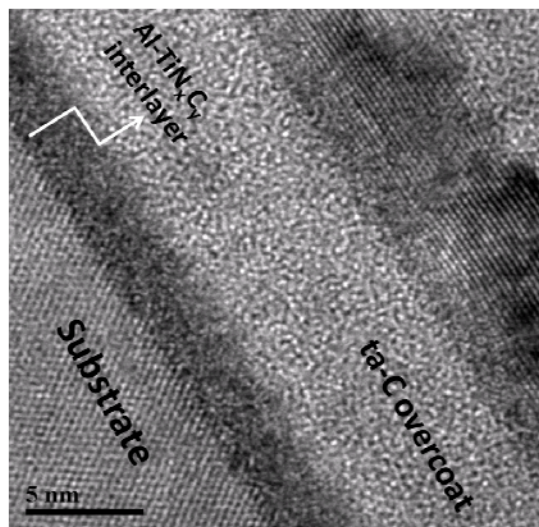


**Figure 7-2** Cross-sectional TEM image of ta-C overcoat with TiN interlayer pre-treated with C$^+$ ions of 350 eV for 25 seconds

### 7.3.1 Bombardment of the TiN-coated AlTiC surface by energetic Ar$^+$ and C$^+$ ions

Before deposition of the ta-C overcoat, the outermost surfaces of the TiN-coated substrates were sputter-etched by Ar$^+$ ions of 500 eV (to sputter-etch the 3.5 nm TiN$_x$O$_y$ layer) followed by C$^+$ ion bombardment at 350 eV (for pre-treatment) and 100 eV (for deposition of the ta-C overcoat). The effects of these three processes on the distribution of the embedded C$^+$ ions as well as the recoiled distribution of the Ti, Al and O atoms at the interface of the TiN layer and the Al$_2$O$_3$ phase of the AlTiC substrate were predicted by SRIM simulation. The distribution of the direct or recoil implanted ions/atoms in a region with a depth of 8 nm (including the TiN/Al$_2$O$_3$ interface) is shown in Figure 7-3.
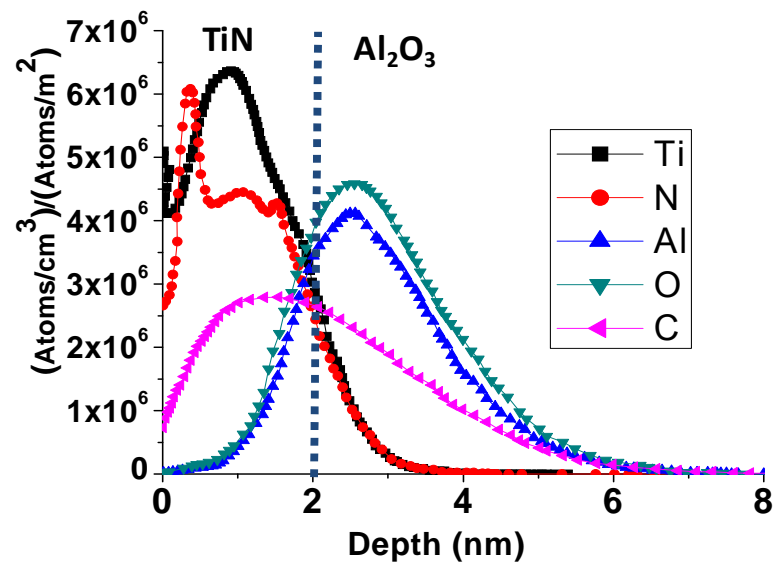


**Figure 7-3** Distribution of the direct and recoil implanted ions/atoms at the TiN/Al$_2$O$_3$ interface due to bombardment of the surface with Ar$^+$ ions with energy of 500 eV, C$^+$ ions with energy of 350 eV, and C$^+$ ions with energy of 100 eV.

As can be seen in Figure 7-3, bombarding the surface with highly energetic Ar$^+$ and C$^+$ ions can lead to the embedment of Ti and N atoms from the interlayer into the Al$_2$O$_3$ phase of the AlTiC substrate due to the knock-on events. At the same time, this bombardment created recoil cascades, which gave the substrate atoms (Al and O) near the interface enough energy to be driven away from the Al$_2$O$_3$ surface into the TiN

region. This atomic transport phenomenon gave rise to an interface mixing, which can be a desirable effect when modification of the interface between the two layers is required. While Ar$^+$ ions are less likely to react with the species in this mixed layer, implanted C$^+$ ions can potentially react with the radicals and broken bonds available in the mixed interface, and form new chemical bonds between the substrate, interlayer and overcoat elements.

As can be seen in Figure 7-3, a considerable portion of energetic C$^+$ ions could pass through the TiN layer and were stopped inside the Al$_2$O$_3$ region, which was already implanted by Ti and N atoms due to the knock-on effects as explained above.

### 7.3.2 *Chemical characterization of the overcoat and the AlTiC/TiN/ta-C interface*

The possibility of the formation of an intermixing layer at the AlTiC/TiN/ta-C interface due to bombardment by energetic ions was further examined by XPS depth profiling (Figure 7-4). In the XPS depth profile, the interlayer can be determined as a region with maximum atomic concentration of Ti and N. As can be seen in Figure 7-4, there were no well-defined ta-C/TiN or TiN/AlTiC margins. In addition to Ti and N, the interlayer region showed considerable amounts of C, Al, and O atoms.

This result indicated the embedment of C$^+$ ions into the interface, and confirmed the formation of an atomic mixing layer at the AlTiC/TiN/ta-C interface as predicted by SRIM simulation. It also supported the idea of the displacement of the Ti and N atoms into the substrate as well as the diffusion of the substrate elements (Al and O) into the TiN interlayer as a result of collision cascades.
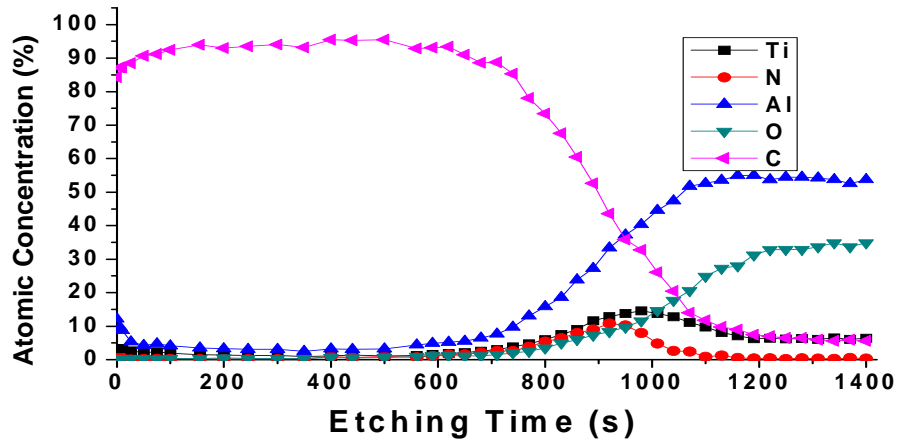
**Figure 7-4** Depth profile of the sample with 8 nm ta-C overcoat and 2 nm TiN interlayer, pretreated with C$^+$ ions of 350 eV. The TiN interlayer is considered as the point at which Ti and N have the maximum concentration.
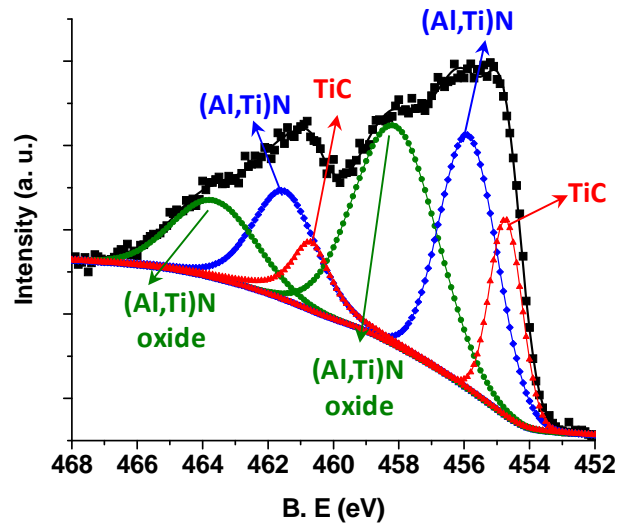


**Figure 7-5** High resolution Ti$_{2p}$ XPS spectrum with Gaussian fits of TiN interlayer pretreated with C$^+$ ions suggesting formation of Ti-C, Al-N-Ti and (Al,Ti)N$_x$O$_y$ bonds in the structure of the interlayer

To examine the chemical structure of the TiN intermediate layer, the XPS high resolution scan of the Ti$_{2p}$ spectrum of the TiN-coated sample pre-treated by C$^+$ ions was studied in detail (Figure 7-5). The Ti$_{2p}$ spectrum of the sample (corresponding to the depth level with maximum concentration of Ti and N) was deconvoluted with six Gaussian/Lorentzian distributions (three doublets pertinent to Ti2p$_{1/2}$ and Ti2p$_{3/2}$ peaks) corresponding to the potentially available bonds existing in the interlayer region.

According to Figure 7-5, the Ti$_{2p}$ core level spectrum of the sample consisted of two peaks at 454.4 eV and 460.7 eV, which were attributed to Ti-C (or TiNC) bonds (Ti2p$_{3/2}$ and Ti2p$_{1/2}$ respectively) [159-161]. There was a dominant doublet with two peaks at 455.8 eV and 461.5 eV corresponding to the (AlTi)N bonds [162, 163]. The other doublet with the peaks at 458.1 eV and 463.8 eV was pertinent to the (Al,Ti)N$_x$O$_y$ structure [163].

It can be inferred that a considerable number of the Ti atoms (broken Ti-N bonds) in the interlayer film have reacted with the C$^+$ ions to form Ti–C bonds. In addition, the results implied that the majority of the Ti and N atoms have reacted with the Al and O atoms. According to SRIM results, these bonds may form either by recoil implantation of Al and O into the TiN layer or direct implantation of Ti and N into the Al$_2$O$_3$ phase of the AlTiC substrate. It would be very likely that the sputter-etching of the substrate surface before deposition of TiN as well as implantation of C$^+$ into the substrate were able to destroy a number of Al–O bonds near the interface, and form radicals containing O and Al. In addition, bombardment of the surface with these ions can lead to the recoil implantation of Al and O atoms (radicals) into the TiN interlayer. These resultant radicals were able to react with either the existing Ti and N atoms in the interlayer or with the implanted Ti and N ions within the Al$_2$O$_3$ substrate to form Al-N-Ti bonds or (Al,Ti)N$_x$O$_y$ compounds.

The existence of strong Al-N-Ti and (Al,N)N$_x$O$_y$ components (peaks) within the Ti$_{2p}$ peak of the samples demonstrated the effective role of pre-treatment of the interlayer by energetic carbon ions in the formation of strong (covalent) bonds between the substrate, interlayer, and overcoat. As mentioned before, most of the Ar$^+$ and C$^+$ ions with higher energy were implanted into the interlayer and substrate, causing strong collision cascades. This phenomenon enhanced the development of a mixed layer

between the interlayer and the substrate due to more effective direct and recoil implantation of the species, and promoted formation of chemical bonds between the existing radicals at the intermixing layer. These chemical bonds may strongly attach the interlayer to the substrate.

### 7.3.3 Ball-on-flat wear tests

As mentioned in Section 4-5-2, tetrahedral amorphous carbon overcoats are able to maintain a very low coefficient of friction between the substrate surface and the counterface. As long as the coating is still on the surface, the friction remains low. The failure mechanism of the DLC-coated AlTiC substrates was reported as delamination due to the lack of adhesion to the substrate. At the onset of failure of the coating, the friction suddenly increased to higher values and then kept increasing with considerable fluctuations. This behavior can be used as a scale to compare the wear lives of the tested samples. Figure 7-6 shows the frictional (ball-on-flat wear test) behavior of the AlTiC substrate coated with an 8 nm ta-C overcoat on a pre-treated TiN interlayer. The wear lives of the samples with and without pretreatment are shown in Figure 7-7.
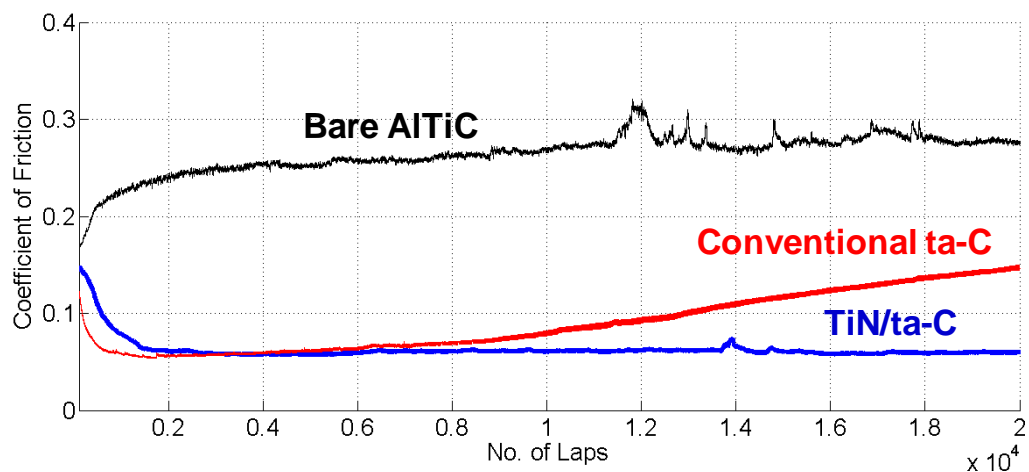


**Figure 7-6** Comparison of the friction coefficients of AlTiC substrate with no overcoat, with 10 nm conventional ta-C overcoat, and with 8nm ta-C overcoat with 2nm TiN interlayer pre-treated by energetic Ar$^+$ and C$^+$ ions.
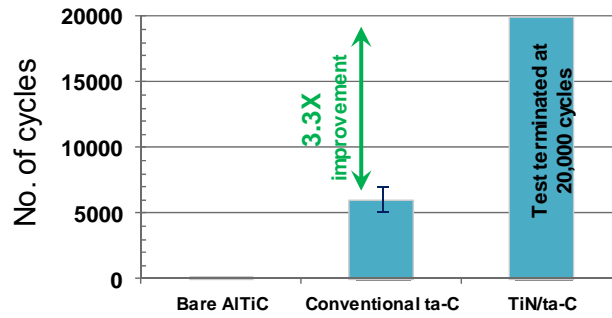
**Figure 7-7** Comparison between wear lives of AlTiC surfaces coated with 10 nm conventional ta-C overcoat and with 8 nm ta-C overcoat with 2 nm TiN interlayer pre-treated by $C^+$ ions (Note that in the case of the TiN/ta-C sample, the test was terminated at 20,000 cycles due to its long duration.

In order to verify the removal or existence of the ta-C film on the wear tracks of the samples after 10,000 cycles for conventional ta-C coating and after 20,000 cycles for ta-C coating with TiN interlayer, the surface of the wear tracks and the not-worn film in their vicinities were observed by AES surface imaging (Figure 7-8). The brighter regions in each window correspond to areas on the surface with higher concentrations of a specific element or compound, while the darker regions show the areas with lower concentrations of that element or compound.
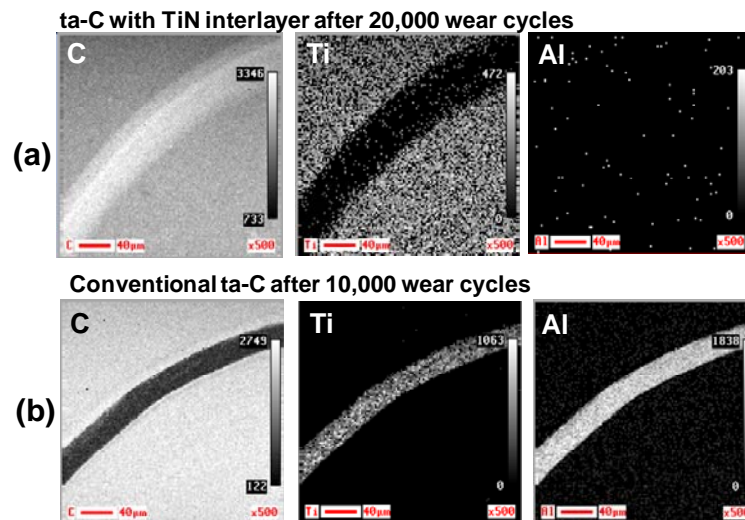


**Figure 7-8** Aluminum, titanium, and carbon AES surface images of wear tracks formed on the AlTiC substrates (a) with ta-C coating with TiN interlayer after 20,000 wear cycles and (b) conventional ta-C coating after 10,000 wear cycles

As can be seen in Figure 7-8(b), the Al and Ti windows showed shinier wear tracks as compared to their unworn neighborhood. This result confirmed the exposure of the Al- and Ti-containing substrate due to the removal of the ta-C overcoat. The wear track of sample C (with pre-treated Si interlayer) is depicted in Figure 7-8(a). As shown in the Al window of Figure 7-8(a), the intensity of the Al signal on the wear track was much less (the wear track appears darker) than that of the intact region in its vicinity which had a uniform ta-C overcoat. This result implied that the wear track was still covered with carbon which prevented the Al from the substrate from being exposed. The Ti image of sample C also showed no evidence of the existence of Ti on the wear track, indicating that the AlTiC surface remained covered with a continuous ta-C overcoat.

A comparison between the wear behaviors of samples with and without the pre-treated TiN interlayer implied that the shorter wear life of the conventional ta-C overcoat (without interlayer) constituted evidence of its weaker adhesion to the substrate. In contrast, the ta-C coating with a TiN interlayer having considerably large amount of chemical bonds between overcoat and the substrate, exhibited much improved adhesion to its substrate, resulting in enhanced wear resistance.

## 7.4   Conclusion

The results of this investigation showed the potential of bombarding the TiN interlayer with energetic Ar$^+$ and C$^+$ ions as a novel surface treatment method for improving the adhesion and durability of the carbon coating on the head substrate.

Simulation and experimental tests were conducted to study the effect of pre-treatment of the TiN interlayer by bombarding the surface with more highly energetic C$^+$ ions prior to deposition of the ta-C overcoat on the chemical state and tribo-mechanical behavior of the coated surfaces. The effect of bombardment of the TiN interlayer with ions of different energies on the distribution of elements in the TiN/AlTiC interface

was studied by SRIM simulation. The chemical state of the interlayers was investigated by means of XPS analysis. Nanotribological properties of the ta-C coated AlTiC substrates with and without a TiN interlayer were studied by ball-on-flat tests. The results showed a remarkable improvement of 3.3 times in the wear life and durability of the ta-C coating when it was deposited on the AlTiC surface with a TiN interlayer. The formation of a Ti–C network between the TiN interlayer and ta-C overcoat as well as the formation of strong Al–N–Ti and (Al,Ti)N$_x$O$_y$ covalent bonds between the interlayer and the substrate were found to be the two main phenomena responsible for the adhesion of the ta-C films to their substrates.

These findings are promising and provide insights for further investigations of FCVA plasma treatment in order to produce coated magnetic tape recording heads that can solve or reduce the tribological problems at the head-tape interface in magnetic tape drives for ultra-high density magnetic recording. The next chapter investigates the effect of this surface treatment on the wear life of ta-C films coated on magnetic tape heads, studied in a real tape drive.

# Chapter 8: Effects of different surface modification (pre-treatment) techniques on the tribological performance of ta-C coating in a real head/tape interface

## 8.1 Introduction

In the previous chapters (chapters 5, 6, and 7), the effects of different surface modification (pre-treatment) techniques on the tribological behaviour of the ta-C coatings deposited on the AlTiC flat substrates were studied. These techniques can be summarized as follows:

- Pre-treatment of the surface by bombarding the AlTiC substrate with $C^+$ ions

- Developing an Al-Si-C composite interlayer

- Developing an $AlTiN_xC_y$ mixed interlayer

Pre-treatment of the AlTiC substrate by bombarding the surface with energetic (350 eV) $C^+$ ions, prior to deposition of a 10 nm ta-C overcoat by the FCVA method (at 100 eV), was shown to considerably improve the wear durability of the ta-C overcoat on AlTiC flat samples (chapter 5). In order to increase the durability of the ta-C overcoats, as shown in chapter 6, bombardment of a thin Si film with energetic $C^+$ and $Ar^+$ ions resulted in the formation of a composite interlayer which chemically bonds the substrate, interlayer, and the overcoat together. This method led to a significant improvement in the wear life of a 5 nm ta-C overcoat on the flat AlTiC substrate [164]. Bombarding the TiN interlayer with energetic Ar+ and $C^+$ ions (chapter 7) also caused the formation of an $AlTiN_xC_y$ intermixing layer between the AlTiC surface and the ta-C overcoat. Formation of such an intermixed layer remarkably increased the durability of the ta-C coating as well. It is noteworthy that the aforementioned methods have

been tested only on flat AlTiC wafers and the behaviors of the treated surfaces were investigated using fundamental tribological tests such as ball-on-flat or scratch tests. Although these fundamental tests have shown remarkable improvements in the tribological properties of the ta-C coatings on the AlTiC flat surface, they did not exactly represent the actual contact situation at the head/tape interface in real tape drives.

In this chapter, the effect of the mentioned three different surface modification methods on the wear life of the coating of magnetic tape drive heads has been studied. In this research, the heads were coated with 10 nm tetrahedral amorphous carbon (ta-C) film using filtered cathodic vacuum arc (FCVA) technique. The surface of the heads was pretreated by bombardment of energetic carbon ions, thereby forming the Si-Al-C and $AlTiN_xC_y$ interlayers prior to deposition of the ta-C coating. The coated heads were tested in a real head/tape interface of a tape drive. Surface characterization and the tribological behavior of the head coatings with and without surface modification have been studied by transmission electron microscopy (TEM), Auger electron spectroscopy (AES) and scanning electron microscopy (SEM).

## 8.2 Experimental procedure

### 8.2.1 Specimens and sample preparation

Generation 4 of the LTO recording heads (LTO-4 heads) manufactured by *Oracle America Inc., Broomfield, CO, USA* were used as the specimen. A recording head consists of 32 read-write elements located in two parallel rows of 16 at both sides of the head. Figure 8-1 shows the optical and SEM images as well as schematic of one read/write element of the recording head.
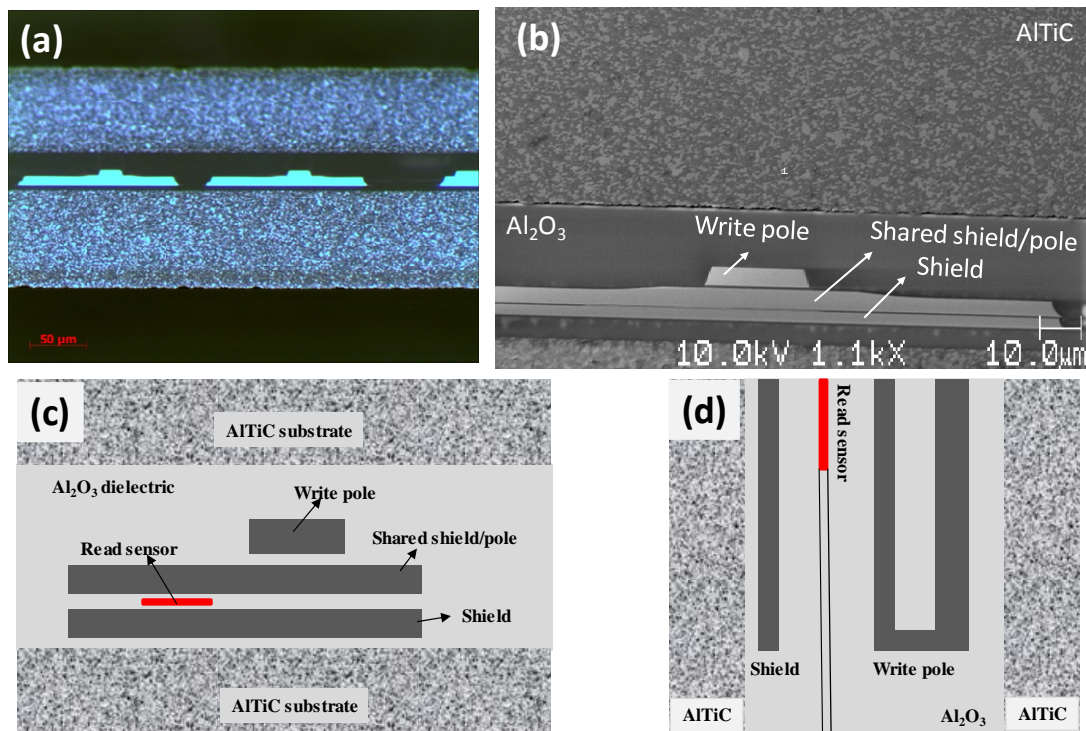
**Figure 8-1** Optical microscope image of the read/write elements, schematic drawing of (b) top view and (c) cross-section of one of the head read/write channels

**Table 8-1** Description of the procedure for surface modification of the heads prior to deposition of 10 nm ta-C

| Sample name | Description of the surface treatment before deposition of 10 nm ta-C overcoat |
|---|---|
| *Head-1* | No surface treatment |
| *Head-2* | Bombarded by energetic $C^+$ ions of 350 eV for 25 seconds |
| *Head-3* | 2 nm Si interlayer bombarded with energetic $Ar^+$ ions of 500 eV followed by $C^+$ ions of 350 eV for 25 seconds |
| *Head-4* | 2nm TiN interlayer bombarded with $Ar^+$ ions of 500 eV followed by $C^+$ ions of 350 eV for 25 seconds |

Each read-write element consists of write poles and shield made of cobalt-zirconium-tantalum (CZT) and the read sensor is made of NiFe. Read-write elements are electrically insulated from each other and also from the substrate by a sputtered $Al_2O_3$ film. These elements are sandwiched and supported by a hard composite ceramic (AlTiC) consisting of about 70% $Al_2O_3$ and 30% TiC by weight (Figure 8-1). In this

study, four different sets (batches) of samples with 10 nm ta-C overcoats were prepared as described in Table 8-1.

Before deposition of the coatings, the heads were ultrasonically cleaned with acetone and IPA for 20 minutes, rinsed with deionized water and dried with pure nitrogen. In order to decrease the out-gassing in the deposition chamber due to the release of the adsorbed moisture or other chemicals from the heads, cleaned heads were baked at 50 °C for 20 minutes. The head surfaces were also cleaned by $Ar^+$ sputter-etching to increase the adhesion of the coatings to their substrates.

The deposition of Si was conducted in a magnetron sputtering tool (AJA international Inc, MA, USA.) using an RF power of 150 Watts. Deposition of the 10 nm ta-C overcoat and pre-treatment of the head surfaces (with or without Si interlayer) was performed using filtered cathodic vacuum arc (FCVA: *Nanofilm Technologies International Pte. Ltd.,* Singapore). Details of deposition of the ta-C overcoats, surface pre-treatment and development of the Al-Si-C and $AlTiN_xC_y$ composite interlayers have been extensively explained elsewhere (in sections 5-2, 6-2-1 and 7-2-1 respectively). All sample preparation stages were undertaken in a class 1000 clean room with a controlled temperature and relative humidity of 22±0.5 °C and 50±5 % respectively.

### 8.2.2    *Characterization procedure*

In order to precisely measure the film thickness as well as to study the structural characteristics of the substrate/interlayer/coating interface, the cross-sectional structure of the ta-C overcoat with Si (with and without pre-treatment) and TiN interlayer was observed by TEM (JEM, 3200FS, JEOL Ltd). The sliding wear tests on the coated heads were conducted using a SDS tape transport system provided by *Imation Corp.,*

*Oakdale, MN, USA*. In this work, Imation LTO Ultrium Generation 3 (LTO-3) tape cartridges were employed for the sliding wear tests. 660 meters out of the total length of 680 meters of the tape cartridge were used for the wear test. In order to keep the tape condition consistent for all the heads, the usable length of the tape was divided into four equal sections whereby each section was slid back and forth only against one head. To study the durability of the coatings, the heads of each batch were tested for three different tape lengths of 170 km, 340 km, and 1000 km. During the experiment, the tape speed and tape tension were fixed at 5 m/s and 0.7 N respectively. The test parameters used for these experiments are summarized in Table 8-2.

**Table 8-2** Parameters of the tape used for sliding wear on the coated heads

| Tape speed | Tape tension | Tape total length | No. of cycles |
|---|---|---|---|
| 5 m/s | 0.7 N | 170 km | 515 |
| | | 340 km | 1030 |
| | | 1000 km | 3030 |

Following the wear tests, the coated heads surfaces were examined using Auger electron spectroscopy (AES:JEOL model JAMP-10SX). Because of the thinness of the coating (less than 10 nm) and the small size of the head features (read/write elements), AES was considered as the most suitable tool to investigate the head surface after the wear test.

For all the heads, in order to eliminate or minimize the effect of airborne contamination, the head surface was slightly cleaned by $Ar^+$ sputter-etching with low ion energy of ~500 eV. Next, the area near one of the read-write elements (see Figure 8-1(b)) was first scanned with an electron beam to acquire a wide AES spectrum to check which elements existed on the surface. With this data, Auger elemental mapping

with a quality of 128×128 pixels was performed to determine the distribution of the available elements on the surface.

The thickness of the coatings after the wear tests, as well as the composition of the coatings and their underlayer (if any), was analyzed by AES depth profiling. By comparing the time needed to etch the ta-C coating and reach the substrate, and also by knowing the actual thickness of the unworn overcoat (measured by TEM), the thickness of the coating after the wear test was calculated. To have a high spatial depth resolution, $Ar^+$ plasma with ion energy of 500 eV and etching time of 10 sec/cycle was used in all experiments.

## 8.3   Results and discussion

### 8.3.1   Comparison between wear resistances of ta-C head coatings with different surface treatments

After running the 170 km and 340 km length of the tapes over the coated heads with different surface treatments (as described in Table 8-1), the surface of the heads was analyzed by AES. Figure 8-2 shows the wide scan AES spectrum of a part of the head surface, which includes the read/write element, AlTiC substrate, and $Al_2O_3$ insulator.

Figure 8-2(a) shows the AES spectrum *Head-1* after the sliding of 170 km tape. Very clear peaks of Ti, Al, and O belonging to the AlTiC and the insulator as well as the peak of Co pertinent to the read/write elements are evident in this spectrum. From this result, it can be inferred that the 10 nm carbon overcoat of the head had been completely worn off after the wear test, and the surface of the head components had been exposed to the electron beam.
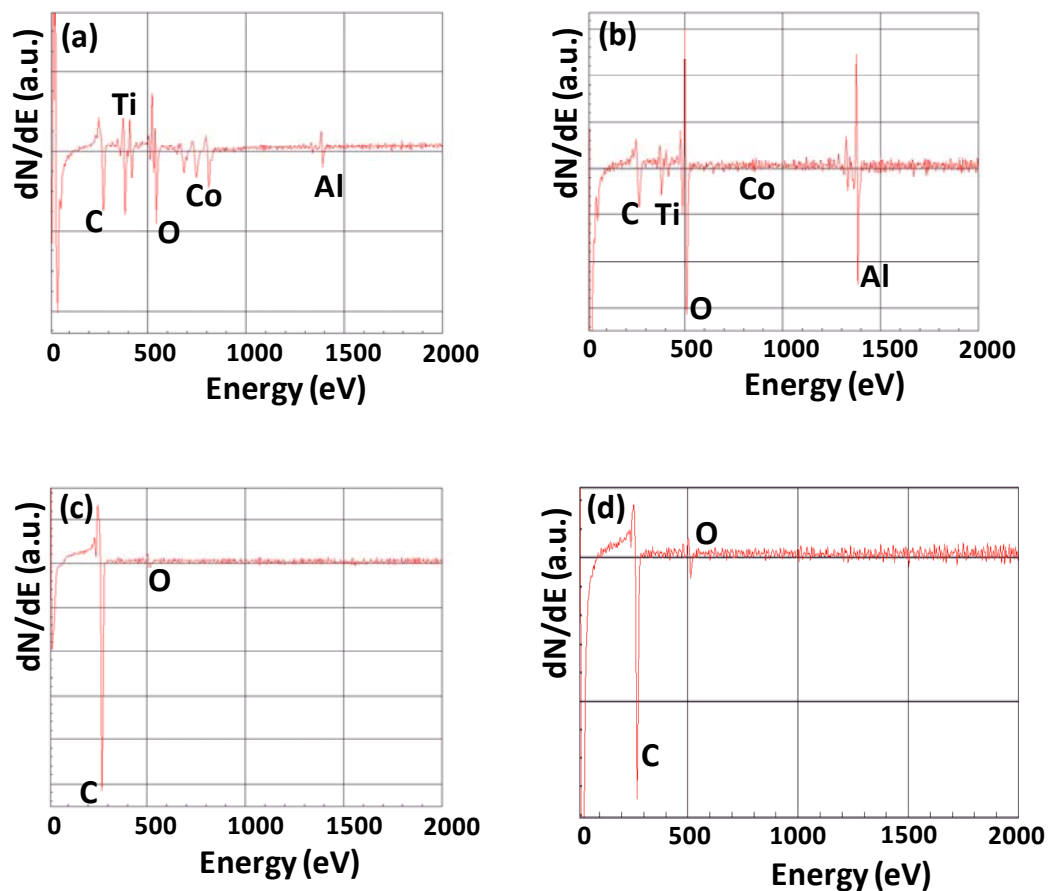
**Figure 8-2** Wide scan AES spectra of heads with 10nm ta-C coating (a) with no surface treatment after 170 km, (b) pre-treated with energetic $C^+$ ions after 170 km, (c) with Si-Al-C composite interlayer after 340 km, and (d) with $AlTiN_xC_y$ interlayer after 340 km wear test.

The AES spectrum of *Head-2* after 170 km is depicted in Figure 8-2(b). As can be seen in this spectrum, strong peaks of Al, O, and Ti are visible, implying that the coating on the AlTiC was damaged due to wear. However, in contrast with Figure 8-2(a), there is no strong obvious Co peak in the spectrum. From this result, it can be inferred that the surface of the read/write elements might still be covered with a thick ta-C film (thicker than the escape depth of the Auger electrons).

Finally, the wide spectra of *Head-3* and *Head-4* after the 340 km wear test are illustrated in Figures 8-2 (c) and (d) respectively. In spite of their longer wear test (two times longer than that of the others), there is no evidence of the substrate elements in the spectra and only a strong C peak is detectable on the surfaces of both heads. This

result implies that the surface of the *Head-3* (with Al-Si-C interlayer) and *Head-4* (with AlTiN$_x$C$_y$ interlayer) were still uniformly covered with the ta-C overcoat.

Although AES wide spectra can accurately determine the existence of the elements on the surfaces, they are not able to determine the distribution of the existing elements on the surface. In order to gain a better understanding of the quality of the coatings and the distribution of the existing elements on the surface of the head, AES surface elemental mapping (AES images) for Al, C, and Co was acquired for all the samples. In these images, a higher concentration of an element in its specific window is shown with warm or lighter colors while the absence or lower concentration of the elements is shown by cold or darker colors.

Figure 8-3 shows the distribution of Co, C, and Al on the surface of the *Head-1* after the 170 km wear test. As can be seen in the C and Al windows, the surface of the AlTiC substrate has completely lost its carbon overcoat (this surface is in darker and blue color in the C image, and is in red and light pink color in the Al image). The AES image for the Co window also indicates that the carbon coating of the read/write elements had been worn off and the Co was clearly exposed. It can be concluded from this result that the conventional ta-C coating without proper surface modification is not durable and cannot protect the surface.

Figure 8-4 shows the AES images of *Head-2* after the 170 km wear test. This result indicates that the AlTiC surface was still partially covered with C in some regions; however, in some other areas of the probed surface, the C film was absent and Al was completely exposed. Nevertheless, the results do not show any wear on the read/write elements. As can be seen in the windows of C and Co, the surface of the recording channels was still uniformly covered with C and there was no signal of Co pertinent to the CZT material of the poles.
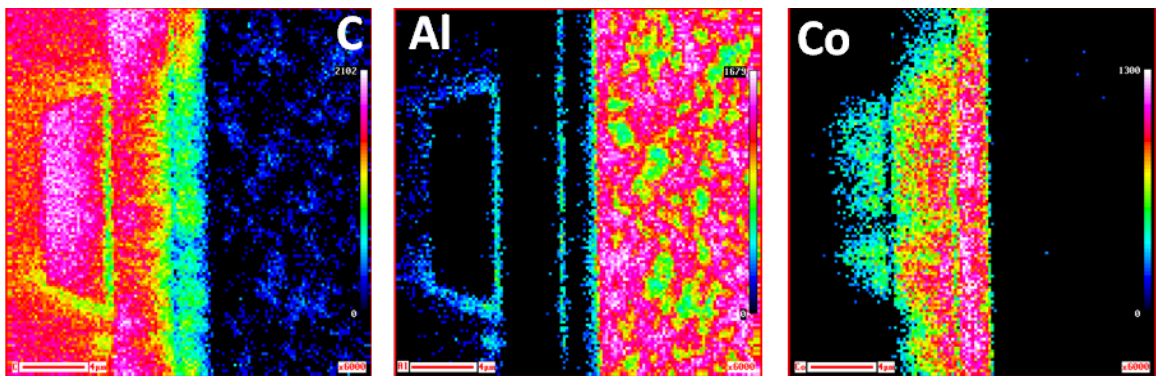
**Figure 8-3** AES surface elemental mapping image of Head-1 after 170 km wear test
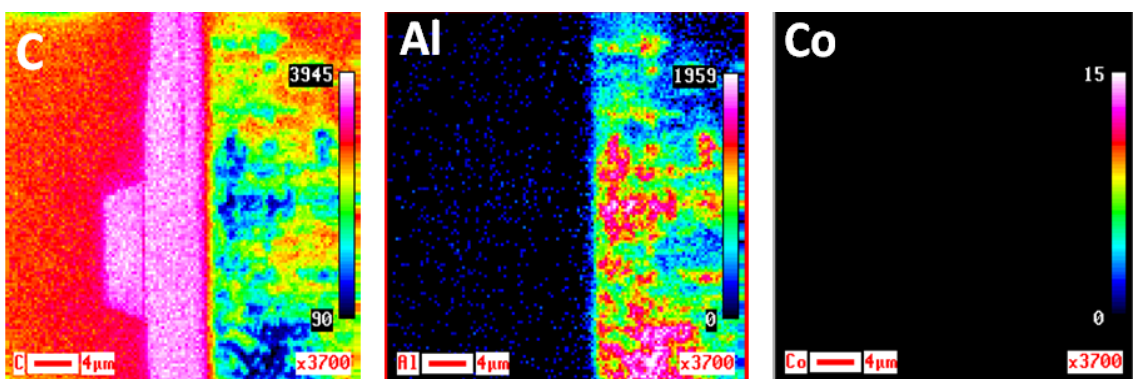


**Figure 8-4** AES surface elemental mapping image of Head-2 after 170 km wear test

Based on these results, one can conclude that bombarding the surface with energetic $C^+$ ions led to an improvement in the durability of the ta-C overcoats on the head surface as compared to the conventional ta-C coating. This improvement is more evident in the metallic surfaces of the head. The partial removal of the overcoat from the AlTiC ceramic can be attributed to the delamination of the film, due to insufficient adhesion. Although this method of pre-treatment could improve the adhesion of the ta-C to the AlTiC, the improvement was not enough to prevent the delamination completely.
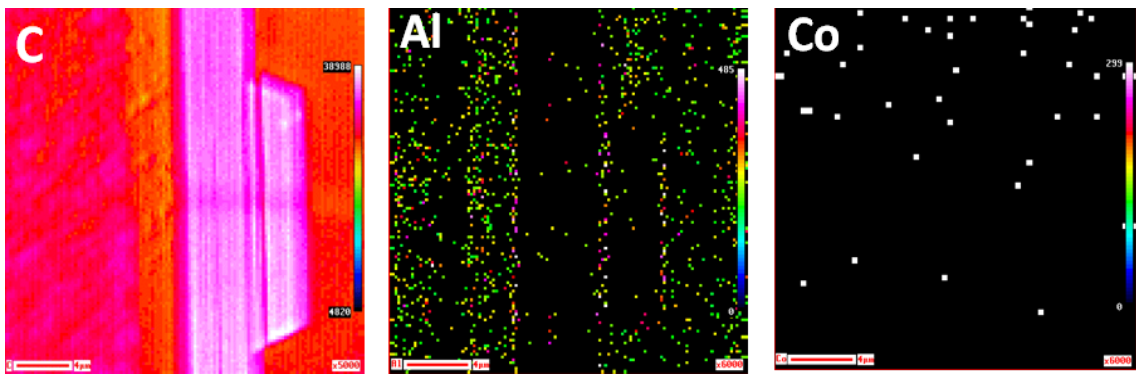
**Figure 8-5** AES surface elemental mapping image of Head-3 after 340 km wear test
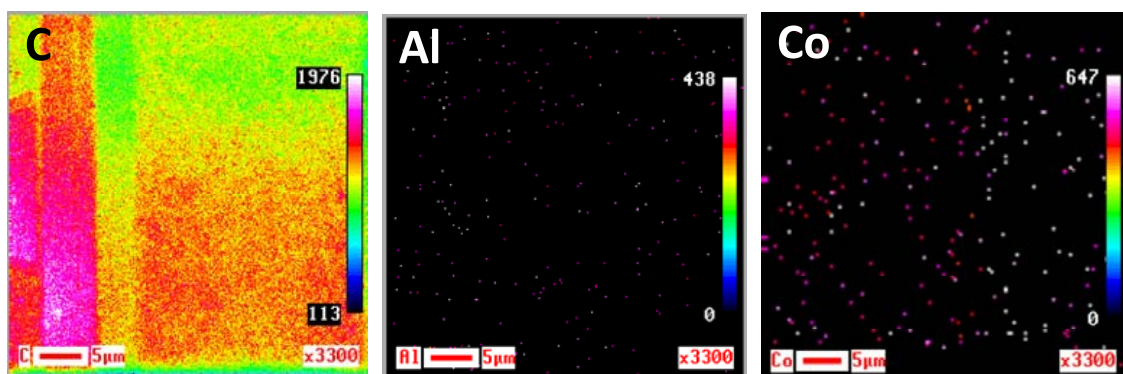


**Figure 8-6** AES surface elemental mapping image of Head-4 after 340 km wear test

The AES images of *Head-3* and *Head-4* after the 340 km wear test are shown in Figures 8-5 and 8-6 respectively. It is very clear from these images that even after a wear test that was two-times longer as compared to the other two samples, the surfaces of the both heads were still completely covered with a uniform ta-C overcoat without any wear or delamination. This result showed the effectiveness of the application of a composite interlayer (Al-Si-C or $AlTiN_xC_y$) to bond the ta-C overcoat to its substrate. These findings are in agreement with the ball-on-disk tribology results of the flat AlTiC surfaces reported in chapters 6 and 7.

In order to have a better understanding of the wear rates of the ta-C coatings, the thicknesses of the ta-C overcoats that remained on the surface after the wear test were measured by means of AES depth profiling. For constant etching parameters, the etching time required to reach the substrate can represent the thickness of the coating.

The thicknesses of the unworn (reference) coatings have been accurately measured by TEM (Figure 8-7). According to the TEM images, the thicknesses of the ta-C coatings on the heads pre-treated with $C^+$ ions, with Al-Si-C, and with Al-TiN$_x$C$_y$ interlayer were 10.8 nm, 10.5 nm, and 8 nm respectively.
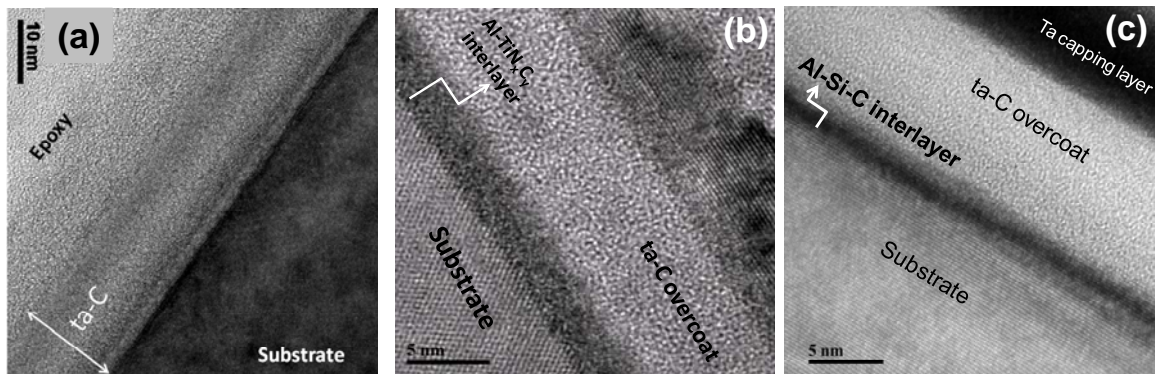


**Figure 8-7** TEM cross-section image of ta-C coating pre-treated by (a) $C^+$ ions, (b) Al-TiN$_x$C$_y$, and (c) Al-Si-C composite interlayer

Figure 8-8(a) shows the depth profile of the coating of *Head-2* on an unworn region. In this profile, the 10 nm coating was completely etched and the substrate was reached after about 1100-1200 seconds. The depth profile of the coating on the write pole is shown in Figure 8-8(b). Based on this result, about 800 seconds were required to etch the overcoat of this region which implied that more than half of the coating has still remained on the write pole. To measure the thickness of the remaining coating of the AlTiC substrate of *Head-2*, depth profiling was conducted on an area on which the overcoat was not delaminated yet (top-right part of C image in Figure 8-4). The depth profile (Figure 8-8(c)) indicated that the region was still covered with a carbon film of about 3 nm.
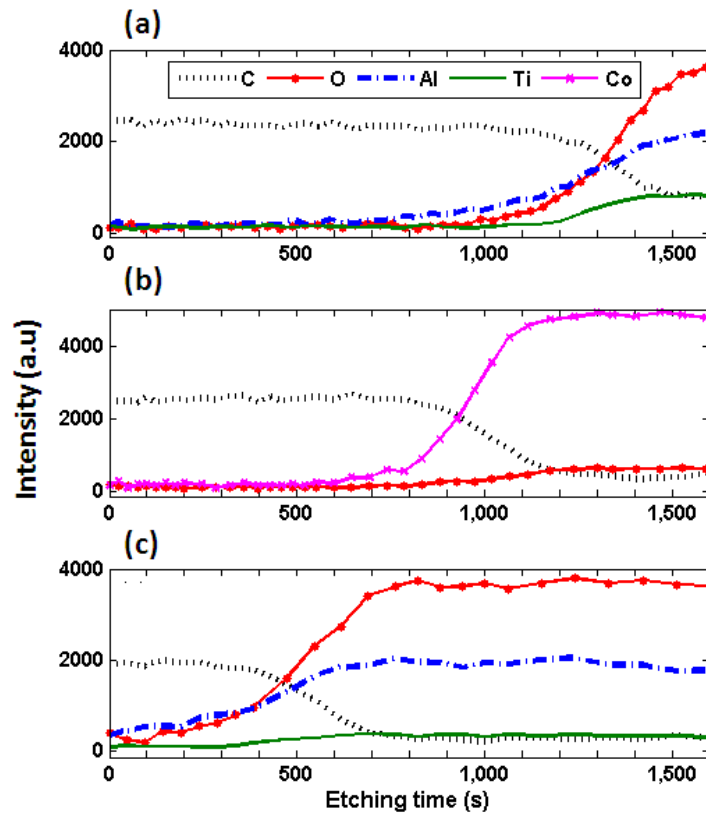
**Figure 8-8** Depth profile of the ta-C coating of the Head-2 on (a) unworn area, (b) read/write element, and (c) on the remaining overcoat of AlTiC substrate after 170 km wear test
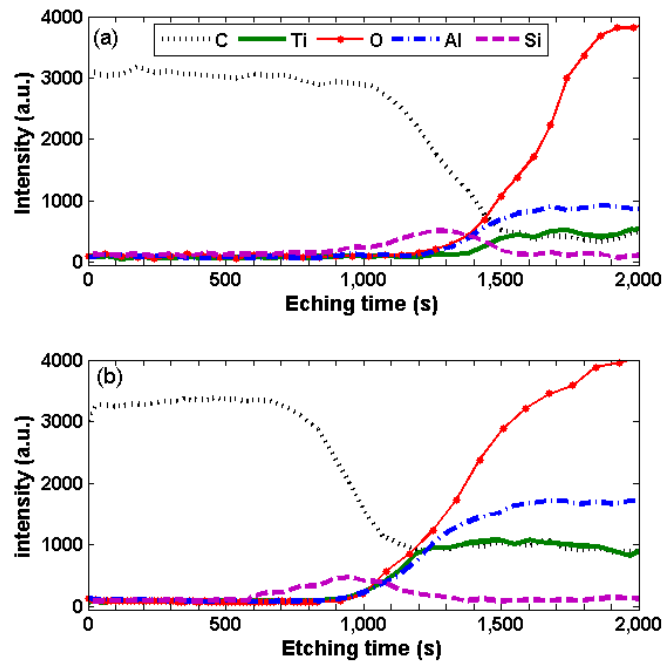


**Figure 8-9** Depth profile of the ta-C coating of the Head-3 (with Al-Si-C interlayer) on (a) unworn area, and (b) AlTiC substrate after 340 km wear test
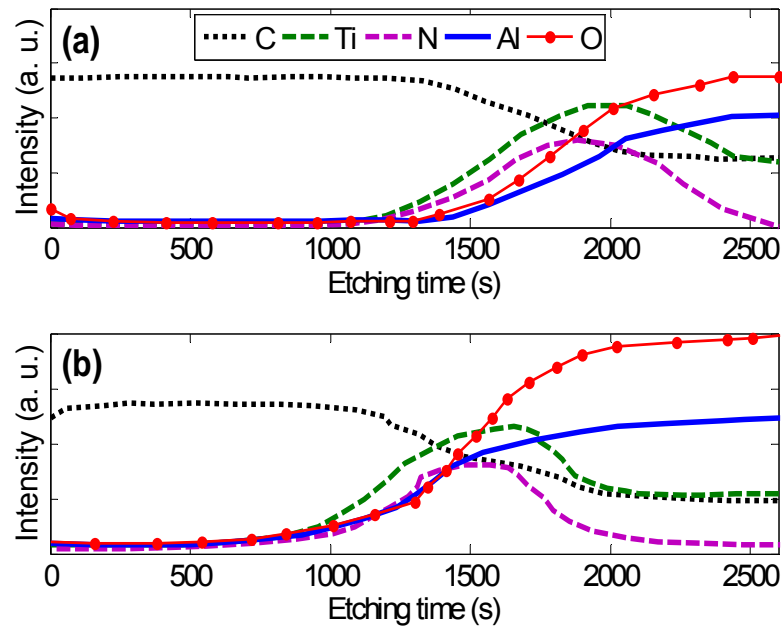
**Figure 8-10** Depth profile of the ta-C coating of the Head-4 (with Al-TiN$_x$C$_y$ interlayer) on (a) unworn area, and (b) AlTiC substrate after 340 km wear test

The depth profile of the reference coating of *Head-3* (with Al-Si-C composite interlayer) is depicted in Figure 8-9(a). The existence of a mixed layer containing Si, O, Al, C and Ti at the coating/substrate interface is clearly depicted in this figure. The thickness of the reference coating as measured by TEM was ~10.5 nm (Figure 8-7(c)). By comparing the depth profile of the reference coating and that of the worn area on the AlTiC surface (Figure 8-9(b)), the thickness of the coating of AlTiC after the 340 km wear test was estimated to be about 7 nm.

A similar depth profiling process was repeated on the surface of *Head-4* with Al-TiN$_x$C$_y$ interlayer. As can be seen in Figure 8-10(a), about 1200 seconds is required to etch the 8 nm ta-C on the reference surface. According to Figure 8-10(b), the etching time required to reach the AlTiC substrate for the worn coating of the AlTiC substrate of the *head-4* is about 1000 seconds. This result implies that about 80% (thickness is estimated to be about 6.4 nm) of the coating on the AlTiC substrate of *Head-4* is still not worn.
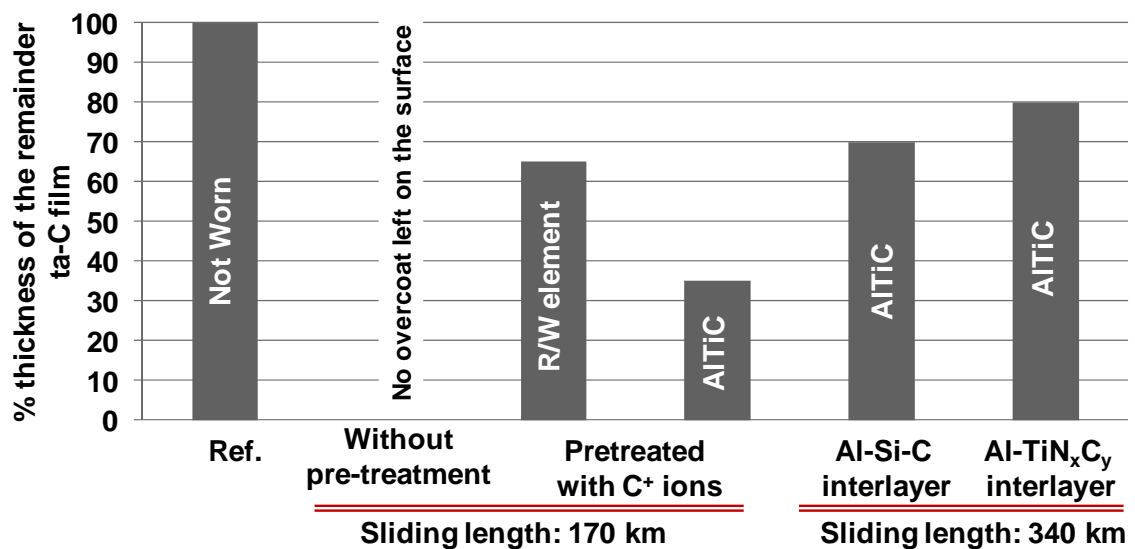
**Figure 8-11** A comparison between the thicknesses of ta-C overcoats on different regions of the coated heads with different surface modifications

Figure 8-11 shows a summary of the thickness of the head coatings with different surface pre-treatments on different regions of the heads. In this figure, the percentage of the remaining thickness of the coatings is used as a scale for comparison. Based on the results, it can be generally concluded that the conventional ta-C deposited without any surface modification was not durable in the severe tribological conditions of the head/tape interface. By bombarding the head surface with energetic carbon ions, the $sp^3$ content and durability of the coating was increased because of the formation of a dense and atomically mixed interface between the ta-C and the substrate [120]. However, this improvement on the AlTiC surface was not enough to prevent the ta-C film from peeling off, and the coating was partially delaminated. In contrast, the coating of the metalic read/write element of *Head-2* was not delaminated and still remained thick and uniform. A comparison between the behavior of the coating on ceramic and metallic surfaces highlights the role of adhesion of the coating on its substrate. It can be speculated that by bombarding the metallic surfaces (read/write elements) with $C^+$ ions, a network of Co-C bonds [165, 166] is formed that enhances

the adhesion of the ta-C overcoat to the metallic elements, which are mostly made of Co. The formation of such strong bonds between the ta-C coating and the ceramic substrate when its surface is saturated with strong ionic or covalent Ti-C or Al-O bonds is less likely. This may lead to the weaker adhesion of the carbon coating to the AlTiC surface, which causes the delamination of the coating in this region.

Through the application of a composite interlayer (Al-SiC or Al-TiN$_x$C$_y$), the problem of delamination of the coating on AlTiC can be solved. Bombarding the thin Si or TiN interlayer with energetic Ar$^+$ and C$^+$ ions prior to the deposition of the ta-C overcoat promoted the formation of strong bonds between the Si or TiN interlayer and the Al$_2$O$_3$ phase of the substrate [147, 148, 164]. The characterization of the chemical structure of these composite interlayers (as discussed in chapters 6 and 7) has confirmed the formation of strong covalent bonds between the substrate, interlayer and the ta-C coating. In addition, the formation of a very strong Si-C or TiC covalent network remarkably bonds the ta-C overcoat to the interlayer. These two phenomena are directly responsible for enhancing the adhesion of the ta-C overcoat to the AlTiC substrate and clearly justify the absence of delamination and improved durabilities of the coatings on *Head-3 and Head-4*.

### 8.3.2  *Difference between conventional Si and composite interlayer*

A thin Si interlayer (less than 2 nm) has been working well for hard disk head sliders [114, 128] in improving the durability of the head overcoat. A question could be asked as to whether conventional pure silicon can effectively be used as an adhesion layer on tape drive heads. To answer this question, the durability of the coatings of tape drive heads with conventional Si interlayer and with composite interlayer was compared in a real head/tape interface. In this experiment the thickness of both interlayers was almost

the same at about 2 nm, and the thickness of the ta-C overcoats was about 10 nm. In the wear tests, 340 km of tape was run over both heads and finally the surfaces of the heads were studied using SEM and AES. SEM images of the coated head surfaces with conventional Si and composite interlayers are shown in Figure 8-12(a) and (b) respectively. The formation of deep scratches on the coated head surface with conventional Si interlayer after the wear test is clearly evident in Figure 12(a). However, the situation of the head surface with a composite interlayer (Figure 12(b)) was in marked contrast to that with a conventional interlayer as shown in Figure 12(a).
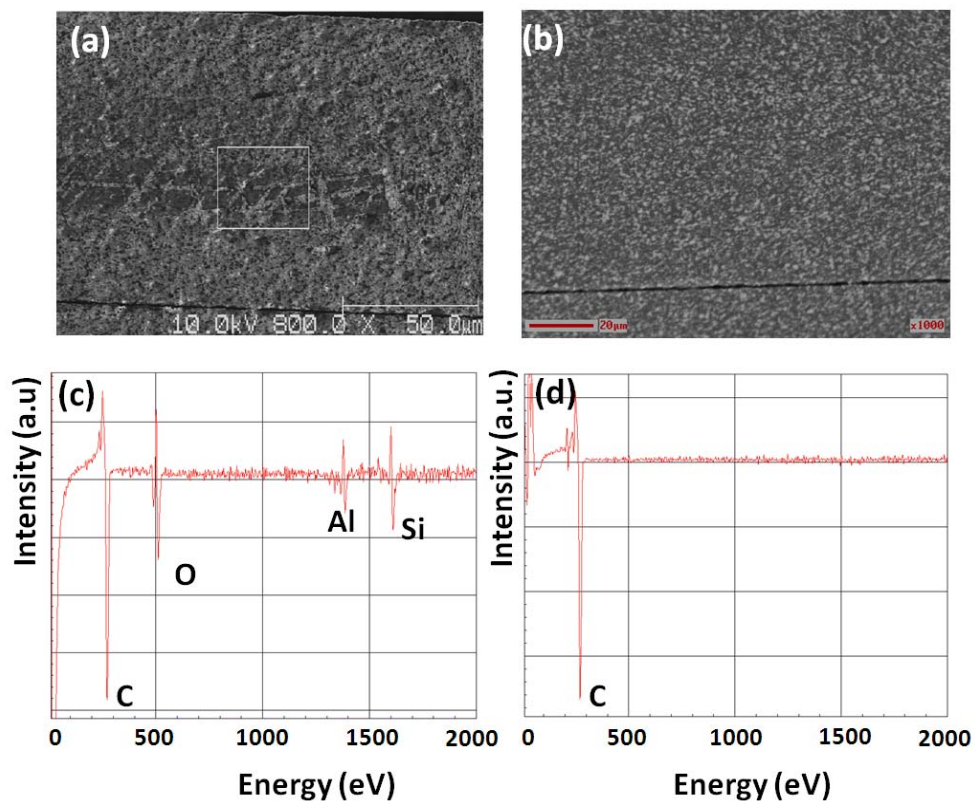


**Figure 8-12** SEM image of the surface of the head with (a) conventional Si interlayer, (b) with composite interlayer, AES spectrum of the head coating with (c) conventional Si interlayer, and (d) with composite interlayer after running 340 km of tape over the heads

The latter surface still looked uniform and had no visible scratches. The AES wide spectra of the head surfaces with conventional Si and with composite interlayers are shown in Figure 8-12(c) and Figure 8-12(d). As can be seen in Figure 8-12(c), the

spectrum shows a strong C peak, implying that there was still a considerable amount of carbon on the head surface. However, the existence of the clear peaks of Al, O, and Si indicated that this carbon film was scratched and the scratches were deep enough to reach the Si interlayer and AlTiC substrate. In comparison, the surface of the head with a composite interlayer (Figure 8-12(d)) did not show any evidence of the Si or AlTiC elements, which supports the idea of the existence of a uniform ta-C overcoat on the head surface.

From this result, it is understood that although a conventional Si interlayer can improve the adhesion of the ta-C coatings on the AlTiC ceramic (in comparison with ta-C coatings without any interlayer or ta-C coating pre-treated with $C^+$ ions), its improvement is not as good as that of the composite interlayer, and is still not enough to completely prevent the coating from delamination or being scratched in longer wear tests. This difference in the behavior of these two coatings is directly associated with the mechanism by which Si or the composite interlayer adheres to the AlTiC surface [164].
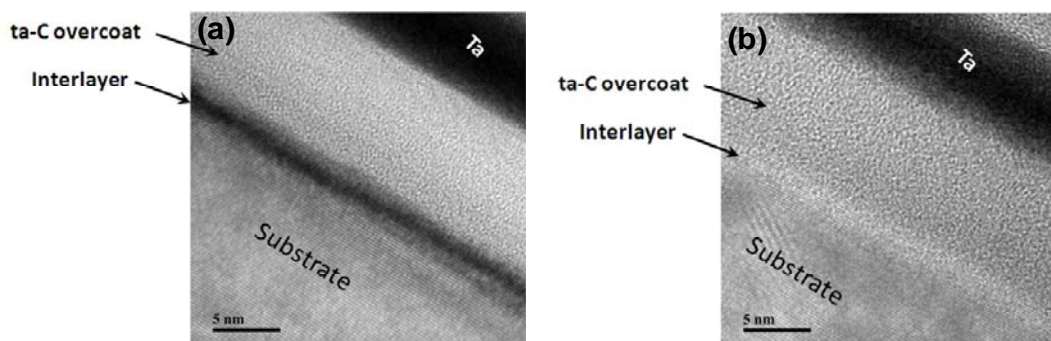


**Figure 8-13** Cross-sectional TEM image of 10 nm ta-C overcoat (a) with composite interlayer and (b) with conventional Si interlayer

The cross-sectional structure of the ta-C overcoats with conventional Si and composite interlayers are depicted in Figure 8-13. As explained earlier, the formation of chemical bonds such as Si-O-C and Al-O-Si is responsible for the improved adhesion of Si to

the AlTiC surface. However, when the Si layer is bombarded by energetic $Ar^+$ and $C^+$ ions, more effective direct and recoil implantation of ions at the AlTiC/Si interface will take place. This phenomenon leads to the formation of an atomically mixed interlayer that, in addition to Si, contains a considerable amount of Al, O, and C. The development of such a mixed interface greatly increases the possibility of the formation of Si-O-C and Si-O-Al bonds between the interlayer and substrate. On the other hand, due to the bombardment of the interlayer with more energetic $C^+$ ions, more Si-C bonds will be formed compared to the conventional Si interlayer.

### 8.3.3 *Wear-life of ta-C coating with Al-Si-C or Al-TiN$_x$C$_y$ composite interlayer*

In order to measure the wear life of the ta-C coating with a composite Al-Si-C or Al-TiN$_x$C$_y$ interlayer, 1000 km of tape was run over the *Head-3* and *Head-4* in longer wear tests. After the tests, the surfaces of the heads were analyzed by AES. Figure 8-14(a) shows the wide AES spectrum of the coating with Al-Si-C interlayer (*Head-3*) near the read/write elements. This spectrum shows strong C and Si peaks accompanied by smaller Al and O peaks. There is no clear evidence of Co in this spectrum. On the other hand, in the AES spectrum of the surface of *Head-4* (with Al-TiN$_x$C$_y$ interlayer), as can be seen in Figure 8-14(b), only a strong C peak and a very small O peak are detectable. In addition, there is no clear peak of Al, Ti or Co from the substrate in this spectrum, implying that the surface is still covered with a carbon film thicker than 2 nm.
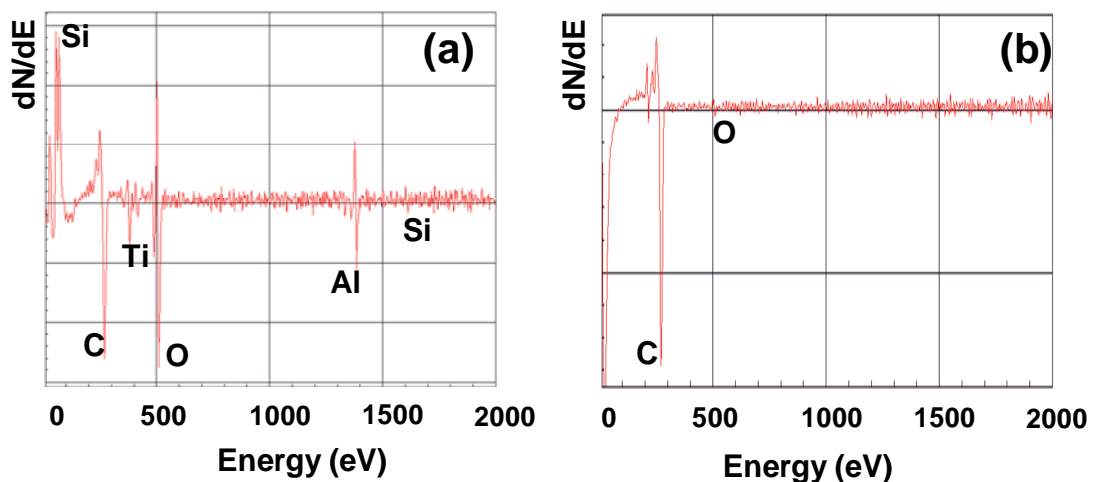
**Figure 8-14** AES spectra of (a) *Head-3* with an Al-Si-C composite interlayer and 10 nm ta-C coating after the running of 1000 km tape over the head, and (b) *Head-4* with an Al-TiN$_x$C$_y$ composite interlayer and 10 nm ta-C coating after the running of 1000 km tape over the head

The distribution of the available elements on the surface of *Head-3* (i.e. Si, O, Al, Ti, and C) is illustrated in the AES elemental mapping image (Figure 8-15). It can be seen that the surface of the AlTiC is covered with a mixture of C and Si. There is also minor evidence of Al belonging to either the existing aluminium in the composite interlayer or the Al$_2$O$_3$ phase of the AlTiC, which was detected because of the thinness of the remaining film on the surface. This data indicates that after the sliding of 1000 km tape, the head coating has become thin enough to either reach the composite interlayer or to detect the Auger electrons from the substrate.
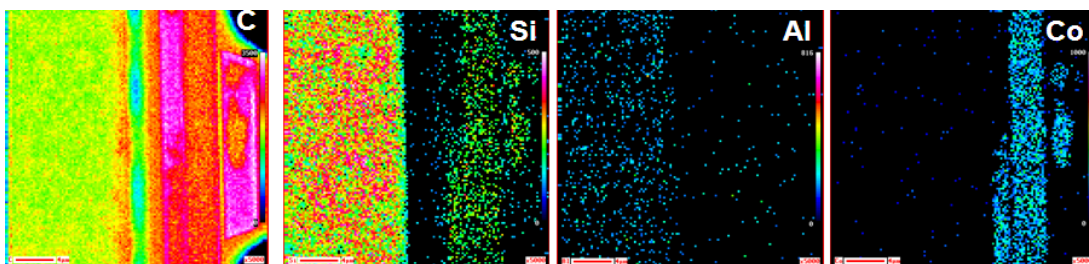


**Figure 8-15** AES surface elemental mapping image of Head-3 with composite interlayer and 10 nm ta-C overcoat after 1000 km wear test

According to this result, the thickness of the carbon coating on the read/write element is generally higher than that of the other regions. For this reason, on the major parts of

this area, the intensity of Si is not as high as that on the AlTiC surface. The Co AES image also suggests that the coating on the magnetic pole and shield is thicker and only small worn patches (with exposed Co) are detectable. However, the ta-C coating on the shared shield/pole was almost worn out and the Si was reached. As can be seen in the Si and Co windows, the intensities of Si and Co (especially) are strong in these areas. This result generally indicates that through the application of a composite interlayer, the problem of delamination has been completely solved and the protective overcoat was gradually worn off rather than being peeled off the surface.

AES elemental mapping was repeated for *Head-4* (with Al-TiN$_x$C$_y$ interlayer) after the wear test against 1000 km tape. It is very clear from this result that even after a wear test with 1000 km tape length, the whole surface is still covered with a uniform ta-C overcoat without any delamination. As can be seen, the C film was still thick enough to prevent any signal from the Ti, N, or Al elements in the interlayer from being detected. This result again proves the effectiveness of the application of an AlTiN$_x$C$_y$ composite interlayer to bond the ta-C overcoat to its substrate. These findings are also in agreement with the ball-on-disk tribology results on the flat AlTiC surfaces as reported in chapters 7.

AES depth profiling was used to estimate the thickness of the ta-C coating left on the AlTiC substrate and read/write elements of *Head-4* after the wear test. By a comparison between the depth profile of the reference surface (not worn area) of this sample (Figure 8-10(a)) and those of the head coating on the AlTiC substrate and read/write elements after the wear test (shown in Figures 8-17 (a) and (b)), and also by considering the initial thickness of the ta-C coating (8 nm as measured by TEM in Figure 8-7(b)), the minimum thickness of the ta-C coating left on the AlTiC substrate and read/write elements of the head is estimated to be approximately 3 nm and 6 nm

respectively. In other words, after a wear test with 1000 km of tape, more than 35% of the ta-C coating is still protecting the surface.
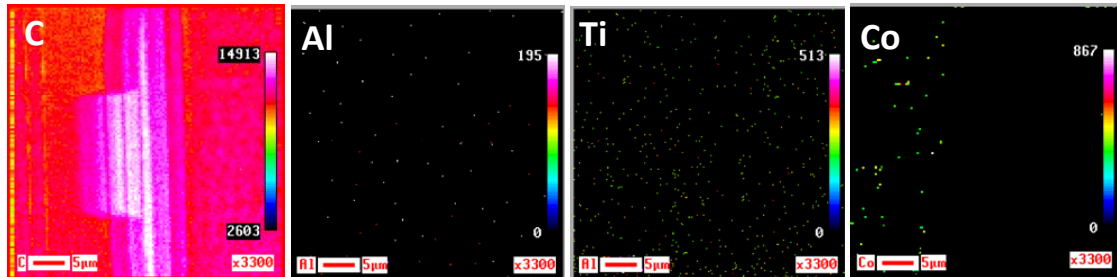


**Figure 8-16** AES surface elemental mapping image of *Head-4* with AlTiN$_x$C$_y$ composite interlayer and 8 nm ta-C overcoat after 1000 km wear test
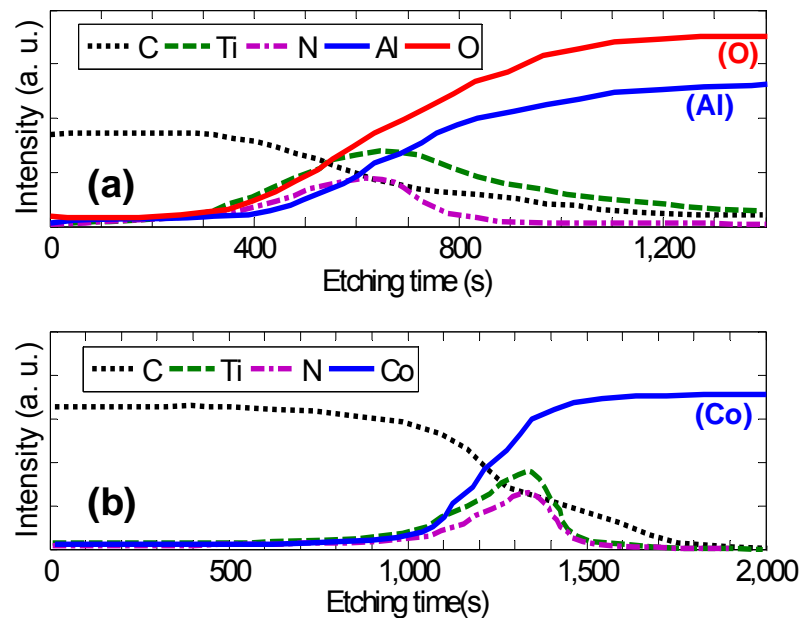


**Figure 8-17** Depth profile of the ta-C coating of *Head-4* (with Al-TiN$_x$C$_y$ interlayer) on (a) AlTiC substrate, and (b) on read/write element after 1000 km wear test

Comparing the performanace of the ta-C coated heads with Al-Si-C and Al-TiN$_x$C$_y$ interlayers (using a linear extrapolation for the wear rate of the coating), we can conclude that durability of ta-C coating with Al-TiN$_x$C$_y$ interlayer has been improved by 60%. In other words, this coating is able to protect the surface of the head up to about 1.6 million meters after which the tape will make contact with the interlayer.

The durability of the ta-C coating on the read/write elements is expected to be much better than that on the AlTiC substrate.

Pole tip recession and stain build-up are the main sources of increased magnetic spacing in tape drives. In this study, we have demonstrated how the proposed surface pre-treatment techniques are able to enhance the wear resistance of the coatings. Even though the coatings developed with the composite interlayers may not be able to completely protect the head over the life of the drive, they are still able to considerably postpone the pole tip recession and stain build-up, and thus keeping the magnetic spacing low for much longer time.

## 8.4 Conclusion

In this work, the effect of application of two different composite interlayers (Al-Si-C and Al-TiN$_x$C$_y$) on the wear life of magnetic tape drive heads with ≤10 nm ta-C coating was studied, and the results were compared with that of conventional ta-C coatings. The results confirmed that conventional ta-C coatings were not able to protect the surface for a long time. It was also understood that bombarding the surface with energetic C$^+$ ions prior to deposition of the ta-C coating was able to improve the durability of the coating on the metallic elements of the head (read/write elements). However, this improvement on the AlTiC surface was not that significant. Although this method could prevent the complete removal of the ta-C coating from the surface of read/write elements, the coating on the ceramic part of the head was partially delaminated after the 170 km wear test. In contrast, the application of composite interlayers was able to dramatically increase the durability of the coating. These interlayers chemically bonded the ta-C overcoat to the substrate, and hence enhanced the resistance of the ta-C films to delamination. These films did not peel off from the

surface even after the 1000 km sliding wear test. The ta-C film with an Al-TiN$_x$C$_y$ composite interlayer also functioned better than a coating with an Al-Si-C interlayer, and presented 60% better durability. The ta-C coating with an Al-Si-C interlayer was worn off and reached the Si containing interlayer after the 1000 km wear test, whereas the head coating with Al-TiN$_x$C$_y$ composite interlayer had at least 3 nm of ta-C film left on the surface after the wear test for the same duration. These results are very promising and the application of such interlayers to improve the durability of the coating can be introduced to develop head coatings that can protect the tape drive heads based on the current standards of the tape drive industry.

# Chapter 9: Effect of relative humidity on tribological performance of the ta-C head coating

## 9.1 Introduction

In the previous chapters, the effects of different surface pre-treatment methods on the wear life and tribological performance of ta-C coatings on recording heads were studied. In these investigations, the coated recording heads were tested against LTO3 tapes in the normal environment of a clean booth (26±2.0 °C and 45±5% RH). According to the results, among different tested coatings, a ta-C overcoat with an AlTiN$_x$C$_y$ interlayer showed the best performance (wear life of ~1.6 million meters in terms of the length of the tape passed over the head).

Previous studies have shown that the tribological properties (wear durability and friction) of DLC films and, more specifically, ta-C films, strongly depend on environmental parameters such as the type of constituent gases (air, inert gas, etc.), temperature, and relative humidity (RH) [167-174]. The effect of these parameters have been extensively studied for different types of DLC films (hydrogenated, hydrogen-free, and doped DLC) with a broad range of thicknesses in various environments such as normal, dry and humid air, as well as inert (nitrogen or argon) ambient gases. A good summary of all these can be found in a review done by Ronkainen and Holmberg [175]. The general findings of all these studies imply that among different types of DLC films, ta-C films have shown the best tribological properties in a normal environment (where humidity and hydrocarbon species exist). In dry air (RH<10%) or inert environment, hydrogenated DLC coatings have shown a super-low friction and wear rate. However, the wear resistance of hydrogen-free DLC films (a-C or ta-C) was observed to have degraded in dry environments. Although

these earlier studies provide a valuable insight into the performance of amorphous carbon coatings in different environments, it should be noted that almost all of these findings were based on results of fundamental tribological tests such as ball-on-disk tests rather than functional tests in real applications.

The effect of environmental conditions on the performance of magnetic tape drives and, more specifically, tribological interactions at the head/tape interface, is an important area for research. In some earlier studies, it has been shown that environmental factors (humidity and temperature) have important effects on the wear, pole tip recession and stain build-up of the recording heads with or without protective coatings (e.g. $Cr_2O_3$ coatings) [16, 176, 177]. However, the effect of environmental conditions on the wear durability and tribological performance of DLC-coated heads has not been well studied.

According to the 2008 INSIC International Magnetic Tape Storage Roadmap [178], the generic operating temperature and humidity ranges for tape are stated as 10-45 $^\circ$C and 10-80% RH, respectively. ta-C are quite stable films at room temperature and their properties do not change in the above-mentioned temperature variation range [106, 179-181]. However, it is still important to study the effect of humidity variation. Considering that air is the most commonly – if not the only – used environmental element in magnetic tape drive applications, and that relative humidity is one of the main factors affecting the tribological properties of DLC coatings, the wear performance of a 10 nm ta-C coating with a $TiN_xC_y$ interlayer was investigated as a function of relative humidity, and the results are reported in this chapter.. In this study, a newer generation of LTO tape (i.e. LTO5) was used for the wear tests and its effect on the wear life of the coating was investigated.

## 9.2   Experimental Procedure

The procedures of surface modification of LTO4 heads with a 1.5 nm $AlTiN_xC_y$ interlayer and deposition of a 10 nm ta-C overcoat have been extensively explained in Chapters 7 and 8. After being coated, the heads were installed on the positioning stage and load cell assembly of the functional tape drive tester. LTO5 tape cartridges (provided by *Hewlett-Packard, Boise, Idaho, US*) were used for the wear tests. These tapes are less abrasive and smoother ($R_a$= 1.5 nm, based on a scan size of $1\times1$ $\mu m^2$) than the older generation of LTO3 ($R_a$= 2.5 nm). The wear tests were conducted using almost the whole length of the tape cartridge (~800 m) at a constant speed of 5 m/s and a tension of 0.7 N over 665 cycles, which corresponds to ~1000 km of tape length. In order to control the wear test environment (relative humidity), the tape drive was enclosed in a chamber properly sealed from the outside ambient environment (Figure 9-1).



**Figure 9-1** Wear tests setup enclosed in the environmental chamber connected to pure dry air cylinder

The humidity of the chamber was controlled by purging the chamber with pure dry air (mixture of 21.0±1.0% $O_2$ and 79±1.0% $N_2$ with water content of <3.0 ppm and total hydrocarbon content of < 5 ppm). The temperature, relative humidity and dew point of

the chamber were continuously monitored using a hygrometer (in real time), and the flow rate of the dry air was adjusted to maintain the required RH in the chamber. Wear test experiments were conducted at a constant temperature of 28±0.5 °C and at three different RH values of 40%, 10% and <1.0%. In order to maintain RH<1.0% (the minimum RH that the hygrometer could measure), the flow rate of dry air was increased (the pressure of the chamber was maintained to be slightly higher than the outside atmosphere) such that the pure air was always flowing out from the chamber vent. The test conditions are summarized in Table 9-1.

**Table 9-1** Tape and environmental conditions used for the wear tests

| Test conditions | Environment | | Tape | | |
|---|---|---|---|---|---|
| | RH | Temperature | Tension | Speed | Length |
| Test 1 | 40% | 28±0.5 °C | 0.7 N | 5 m/s | 1000 km |
| Test 2 | 10% | | | | |
| Test 3 | <1.0% | | | | |

The first test condition (28°C, 40% RH) is referred to as *normal atmospheric* condition, whilst the two other conditions (28°C, 10% RH and 28°C, <1% RH) are referred to as *dry air* and *pure air* conditions respectively. Following each wear test, the coating on each of the heads was examined using scanning electron microscopy (SEM) and Auger electron spectroscopy (AES).

## 9.3 Results and discussion

The surfaces of the coated heads after the wear test were assessed using AES wide scanning. Figure 9-2(a) shows the AES wide scan of the region near the read/write channel (Figure 9-2(b)), which consist of the AlTiC substrate, read/write elements and

the Al$_2$O$_3$ insulator. According to this spectrum, the surface of the head was completely covered with ta-C film. Although this result confirmed the existence of a carbon coating thicker than the AES information depth (which is about 0.5-2 nm) on the head surface, it did not provide any information about the real (absolute) thickness of the coating.
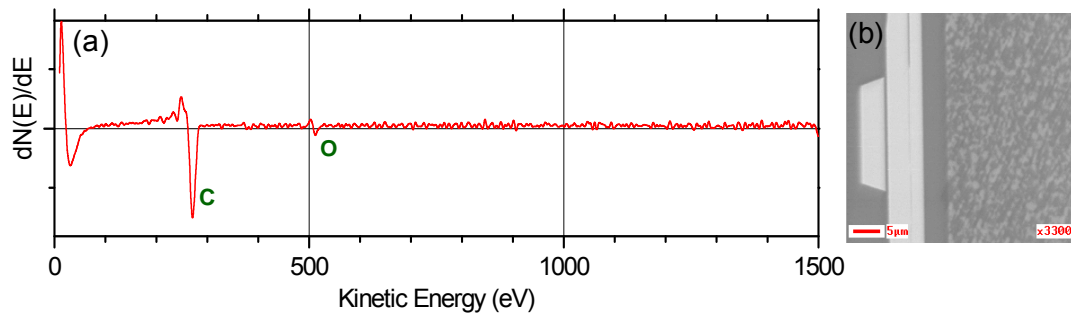


**Figure 9-2 (a)** AES wide scan of the region near the read-write channel of the coated head after the wear test in normal environment (RH=40%) **(b)** SEM image of the region from which the AES spectrum has been acquired.

AES depth profiling on the worn (Figure 9-3(a)) and unworn (Figure 9-3(b)) regions of the head was used to estimate the thickness of the coating of the head after the wear test in a normal environment. As can be seen in Figure 9-4, the sputtering time corresponding to 10 nm of ta-C was 1,200 seconds (i.e. a timing of 1,200 seconds was required to sputter-etch the 10 nm ta-C overcoat and reach the interlayer). Using the same ion parameters for depth profiling of the worn coating, a timing of about 900 seconds was required to reach the interlayer. According to this result, the thickness of the ta-C coating after the 1,000 km wear test against LTO5 tape in a normal environment was estimated to be about 7.5 nm. In other words, the running of 1,000 km of tape over the head was able to remove about 2.5 nm of the ta-C coating. Assuming a linear relation between the distance of the tape run over the head and the removal rate of the ta-C coating, the wear life of the ta-C can be estimated to be about

4,000 km. This value is about 2.5 times more than the wear life of the same coating

running in contact with LTO3 tape.
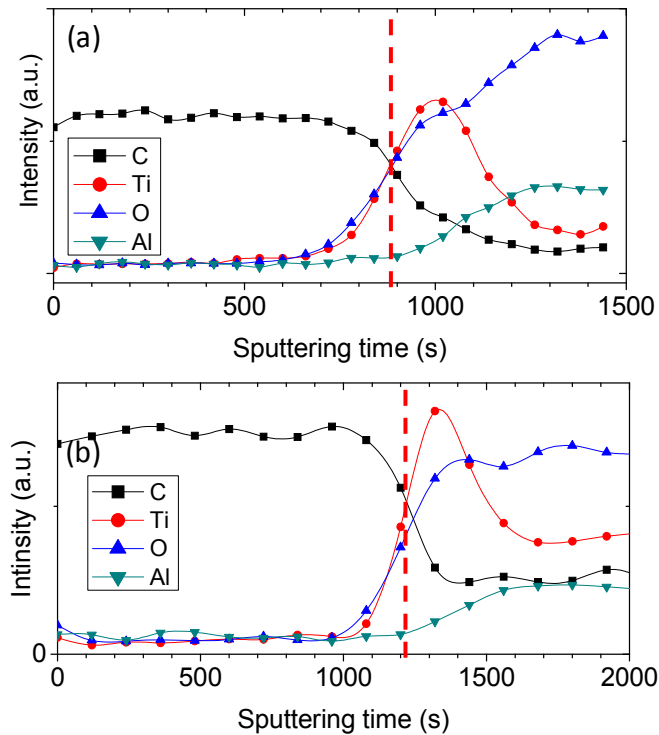


**Figure 9-3** AES depth profile of (a) ta-C coating after1000 km wear test in normal environment and (b) reference coating (not worn). This result implies that the thickness of the ta-C coating after the wear test is about 7.5 nm.
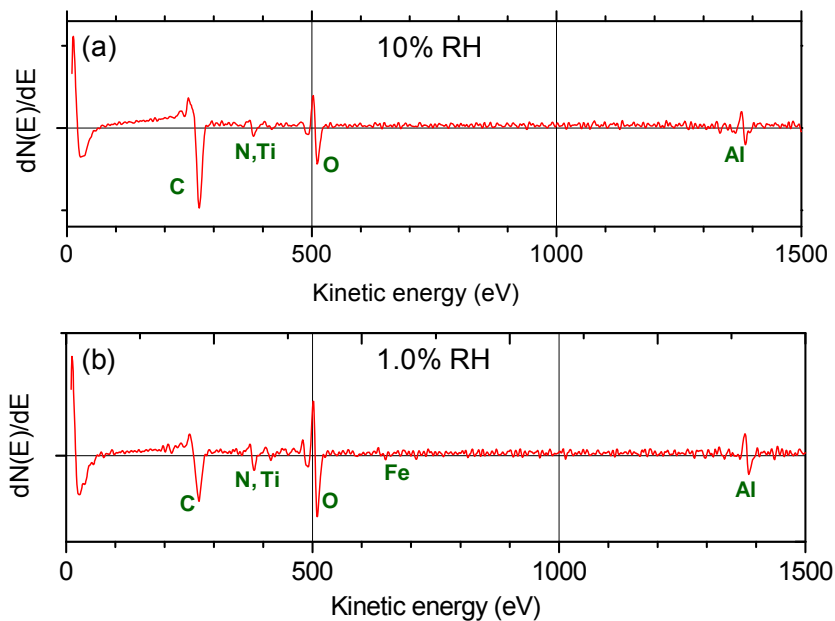


**Figure 9-4** AES wide scan from the region near the read/write channel of the ta-C coated heads after 1,000 km wear test in (a) dry (10% RH) and (b) pure (1.0% RH) air. The existence of Al, O, and Ti peaks imply that the coating has been damaged and the AlTiC is exposed.

In order to gain more insights into the effect of humidity on the wear of the ta-C coating, the surface of the coated head tested in dry and pure air was also assessed by AES. Figures 9-4(a) and 9-4(b) show the AES spectra of the heads at the region near the read/write channels, after the 1,000 km wear tests in dry (10% RH) and pure (1.0% RH) air, respectively. In these spectra, the peaks of Ti, Al, and O belonging to the AlTiC and the $Al_2O_3$ insulator are clearly evident. From this result, it can be inferred that the 10 nm ta-C of these heads after the wear test had been worn off and the surface of the heads (at least in some regions) was exposed to the electron beam.

In order to gain a better understanding of the quality of the coatings and the distribution of the existing elements on the surface of the head, AES surface elemental mappings (AES images) for the elements detected in the AES spectra shown in Figure 9-4 were acquired for the samples tested in low humidity. In these images, a higher concentration of an element in its specific window is shown in a lighter color while the absence or a lower concentration of the elements is shown to be in a darker shade.
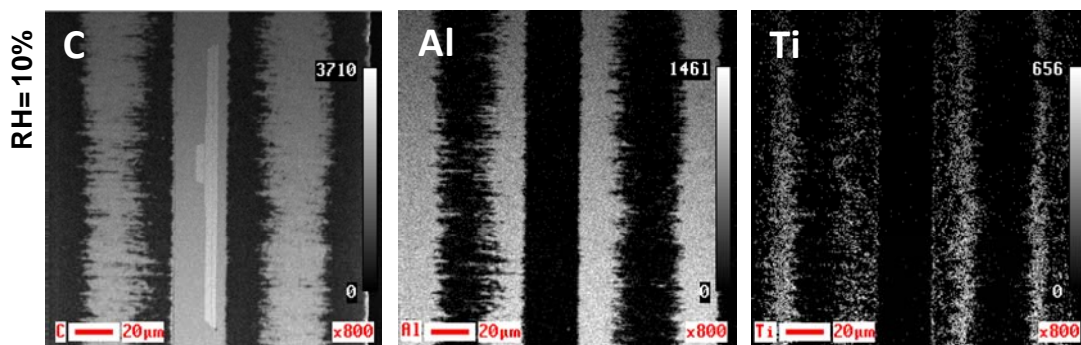


**Figure 9-5** AES surface elemental mapping image of the ta-C coated head tested in dry air (10% RH) after 1000 km wear test, indicating partial removal of the coating

Figure 9-5 shows the distribution of C, Al, and Ti on the surface of the head tested in dry air (10% RH). As can be seen in the C, Al, and Ti windows, the surface of the AlTiC substrate near the edges of the AlTiC block has partially lost its carbon overcoat (this surface is darker in the C image, and is in lighter in the Al image). The removal

of the carbon overcoat in the regions very close to the edges of the AlTiC substrate (as can be seen in the left and right extremities of the C image in Figure 9-5) could be due to the re-profiling of the sharp edges of the AlTiC block, which usually occurs for new heads, and cannot be relied on to gauge the wear resistance of the coating. However, in addition to the worn edges of the AlTiC block, wear-susceptible regions can be found near the read/write channels as well. In Figure 9-5, these regions are detectable in the central parts (near the read/write channel) of the C image (darker regions) or the lighter regions of the Al image. Except for these worn stripped off regions, the rest of the probed area was still covered with a ta-C coating. In the Al and Ti windows of Figure 9-5, these regions can be seen in black color. This result mainly implied that the head coating tested in dry environment has generally undergone severe overcoat damage. In other words, by decreasing the humidity of the test environment, the wear resistance of the coating degraded.

Figure 9-6 shows the AES image of the head tested in pure air (<1.0% RH). This result indicated that the ta-C coating of the AlTiC substrate of the head (left side of the C image in dark gray color) was completely stripped off. It can be seen that the ta-C coating of the AlTiC closure (on the left side of the read/write channel) was also severely damaged and only a small area was still covered with carbon. Generally, it can be concluded that the wear of the ta-C coating in pure air was more severe than that in dry air with finite water content. The results clearly highlight the important role of the humidity content of the environment on the wear performance of the head ta-C coating.
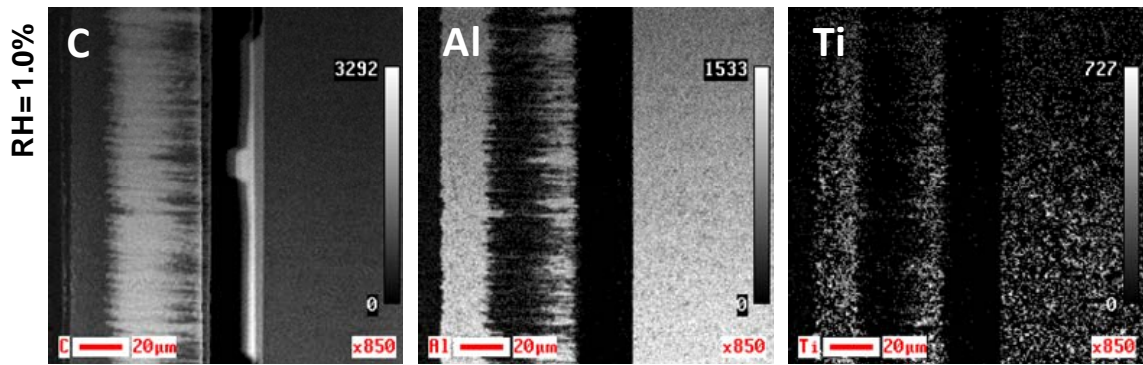
**Figure 9-6** AES surface elemental mapping image of the ta-C coated head tested in pure air (1.0% RH) after 1000 km wear test, indicating severe damage of the coating.

According to the literature, the performance of ta-C films in different environmental conditions (different RH values) can be explained in terms of their surface chemical state. As explained in Chapter 3, the majority of the C atoms in the structure of the ta-C film are connected together by tetrahedral C-C $sp^3$ ($\sigma$) bonds. On the surface, a $sp^3$ hybridized C atom is connected to its three neighboring atoms by three $\sigma$ bonds, leaving the fourth $\sigma$ bond free and dangling out of the surface. In a normal (humid) environment, water molecules or hydrocarbon airborne species can get adsorbed (by physisorption or chemisorption) on the surface of the ta-C film and passivate the surface by terminating the existing dangling bonds. During the wear test in a dry environment (pure air, inert gas, or vacuum), mechanical interaction (friction) between the surfaces and/or the consequent thermal desorption may remove these adsorbed species and expose the dangling bonds. These exposed $\sigma$ bonds are very active and are able to form strong covalent interactions with the atoms on the surface of the counterface [171, 182, 183].

According to our results, the ta-C coating presented good wear resistance in a normal environment (RH 40%). However, decreasing the humidity content of the environment had an adverse effect on the wear life of the coating, and this effect worsened with a further decrease in the relative humidity. This behavior can be explained based on the

above-mentioned mechanism. In a humid environment, the existing water molecules and/or hydrocarbon species can serve as a reservoir and continuously replenish and terminate the new dangling bonds, which had been formed on the surface due to wear and/or thermal desorption. This mechanism is able to decrease the bond strength between the interacting surfaces (i.e. the active dangling $sp^3$ sites of the ta-C film and the tape material) to, for example, about 0.21 eV per bond, which is typical for the hydrogen bonding of water molecules at C=O sites [184]. Decreasing the bond strength between the interacting surfaces weakens the atomic adhesion junctions between the contacting surfaces. On the other hand, in dry air condition, this surface passivation process fails to function due to the lack of a sufficient number of water molecules. This leads to the formation of strong bonds between the surface of the coating and that of the tape counterface, giving rise to material removal from the ta-C coating due to adhesive wear [185]. This interaction at the head/tape interface is more severe in a pure air environment (with almost zero content of hydrocarbon species or water molecules) and leads to further wear of the ta-C coating.

By removing the ta-C film, the head bearing surface (AlTiC ceramic) will be in direct contact with the tape. In a normal environment, $H_2O$ molecules could saturate the active sites on the head material surface; however, in pure air (RH < 1%), the head surface remains active after removal of the coating, at where strong chemical (electrostatic, ionic, or covalent) bonds and therefore strong adhesive junctions may form between the different components of the head and the tape media. If the bond strength of these newly formed adhesive junctions is greater than that between the tape components (e.g. magnetic layer and the polymeric binder of the tape), material transfer from the tape to the head surface may take place. This is technically known as

stain formation [10, 11, 17, 176, 186].
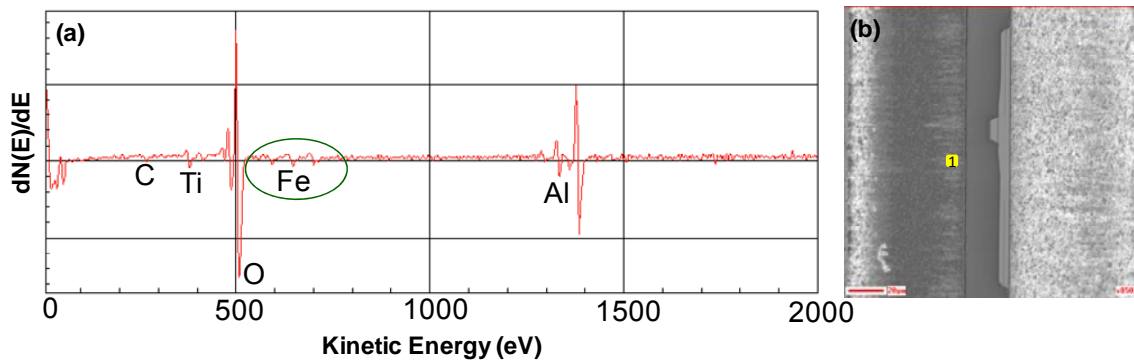


**Figure 9-7** (a) AES spectrum from the head surface after wear test in pure dry air, indicating formation of a Fe-containing transfer layer on the head surface. (b) SEM image of the worn head showing the point on which the AES spectrum has been acquired.

Figure 9-7(a) shows the AES point spectrum of an area near the read write channels of the head tested in pure air (labeled as point-1 in Figure 9-7(b)). The presence of Fe peaks in this spectrum imply that material transfer from the head magnetic layer ($Fe_2O_3$ magnetic pigments embedded in polymeric binder) to the head surface has taken place. This result is consistent with the mechanism described for adhesive material transfer between the head and media in low humidity conditions.

## 9.4 Conclusion

In this chapter, the effect of relative humidity of the working environment on the tribological (wear) performance of the ta-C coating was studied. In addition, LTO5 tape was used for the wear experiments in this work. ta-C coated heads were tested in three different environments of normal (40% RH), dry (10% RH), and pure (<1% RH) air. After running a total length of 1,000 km tape over the coated heads, their surfaces were assessed using Auger electron spectroscopy. The results revealed that the 10 nm ta-C film with an $AlTiN_xC_y$ interlayer presented the highest wear life in a normal environment (only 2.5 nm of the coating was removed). In addition, it was found that

the application of the LTO5 tape can improve the wear life of the coating by up to 2.5 times compared to LTO3 tape. However, the results showed that at a constant temperature, the wear life of the ta-C coatings was a function of humidity, and wear resistance degraded as the relative humidity decreased. It was also found that very low humidity not only decreased the wear life of the head coating, but it also increased the likelihood of material transfer from the tape to the head surface as well as the formation of head stain. This behavior can be attributed to the surface chemistry at the head/tape interface. In humid air, water and hydrocarbon molecules are able to saturate the dangling bonds and passivate the surface, which decreases the chance of formation of strong adhesion junctions between the two surfaces and therefore decreases the coating removal due to adhesive wear. On the other hand, due to an insufficient supply of $H_2O$ molecules in very dry or pure air, the dangling bonds will remain active and strong adhesion junctions (with high bonding strength) may form between the tape and coating, which gives rise to wear of the coating and, in more severe cases, material transfer from the tape to the head surface. These conclusions were in agreement with the findings of the previous studies investigating the effects of the environment on the wear performance of hydrogen-free carbon films tested by fundamental tribological techniques.

# Chapter 10: Surface modification of Co magnetic media with a mixture of Si and C atoms

In this chapter, the concept of the formation of a mixed (composite) layer by bombarding a thin Si layer by energetic $C^+$ ions (as explained in chapter 6) was used to develop a new surface treatment method for hard disk media. In this work an ultra-thin layer of Si with a total thickness of $\leq 1$ nm was deposited on the cobalt magnetic film. This layer was bombarded with $C^+$ ions at an ion energy of 90 eV using filtered cathodic vacuum arc (FCVA) technique. The structure and tribological properties of the modified surface of the Co media were examined by means of X-ray-photoelectron spectroscopy (XPS), Auger electron spectroscopy (AES), atomic force microscope (AFM) based scratch tests, and ball-on-flat wear tests. Bombarding the Si layer with $C^+$ ions led to formation of an ultrathin Si/C mixed layer. The wear resistance of the Co sample with the Si/C mixed layer was compared to that of a commercial magnetic disk media with a 3 nm carbon overcoat and 1.4 nm of lubricant. In this comparison, a cobalt sample with a Si/C mixed layer showed better tribological properties. The formation of C-C and Si-C bonds at the outermost layer and the bulk of the Si/C film as well as the formation of chemical bonds between the Co surface and the mixed layer was found to be an important factor in improving the tribological properties (such as higher wear resistance and lower friction) of the treated Co surface.

## 10.1 Introduction

As explained in sections 2-1-1 and 3-4-1, hard disk drives (HDDs) of the next generation aim at achieving magnetic recording areal densities beyond 1.0 Tbit/in$^2$ [187, 188]. The properties of the overcoat on the disk media and air bearing of the recording head are very critical for wear and corrosion protection. An ideal material

for this application should be able to form a continuous (pinhole free), hard (but not brittle), dense, and inert ultra-thin overcoat which demonstrates excellent adhesion to the slider and media surface [1, 52, 189].

Decreasing the thickness of conventional carbon overcoats poses significant issues to their tribological and corrosion performance. Ultrathin DLC films (thinner than 2-3 nm) deposited by conventional deposition techniques like direct ion beam or sputtering have failed to form continuous films, such that corrosion protection becomes inadequate [189, 190]. In addition, the $sp^3$ content and consequently, the wear resistance of these films decrease when the films become very thin. This necessitates the development of new processes (in terms of deposition techniques and materials) that can help in decreasing the thickness of the overcoat while improving its desired properties required for the next generation of magnetic recording.

Filtered cathodic vacuum arc (FCVA) is a useful technique which allows deposition of continuous tetrahedral amorphous carbon (ta-C) films with thickness of less than 2 nm [191, 192] (further details about this technique have been explained in section 3-3-3). The critical properties of these films for application in the HDD industry, such as $sp^3$ content, density, hardness, stress, deposition temperature, and thermal stability have been studied by Bhatia et al. [43]. Exploiting the FCVA technique, novel surface modification techniques have been recently developed to produce an overcoat-free magnetic media with improved tribological and performance [193-195]. In this technique the magnetic media (Co or FePt) surface was bombarded with $C^+$ ions at an ion energy of 90 eV to produce a mixed layer of Co or FePt and carbon in the top 1 nm of the magnetic media surfaces. This mixed layer exhibited excellent tribological properties in terms of reduced coefficient of friction as compared with the bare Co or FePt surface and the commercial HDD media.

As a part of this PhD work, in order to further improve the tribological properties (in terms of friction, wear and scratch resistance) of the magnetic media, the concept of the formation of a composite film (as described in chapter 6) was further studied for surface modification of magnetic disk media with more than one element. Application of more than one element will allow us to further engineer the surface properties to achieve improved tribological performance. In this work, an ultra-thin layer of Si with a total thickness of 1 nm (deposited on the Co surface) was bombarded with $C^+$ ions using the FCVA technique to form a Si/C mixed layer. The tribological behavior (friction, wear and scratch resistance) of the modified surface was compared with that of commercial HDD media.

## 10.2 Experimental Procedure

Sample preparations were carried out in a class 1000 clean room with temperature and relative humidity of 22±0.5 °C and 50±5 % respectively. 10 mm × 10 mm square coupons of single crystal silicon wafers, pre-cleaned with acetone, isopropyl alcohol and $Ar^+$ plasma etching, were coated with 40 nm of Co by magnetron sputtering at a DC power of 60 W, with working and base pressures of $3\times10^{-3}$ and $2\times10^{-9}$ Torr respectively.

Surface modification of the cobalt was achieved in a three-step process.

- Step 1: A 5 nm Si film was deposited on the Co surface. The deposition of Si was conducted in the same magnetron sputtering chamber used for deposition of Co without breaking the vacuum while using an RF power of 150 W and working pressure of 3 mTorr.

- Step 2: The Si-coated cobalt samples were transferred to an FCVA chamber (*Nanofilm Technologies International Pte. Ltd., Singapore*). 1-2 nm of the outermost Si film which was exposed to the ambient environment was expected

to be oxidized [12]. The thickness of the Si layer was decreased to 1 nm by removing the top Si/SiO$_x$ layer (4 nm) using Ar$^+$ sputter-etching with ion energy of 500 eV within the FCVA chamber.

- Step 3: The FCVA technique was used for bombarding the surface with C$^+$ ions at 90 eV which embedded the ions into the remaining Si film. The embedment was carried out for 50 s.

Hereafter, this sample is referred to as Co-Si/C sample. Further details about the C$^+$ ion embedment technique used in this study can be found in section 4-2-1 and ref. [193-195]. The characterization of the surface and bulk of this mixed layer as well as the interface between this layer and the underlying magnetic film is very important for the potential application of the developed surface treatment method as a protective layer on the surface of magnetic disk.

For thicker films (thicker than the photo electrons escape depth), XPS depth profiling with argon ion sputtering can be used to identify the composition and chemical structure of the films and their interface with the underlying layers or substrate. However, because of the thinness of the SiC layer ($\leq$ 1nm) developed in the current work, which is below the information depth of XPS, conventional XPS depth profiling will not be able to provide accurate information from different levels of the thin layer.

On the other hand, because of the short mean free path of the photoelectrons, the contribution of different surface layers with respect to their underlying layers (substrate) can be enhanced by changing the photoelectron collection angles. It has been demonstrated that photoelectron emission depth (information depth) decreases by decreasing the photoelectron take-off angle (collection angle); and therefore, more surface sensitive analysis can be done at grazing take-off angles. This technique is known as angle resolved x-ray photoelectron spectroscopy (ARXPS) [109]. The

contribution of the surface atoms can be enhanced by decreasing the photoelectron take off angle with respect to the sample surface. On the other hand, increasing the collection angle increases the contribution of the atoms from deeper levels of the film. ARXPS enables researchers to study the chemical structure of the thin films in a non-destructive manner by acquiring the data at different take off angles (i.e. different surface sensitivities). In this work, because of the thinness of the SiC layer, and in order to acquire the maximum data from the surface and interface of the deposited layers and the Co surface, ARXPS analyses were preferred over XPS sputtering depth profiling to study the chemical structure of the thin layer. In our analysis, the photoelectron take-off angle was varied from 5° to 75° (with respect to sample surface), with intervals of 10°. The chemical structure of each level (associated to each take off angle) was precisely measured by acquiring a high resolution XPS spectrum ($Co_{2p}$, $Si_{2p}$ and $C_{1s}$) with energy steps of 0.1 eV.

In order to precisely measure the thickness of the Si/C mixed layer and also to study the structural characteristics of the substrate/coating interface, the cross-sectional structures of the Co-Si/C sample were observed by TEM. Details of the TEM sample preparation process can be found in section 4-4-1. Since the developed film is very thin and has an amorphous structure, it is very difficult to make a distinction between the Si/C layer and the epoxy adhesive used in the process of TEM sample preparation. To address this problem, a thin layer of a crystalline material (e.g. a metal film) can be deposited on the amorphous Si/C surface before application of the epoxy to the surface. Because of its good adhesion to the substrate, a thin film of Ta was used in this work.

The scratch resistance of the samples was qualitatively compared with that of bare Co and commercial HDD media using an AFM-based single asperity contact scratch test.

This experiment was conducted using a scanning probe microscope (*SPM: Innova, Bruker*) and a probe with a sharp natural diamond tip (with a tip radius of 40 nm as provided by the manufacturer) mounted on a stainless steel cantilever, with a spring constant of 277 N/m and contact sensitivity of 189 nm/V working in contact mode. An area of $1 \times 1$ $\mu m^2$ was scratched using a normal load of ~ 52 $\mu N$ and scanning rate of 0.9 Hz. The topography of the scratched region was measured by scanning a larger area surrounding the scratched area with the same tip but at a much lower normal load (~ 15 $\mu N$) and scanning rate of 1 Hz. A total of three independent measurements were performed randomly at different locations on the samples and an average value was taken for the scratch depth (if any) of every sample.

The effect of surface modification with Si/C mixed layer on the wear and friction properties of the Co media was examined by ball-on-flat testing using a CSM-Nanotribometer (*CSM, Switzerland*). A silicon nitride ball with diameter of ($2.0 \pm 0.1$ mm) was used as the counterface material. Wear tests were conducted at a constant normal load of 20 mN and a constant rotational speed of 100 rpm (linear speed = 0.01 m/s) for 10,000 cycles. The tests were done in a class 100 cleanroom with a temperature and relative humidity of $25 \pm 0.5$ °C and $50 \pm 0.5$ %. To evaluate the effectiveness of the developed mixed layers, the tribological tests under the same conditions were repeated on the commercial media. It should be noted that the commercial media had a 3.0 nm DLC overcoat covered with 1.4 nm of lubricant. At least three repetitions were carried out on different samples of the same batch (Co, Co-Si/C, and commercial media samples) and the average values of the coefficient of friction were reported. Following the wear tests, the surface modified Co-Si/C and commercial media samples were examined using Auger electron spectroscopy (AES).

Auger elemental mapping with image quality of 128×128 pixels was performed to determine the distribution of the C, Si, and Co on the surface.

## 10.3 Results

### 10.3.1 Structure of the Si/C mixed layer

Figure 10-1 shows the TEM image of the cross-section of the Co-Si/C sample. As can be seen from this image, the described method of surface modification led to the formation of an amorphous and continuous Si/C layer, with a thickness of 1.0±0.1 nm on the surface of the Co magnetic film.
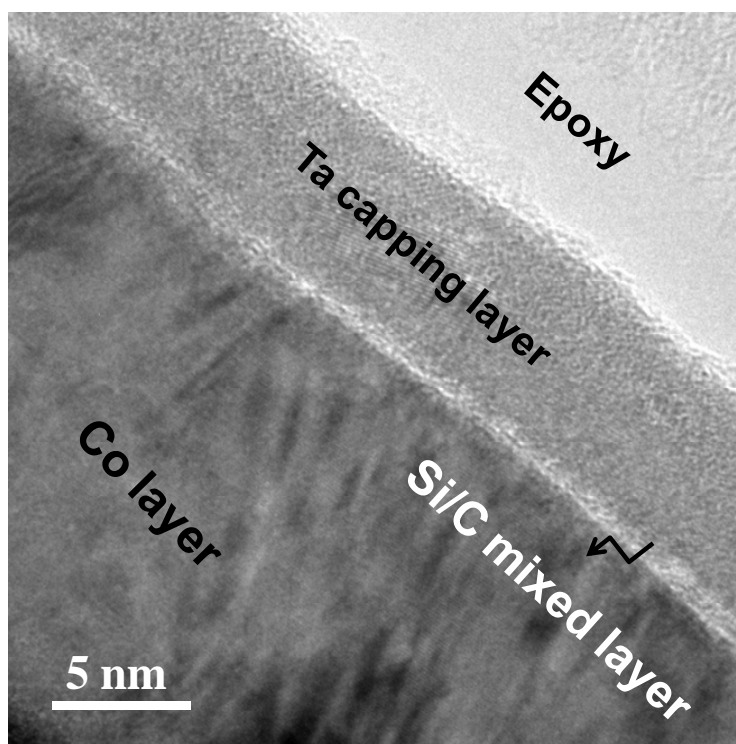


**Figure 10-1** TEM cross-section image of the Co magnetic film modified with Si/C mixed layer

The chemical composition of the formed Si/C layer was examined by ARXPS analysis. For this purpose, XPS spectra were acquired as a function of photoelectron the take off angle. Figure 10-2 shows the $Si_{2p}$, $Co_{2p3}$, and $C_{1s}$ spectra at different take off angles ranging from 5° to 85°.
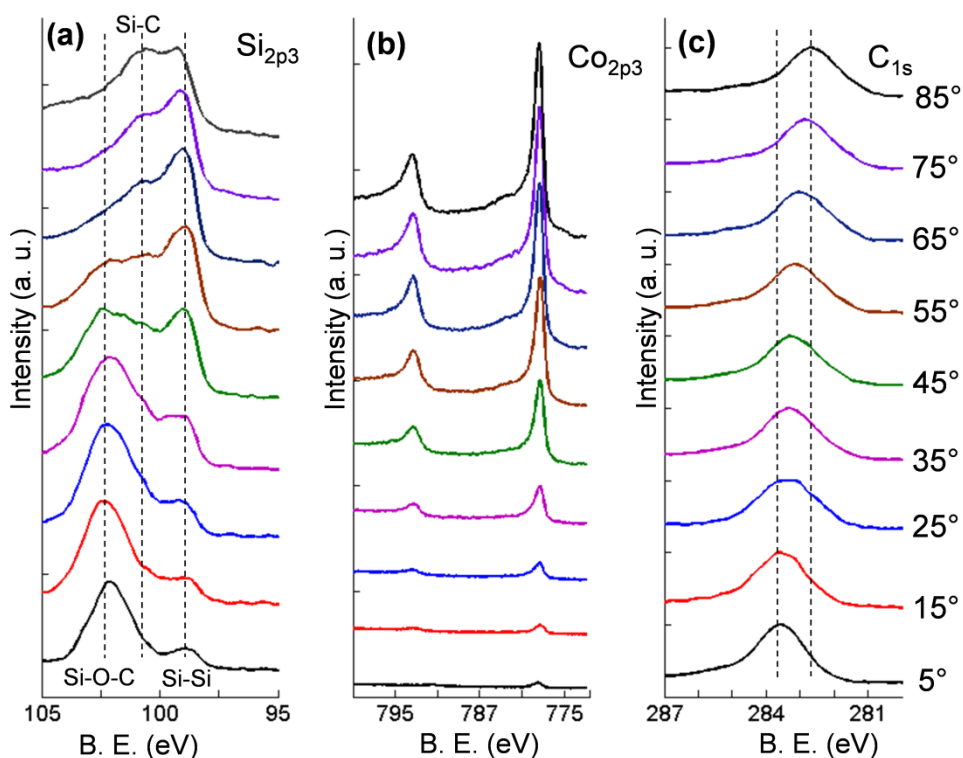
**Figure 10-2** XPS spectra high resolution spectra of (a) $Si_{2p3}$, (b) $Co_{2p3}$, and (c) $C_{1s}$ core levels of 1nm Si/C layer deposited on the Co magnetic film. The spectra were acquired at different photoelectron take off angles measured with respect to the sample surface

As explained earlier, the XPS spectra acquired at grazing angles correspond to the atoms from the outermost layer of the samples. By increasing the take off angle, contribution of the atoms from the bulk of the film and its interface with the substrate will increase. At smaller angles (the outermost region of the Si/C layer), the $Si_{2p3}$ core level spectrum consists of a dominant peak at about 102.2±0.1 eV and a weaker peak located at about 99 eV, corresponding to the Si-O-C (silicon oxycarbide) and Si-Si (Si element) bonds [137, 144-146] respectively. As can be seen, by increasing the take off angle (increasing the contribution of the atoms from deeper levels), the intensity of the oxycarbide peak decreases and the peak shifts to a lower binding energy of about 100.7±0.2 eV corresponding to Si-C bonds [137, 139, 140, 142-144, 196].

Presence of Si-C bonds can be attributed to bombardment of the Si layer with energetic $C^+$ ions. Formation of such bonds between impinging $C^+$ ions of Si surface

due to deposition or ion implantation of C have been reported by many researchers. Existence of silicon oxycarbide on the atomic layers of the sample outermost can be attributed to oxidation of the SiC bonds which was initially formed on the surface. After bombarding the sample with $C^+$ ions, by exposing the sample to the normal environment, oxygen and $H_2O$ molecules can affect the atomic layers on top of the surface and oxidize the SiC bonds. However, this effect was limited to the very shallow regions of the sample and vanishes at deeper levels as can be seen in XPS spectra acquired at larger take of angles (Figure 10-2(a)).

Formation of such chemical bonds between Si atoms and $C^+$ ions on the surface and in the bulk of the Si layer is also supported by the concurrent XPS $C_{1s}$ spectra (Figure 10-2(c)). This result indicates the embedment of $C^+$ ions into the Si thin film. As can be seen in Figure 10-2(c), the maxima of the $C_{1s}$ spectra are located in a range of 283.6-282.7 eV (from top surface to the bulk of the film). These peaks located at low binding energies (compared to that of carbon element at 284.6 eV) can be attributed to carbon atoms in carbide (or carbide-dominant) form. The existence of 0.9 eV peak shift of $C_{1s}$ spectra from top to bulk (interface) of the film could be because of the presence of more C-C bonds on the top surface. By increasing the take off angle, the contribution of these carbon atoms decreases and the $C_{1s}$ peak position shifts to 283.6 eV, corresponding to pure Si-C bonds [114, 132, 140].

The chemical structure of the Si/C mixed layer surface was further studied by the deconvolution of the $C_{1s}$ core level spectrum on the surface (take off angle of 5°). Details of the deconvolution and curve fitting process used in this work have been explained in sections 5-2 and 6-2. From this result, it can be inferred that the C atoms existing on the outermost region of the Si/C layer are in the form of Si-C and $sp^2$ or $sp^3$ boned C-C bonds.
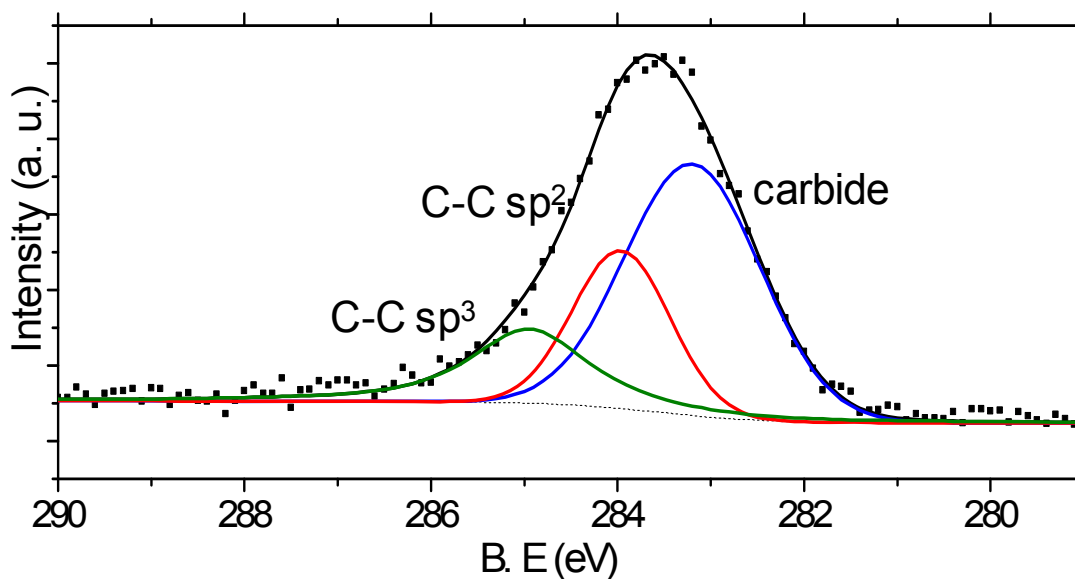
**Figure 10-3** $C_{1s}$ and core level XPS spectra of the top surface of the Co-Si/C sample (take off angle of 5°)

The other important feature of the developed film is presence of Co atoms in the bulk of the Si/C mixed layer. As can be seen in Figure 10-2(b), a very weak peak of Co can be detected on the surface of the sample. However, by increasing the take off angle, the intensity of Co increases. As can be seen, in this figure, at a certain depth (take off angle) of the sample, clear peaks of Si, Co, and C are present; which supports the idea of the formation of a mixed layer rather than separate layers of C and Si on the Co surface. The presence of Co atoms within the structure of the Si/C layer can be attributed to recoil cascades due to bombardment of the surface with $Ar^+$ and $C^+$ ions which provided the Co atoms near the interface enough energy to be driven away from the Co surface into the Si region.
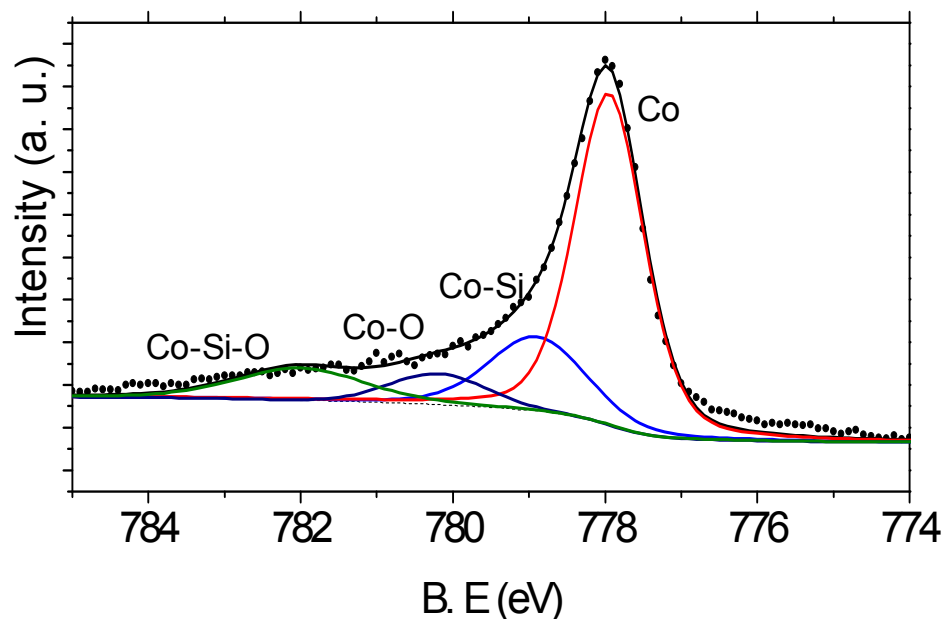
**Figure 10-4** XPS Co$_{2p/3}$ spectrum of the Co/Si mixed layer (interface of Co film and Si/C layer) at take off angle of 75°

The chemical state of the Si/Co mixed layer (interface) was further examined by detailed analysis of the XPS high resolution scans of the Co$_{2p/3}$ spectrum. The Co$_{2p/3}$ spectrum was deconvoluted with four Gaussian/Lorentzian distributions corresponding to the potentially available bonds existing in this region i.e. Co-Co, Co-O, Co-Si, and Co-Si-O. This spectrum (Figure 10-4) consists of one dominant peak at 778±0.2 eV that can be attributed to the Co-Co bonds [142, 197] and also three minor peaks at higher binding energies of about 778.7±0.2 eV, 780 eV, and 781.5±0.2 eV assigned to cobalt silicide (Co-Si) [198], cobalt oxide (Co-O) [142, 199], and cobalt silicate (Co-Si-O) bonds [142, 199] respectively.

### 10.3.2 *Effect of the Si/C mixed layers on the scratch resistance of Co magnetic film*

The effect of surface modification with the Si/C mixed layer on the scratch resistance of the Co film is shown in Figure 10-5. As can be seen in Figure 10-5(a), a scratch of 2–3 nm deep is evident in the surface of bare Co. On the other hand, the surface of the commercial HDD media does not show any deep scratches; however, an initiation of

surface damage (material pile up near the sides of the scratched region) can be observed on the surface of the commercial media, as shown in Figure 10-5(b). Finally, no visible scratch was observed on the Co-Si/C sample as shown in Figure 10-5(c).
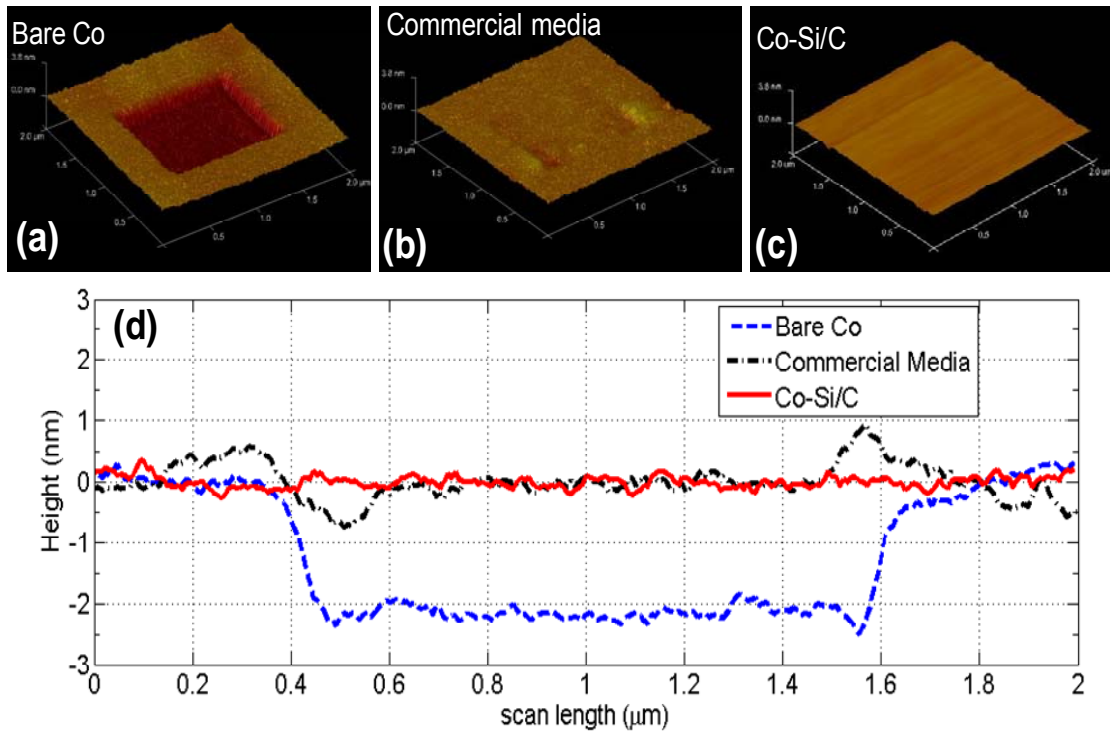


**Figure 10-5** AFM images of the 1×1 µm2 scratched area of (a) bare Co magnetic film, (b) commercial HDD media, and (c) Co magnetic film modified by SiC/C mixed layer. (d) Comparison between the depths of the scratched regions of the samples across the scratched region

The depths of the scratch regions of the samples have been compared using a line profiles across the scratched regions (Figure 10-5(d)). This result signifies a remarkable improvement in the scratch resistance of the Co surface modified with a Si/C mixed layer.

### 10.3.3 *Effect of the Si/C mixed layer on the wear resistance and friction of the Co surface*

A comparison between the typical frictional graphs for bare Co, Co-Si/C, and commercial media is shown in Figure 10-6. A remarkable improvement in the friction of the Co-Si/C sample is evident from the comparison between the coefficient of

friction of this sample (0.18±0.02) and those of the bare Co (0.7±0.06) and commercial media (having an unstable coefficient of friction fluctuating between 0.2 and 0.5). Having maintained a low and stable coefficient of friction until 10,000 wear cycles implies that the Co surface might be still protected by the Si/C mixed layer.
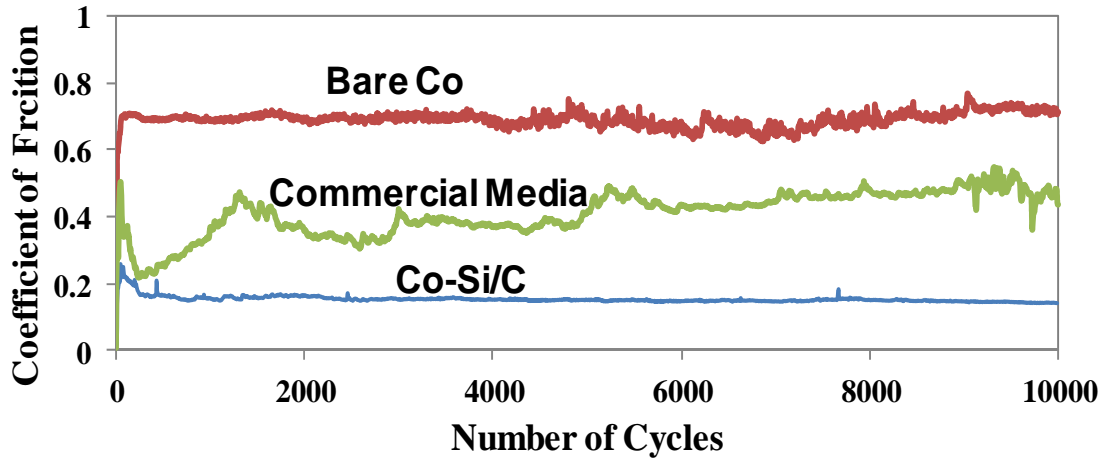


**Figure 10-6** Comparison of typical frictional behavior of Co magnetic film with and without Si/C mixed layer, and commercial magnetic media
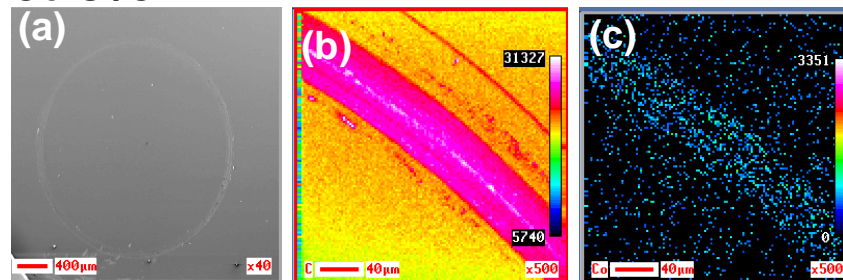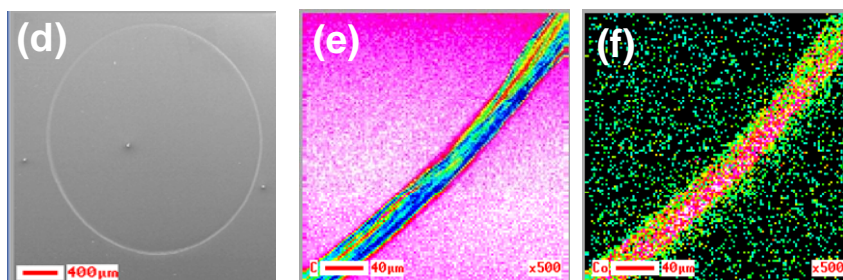


**Figure 10-7** (a, b, and c) SEM images of the wear track and AES elemental mapping of C and Co on sample with Si/C mixed layer and (d, e, and f) on commercial hard disk

The SEM micrographs of the wear tracks on the Co-Si/C and commercial media samples are shown in Figure 10-7(a) and Figure 10-7(d) respectively. As can be seen,

a clear visible wear track is formed on the commercial media. In order to gain a better understanding of the quality of the coating on the commercial media and Co-Si/C sample after the wear test, the surface of the samples was further studied using AES analysis. For this purpose, AES surface elemental mapping (AES images) for C and Co was acquired across the wear track of the samples. In these images, a higher intensity of an element in its specific window is shown with warm or lighter colors while the absence or lower concentration of the elements is indicated by cold or darker colors.

As can be seen from Figures 10-7(b) and 10-7(c), the presence of a uniform Si/C mixed layer (with a stronger intensity of C) on the wear track even after a wear test of 10,000 cycles is evident. This implies that the Si/C mixed layer was able to protect the surface of the Co film against wear. The low friction at the ball/sample interface can be attributed to the existence of this protective layer up to and until the end of the wear test.

Figure 10-7(e) shows the distribution of C atoms near the wear track on the commercial media after the wear test. As can be seen, the C overcoat of the disk (on the wear track) was completely worn off and the Co (from the magnetic layer) was clearly exposed, as shown in Figure 10-7(f). This result clearly explains the high friction and fluctuations in the coefficient of friction of this sample.

## 10.4 Discussion

The improved tribological properties of a Co surface modified with a Si/C mixed layer can be explained in the light of the chemical characteristics of the modified surface. According to the ARXPS results (Figure 10-2 to 10-4), the Si/C film can be considered as a mixture of Si and embedded C atoms that are connected to each other by means of

different types of C-C (with $sp^2$ or $sp^3$ hybridization), Si-Si, and Si-C bonds. XPS analysis demonstrated the existence of a network of C atoms connected by $sp^2$ and $sp^3$ bonds on the outermost region of Si/C mixed layer. In such a mixed layer, a portion of the subplanted C atoms existing in the Si layer was able to form chemical bonds with the Si atoms, forming Si-C bonds. At the same time, these atoms were also able to form C-C bonds with the other carbon atoms existing in the shallower regions of the intermixing layer and also with the C atoms/ions existing/arriving at the outermost area of the Si film.

The improved tribological behavior of the Co-Si/C sample can be attributed to the formation of such a mixed layer containing networks of Si-C and C-C bonds. While SiC itself is a hard material with desirable tribological properties, the formation of a C-C network in conjunction with the Si-C bonds can further improve the wear resistance of the modified surface. The development of such a mixed layer as an interlayer for the overcoat of the recording heads has shown a remarkable improvement in the wear and scratch resistance of the ta-C coating deposited on the AlTiC substrate of the recording heads [123, 200].

The improved tribological performance of the Co-Si/C sample can be further attributed to the formation of silicide bonds between the Si atoms of the mixed layer and the Co atoms of the substrate (Figure 10-4). The formation of such covalent bonds enables the mixed layer to chemically attach to the Co surface and improve its adhesion strength, hence improving the durability of this protective layer.

## 10.5 Conclusion

This proposed surface modification method significantly decreased (more than three times) the friction and improved the scratch and wear resistance of the Co surface. The modified surface with a 1.0±0.1 nm Si/C mixed layer performed much better than

commercial media (with 3 nm of DLC and 1.4 nm of lubricant). These findings show the potential of this novel method to be applied to future generations of hard disk drives with much reduced magnetic spacing. Further improvements in terms of the tribological and corrosion performance of the modified surface may be achieved by applying a thin layer of lubricant to the top surface of the magnetic media which has been modified with the current technique.

# Chapter 11: Conclusion

In order to maintain its position as the most efficient, high capacity, and low-cost form of information storage technology over time, magnetic tape drives have to undergo many improvements in terms of head technology, magnetic media, transport systems, etc. To increase the data recording areal density, the magnetic spacing between the head and magnetic media of the tape (or the hard disk) should be decreased. However, decreasing the magnetic spacing and keeping it within narrow tolerances poses a huge challenge in this technology. Because tape drives are contact recording systems (the head is in contact with the running tape), they experience the problems of mechanical wear and corrosion of the heads, which are the major sources of magnetic spacing.

One way to overcome these tribological problems is to provide an ultra-thin protective coating (not thicker than 10 nm) on the head surface in order to reduce direct interactions between the head materials and the tape media components. The material for such a coating should be atomically dense, compatible with the lubricant, mechanically hard, durable, and have excellent adhesion to the head surface. Tetrahedral amorphous carbon (ta-C), which is a type of DLC with a high fraction of diamond-like ($sp^3$) C-C bonds, has shown promising tribo-mechanical properties which have made it a potential material of choice for protecting magnetic heads in tape drives. However, the serious drawback of ta-C coatings, like all other DLC films, is their poor durability and adhesion to the $Al_2O_3$/TiC (AlTiC) ceramic substrate of the head, which may cause delamination of the coating off the substrate and abrupt failure of the coating.

The main goal of this PhD research work is to investigate various strategies to enhance the durability of ta-C coatings deposited by the filtered cathodic vacuum arc (FCVA)

technique for magnetic tape heads and to develop ultrathin (≤ 1nm) protective layers for hard disk media. In this work, three different methods as listed below were adopted to synthesize durable protective coatings (or surface modifications) on the recording heads or media:

**(a) Pre-treatment of the head surface by bombarding the surface with energetic carbon ions ($C^+$ ions)**

In this work, the effect of pre-treatment of the surface of AlTiC substrate (the main bearing surface of the head in contact with tape) with energetic $C^+$ ions on the structural and tribo-mechanical behaviors of the coated surfaces was studied. This method consisted of two separate stages of surface pre-treatment: bombarding the substrate with energetic $C^+$ ions and deposition of the protective film, and were done by FCVA. The surface characterization results revealed the formation of a broad, atomically dense mixed layer at the ta-C film–substrate interface of the pre-treated samples. Surface pre-treatment was found to have a remarkable effect on increasing the $sp^3$ hybridization fraction in the ta-C overcoat. The tribological behavior of the treated surface was tested using ball-on-flat tests and the results demonstrated the effectiveness of bombardment of the surface with $C^+$ ions to improve the structural and tribo-mechanical properties of the protective ta-C films on the recording head substrate material. According to the tribological tests (ball-on-flat tests), the wear life of the 10 nm ta-C film deposited on the AlTiC flat samples was improved by more than seven times.

**(b) Modification of the head surface by means of formation of an Al-Si-C interlayer between the head substrate and ta-C overcoat**

A 5 nm ta-C overcoat was deposited on Si-coated ceramic substrates by using FCVA technique at ion energy of 100 eV. The chemical state of the ta-C overcoats and

interlayers as well as the nanotribological properties of the ta-C coated AlTiC substrates were studied by means of XPS analysis, nano-scratch and ball-on-flat tests. The formation of a Si-C network between the Si interlayer and ta-C overcoat as well as the formation of Al–O–Si and Si–O–C bonds between the interlayer and the substrate were found to be the two main phenomena which strongly bonded the ta-C film to its ceramic substrate. Prior to the deposition of the ta-C overcoat, the surface of the Si interlayer was bombarded (pre-treated) by $C^+$ ions with ion energy of 350 eV. The effect of this pre-treatment on the structure and tribological properties of the coated surfaces was studied. The results revealed that pre-treatment of the Si interlayer with energetic $C^+$ ions increased the $sp^3$ content of the ta-C film and enhanced the formation of a larger number of strong chemical bonds between the substrate and the overcoat, which improved the durability of the overcoat. In this work, the 5 nm ta-C film with an Al-Si-C interlayer presented approximately two times better durability (wear life) as compared to a ta-C film of the same thickness with a conventional Si interlayer.

The concept of surface modification with more than one element was studied on Co magnetic media (Chapter 10). In this work, an ultra-thin layer of Si with a total thickness of about 1.0 nm (deposited on the Co surface) was bombarded with $C^+$ ions using the FCVA technique to form a Si/C mixed layer. The wear resistance of the surface-modified Co sample was compared with that of a commercial magnetic hard disk with a 3 nm carbon overcoat and 1.4 nm of lubricant. It was found that the Co-Si/C sample showed better tribological properties. The formation of C-C and Si-C bonds at the outermost layer and the bulk of the Si/C film, as well as the formation of chemical bonds between the Co surface and the mixed layer, were found to be important factors in improving the tribological properties (such as higher wear resistance and lower friction) of the treated Co surface.

### (c) Development of a Al-TiN$_x$C$_y$ interlayer to chemically bound the ta-C overcoat to the head surface

In this work, the surface of the heads was pretreated by developing an Al-TiN$_x$C$_y$ composite interlayer prior to deposition of the ta-C overcoat. This composite (mixed layer) was developed by bombardment of a thin (about 1-2 nm thick) TiN film with energetic C$^+$ ions of 350 eV prior to deposition of a 10 nm ta-C overcoat by the FCVA technique. The simulation and experimental results demonstrated the formation of an atomically mixed layer between the ta-C overcoat and AlTiC substrate. It was found that collision cascades – due to bombardment of the TiN layer with C$^+$ ions – were able to embed C$^+$ ions into the TiN and AlTiC regions. In addition, they led to recoil implantation of Al and O atoms from the AlTiC region into the TiN layer. This intermixing process led to the formation of chemical bonds between the existing species in the mixed layer (AlTiN and TiC bonds), which could have chemically bonded the overcoat to the interlayer and the interlayer to the substrate. The effect of this surface pre-treatment on the tribological performance of the coatings with and without an AlTiN$_x$C$_y$ interlayer was studied by ball-on-flat wear tests. The results showed that the developed surface treatment technique was able to improve the wear resistance of the ta-C coating by a factor of 3.3.

### (d) Effects of different surface modification (pre-treatment) techniques on the tribological performance of ta-C coating in a real head/tape interface

In chapters 5 to 7, the effects of different surface treatments on the tribological performance of the ta-C films were studied by using fundamental tribological tests such as ball-on-flat or nano-scratch tests. However, the contact situation in these tests was not similar to the one at the head/tape interface in an actual tape drive. In order to

gain a better insight into the general effects of the developed surface treatment methods on the wear and friction performance of the ta-C film as a protective coating on the recording heads, similar surface treatments were carried out on actual recording heads and the heads were tested in contact with commercial tape media in a real tape drive. According to the results, the conventional ta-C coating was not durable enough to protect the head for a long time, and the coating was completely worn off the surface after running 170 km over the head. ta-C film pre-treated with energetic $C^+$ ions showed better results in comparison with the conventional ta-C. Although the coating was not removed completely, it was delaminated in some regions. Heads with Al-Si-C showed much better wear performance and were able to protect the head after running 1000 km of tape over it. After the wear test it was understood that the ta-C was gradually worn and reached the interlayer.

### (e) Effect of relative humidity on the tribological performance of the ta-C head coating

The effects of different surface pre-treatment methods on the wear life and tribological performance of the ta-C coatings of recording heads were studied in chapters 5-8. In these investigations, the coated recording heads were tested against LTO3 tapes in the normal environment of a clean booth (26±2.0 °C and 45±5% RH). According to the results, among different tested coatings, a ta-C overcoat with an $AlTiN_xC_y$ interlayer showed the best performance (wear life of ~1.6 million meters in terms of the length of the tape passed over the head). In chapter 9, the wear performance of a 10 nm ta-C coating with a $TiN_xC_y$ interlayer was studied as a function of relative humidity. In this study, a newer generation of LTO tape (i.e. LTO5) was used for the wear tests and its effect on the wear life of the coating was investigated. The wear tests were conducted in three different environments of normal (40% RH), dry (10% RH), and pure (<1%

RH) air. The results revealed that the 10 nm ta-C film with an $AlTiN_xC_y$ interlayer presented the highest wear life in a normal environment (only 2.5 nm of the coating was removed). In addition, it was found that the application of the LTO5 tape can improve the wear life of the coating by up to 2.5 times compared to LTO3 tape. However, the results showed that at a constant temperature, the wear life of the ta-C coatings was a function of humidity, and wear resistance degraded as the relative humidity decreased. It was also found that very low humidity not only decreased the wear life of the head coating, but it also increased the likelihood of material transfer from the tape to the head surface as well as formation of head stain. This behavior can be attributed to the surface chemistry of the head/tape interface. In humid air, water and hydrocarbon molecules are able to saturate the dangling bonds and passivate the surface, which decreases the chance of formation of strong adhesion junctions between two surfaces and therefore decreases the coating removal due to adhesive wear. On the other hand, due to an insufficient supply of $H_2O$ molecules in very dry or pure air, the dangling bonds remain active and strong adhesion junctions (with high bonding strength) may form between the tape and coating. This gives rise to wear of the coating and, in more severe cases, material transfer from the tape to the head surface. These conclusions were in agreement with the findings of the previous studies investigating the effects of the environment on the wear performance of hydrogen-free carbon films tested by fundamental tribological techniques.

The application of an $Al-TiN_xC_y$ composite interlayer was shown to be able to solve the delamination problem effectively and increase the wear life of the coating. This coating showed more than 60% improvement in wear life as compared with that of the ta-C film with an Al-Si-C interlayer. These results are very promising and the application of such interlayers to improve the durability of coatings can be introduced

to develop head coatings that can protect tape drive heads based on the current standards of the tape drive industry.

Finally, it should be emphasized that these tests were conducted using a commercially available tape generation which is generally more abrasive than new generations of tapes that are smoother and with lower friction at the head/tape interface. Therefore, the designed coatings are expected to perfom for a longer time when working in contact with the new generations of tapes. Furthermore, the maximum thickness of the coatings used in this study was about 10 nm, while the tape industry road map allows for thicker head coatings (15-17 nm) till 2014. Moreover, by decreasing the film thickness, these surface modification methods can be potentially exploited in the surface modification of recording heads and media as well as the development of overcoat free magnetic disks in the next generation of hard drives with extremely high recording density.

# Chapter 12: Future Recommendations

Tetrahedral amorphous carbon was used as the protective coating on the surface of magnetic tape drive heads. Different surface modifications were developed to improve the durability of these films. These surface pre-treatment methods were able to improve the durability of the 10 nm ta-C films considerably when coated on the surface of the magnetic tape drive heads. In this work, the main focus was on the application of ta-C films deposited with the FCVA technique.

However, there are other wear resistant materials that can potentially be used for protecting the head surface against wear. Hard ceramics such as SiC, SiN, TiN, AlTiN, nitrogenated carbon deposited by FCVA technique, BC, BN, etc. are being used as wear resistant coatings on the surfaces of bearings or tools. Although most of these films with a thickness of less than 20 nm were not able to effectively protect the head surface, super-lattice (multilayer) films such as TiN/SiN or SiN/Al-TiN, etc. with a thickness of about 10 nm can be studied as new coating designs to protect the head against wear and corrosion. In the final months of this PhD work, initial studies on this field were conducted and a TiN/SiN multilayer film (repetition of SiN and TiN layer of 2nm periodicity) with a total thickness 10 nm was used as an overcoat for the tape head. The initial results showed remarkably improved wear resistance as compared with single layer films of TiN or SiN of the same thickness. More interestingly, this multilayer film showed a wear performance as good as that of ta-C films with $AlTiN_xC_y$ interlayer as presented in this work. Further studies and optimizations in terms of materials, thicknesses, order of layers and deposition techniques, is a potentially exiting topic for the future work in this field.

Another important topic which can be studied in future is the role of environmental effects on the tribological performance of the developed coatings in the present work. In the current study, the developed coatings were tested in a fixed temperature but at different values of relative humidity. In the future work, one may study the effects of temperature and relative humidity together well as effect of different gas environments on the wear performance of the coatings.

In this work, LTO3 tapes were used as the counterface in most of the wear tests on coated heads. This generation of tape is much rougher (more abrasive) than the newer generation of tapes with higher data capacity. In order to have a better understanding of the wear life of the developed methodology in the future tape drives, it is suggested that one repeats the tribological tests against more advanced generations of tapes such as LTO5, and especially BaFe tapes, which are smoother (less abrasive) with modified formulations of lubricant.

Finally, this PhD work was mainly focused on the wear performance of the developed coatings. Friction at the head/tape interface is a critical issue and is one of the most important aspects that one may consider in tribological studies of magnetic tape drives. Understanding the complicated mechanisms governing the frictional interactions (causes of static and dynamic friction) at the head/tape interface was out of the scope of the current work. However, this topic, as well as understanding (analytically and experimentally) the effect of different head coatings on the dynamic friction and stiction (static friction) between head and tape media, and also the stick-slip behaviour with very smooth tapes, are suggested as potential areas for future research.

In this study, we mainly focused on the role of humidity (water content) of the normal environment (air + humidity) on the wear resistance of the ta-C coatings. The mechanism provided in this research was that water molecules passivate the dangling bonds of surface carbon atoms. The findings of this study can clearly comment on the role of water molecules on passivation of the surface, which decreases the severity of the wear. However, one may considered the possibility of tribochemical wear due to oxygen. In a normal humid environment, water molecules may out-compete oxygen in adsorption to passivate the carbon surface. However, in a dry environment, adsorption of oxygen will no doubt cause tribochemical wear.

Based on the existing experimental procedure and results, we are not able to confidently comment on the tribo-mechanical wear due to adsorption of oxygen. To have certain conclusion, one needs to design another experiment in which the wear test is carried out in an environment free of oxygen (with and without humidity). This can be done by purging the test chamber with an inert gas such as $N_2$ or Ar. In this way, the effect of only humidity will be studied. This is because in an inert and dry environment, there will be no $O_2$ or $H_2O$ to alter the surface dangling bonds. One can repeat the same thing but in the presence of $H_2O$ and study the surface after the wear tests. By comparing the results of these two experiments with the existing results from the current work, one can comment on whether the wear is due to oxidation of the surface or because of adhesive wear. This topic generally has been extensively studied by other researchers; however, further work can be done in future to study the effect of oxidation on the wear of the head ta-C coatings at the head/tape interface.

# Bibliogarphy

1.      Ferrari, A.C., *Diamond-like carbon for magnetic storage disks.* Surface and Coatings Technology, 2004. **180-181**: p. 190-206.

2.      Wallace, R.L., *The reproduction of magnetically recorded signal.* Bell System Technology  Journal, 1951. **30**: p. 1145-1173.

3.      Harris, J.P., W.B. Phillips, J.F. Wells, and W.D. Winger, *Innovations in the design of magnetic tape subsystems.* IBM J. Res. Dev., 1981. **25**(5): p. 691-700.

4.      Daniel, E.D., C.D. Mee, and M.H. Clark, *Magnetic Recording: The First Hundred Years*. 1999, New York: IEEE Press.

5.      Scott, W.W. and B. Bhushan, *Corrosion and wear studies of uncoated and ultra-thin DLC coated magnetic tape-write heads and magnetic tapes.* Wear, 2000. **243**(1-2): p. 31-42.

6.      Dee, R.H., *Magnetic Tape for Data Storage: An Enduring Technology.* Proceedings of the IEEE, 2008. **96**(11): p. 1775-1785.

7.      Cherubini, G., et al., *29.5-Gbit/in$^2$ Recording Areal Density on Barium Ferrite Tape.* Magnetics, IEEE Transactions on, 2011. **47**(1): p. 137-147.

8.      Watson, M.L., R.A. Beard, S.M. Kientz, and T.W. Feebeck, *Investigation of Thermal Demagnetization Effects in Data Recorded on Advanced Barium Ferrite Recording Media.* Magnetics, IEEE Transactions on, 2008. **44**(11): p. 3568-3571.

9.      *Fujifilm to manufacture 5 TB Tape Cartridge for Oracle's Storage Tek T10000C Drive, Fujifilm News Release, February 1, 2011, http://www.fujifilm.com/news/n110201.html*.

10.     Sullivan, J.L., *Magnetic Recording: Flexible Media, Tribology*, in *Encyclopedia of Materials: Science and Technology*, K.H.J. Buschow, et al., Editors. 2002, Elsevier: Oxford. p. 1-9.

11.     sullivan, J.L., *Magnetic Recording: Flexible Media, Tribology*, in *Concise Encyclopedia of Magnetic and Superconducting Materials*, K.H.J. Buschow, Editor. 2005, Elsevier.

12.     Thomson, T., L. Abelmann, and H. Groenland, *Magnetic Data Storage: Past Present and Future*, in *Magnetic Nanostructures in Modern Technology*, B. Azzerboni, et al., Editors. 2008, Springer Netherlands. p. 237-306.

13.     Childers, E.R., W. Imaino, J.H. Eaton, G.A. Jaquette, P.V. Koeppe, and D.J. Hellman, *Six orders of magnitude in linear tape technology: The one-terabyte project.* IBM Journal of Research and Development, 2003. **47**(4): p. 471-482.

14. *Information Storage Industry Consortium (INSIC), International Magnetic Tape Storage Roadmap.* 2011.

15. Hansen, W.S. and B. Bhushan, *Measurement and mechanism of pole tip recession with advanced metal evaporated tape at low tension in a linear tape drive.* Microsystem Technologies, 2006. **12**(3): p. 193-203.

16. Sourty, E., J.L. Sullivan, and L.A.M. De Jong, *Pole tip recession in linear recording heads.* IEEE Transactions on Magnetics, 2003. **39**(3 II): p. 1859-1861.

17. Shi, B., J.L. Sullivan, S.O. Saied, and M.A. Wild, *A study on the formation and structure of LTO head stains.* Tribology International, 2005. **38**(6-7): p. 709-716.

18. Shi, B., M.A. Wild, J.L. Sullivan, and S.O. Saied, *Contact pressure effects on pole tip recession and head stain in linear digital tape systems.* Tribology International, 2005. **38**(6-7): p. 699-708.

19. Lacey, C. and F.E. Talke, *Measurement and Simulation of Partial Contact at the Head/Tape Interface.* ASME J. Tribol, 1992. **114**(4): p. 646–652.

20. Poorman, P., *The effect of tape overwrap angle and head radius on head/tape spacing and contact pressure in linear tape recording.* Tribology International, 1998. **31**(8): p. 449-455.

21. Shi, B., J.L. Sullivan, M.A. Wild, and S.O. Saied, *Study of Generation Mechanism of Three-Body Particles in Linear Tape Recording.* Journal of Tribology, 2005. **127**(1): p. 155-163.

22. Scott, W.W. and B. Bhushan, *Micro/nano-scale differential wear of multiphase materials: pole tip recession in magnetic-tape heads.* Wear, 2002. **252**(1-2): p. 103-122.

23. Xu, J. and B. Bhushan, *Pole tip recession studies of thin-film rigid disk head sliders I. Mechanisms of pole tip recession growth.* Wear, 1998. **219**(1): p. 16-29.

24. Sullivan, J.L., B. Shi, and S.O. Saied, *Microtribological studies of two-phase Al2O3-TiC ceramic at low contact pressure.* Tribology International, 2005. **38**(11-12): p. 987-994.

25. Harrison, M.J.K., J.L. Sullivan, and G.S.A.M. Theunissen, *Pole tip recession in sandwich heads incorporating a FeTaN soft magnetic track.* Tribology International, 1998. **31**(9): p. 491-500.

26. Spada, F., *Contribution of Electrochemical Processes to Increased Head-Media Spacing in Tape Drives.* presented at INS IC TAPE Research Program Technical Reviews, November 15, 2011, February 14, 2012 and May 15, 2012.

27. Thomson, T., L. Abelmann, and J.P.J. Groenland, *Magnetic data storage: past, present and future*, in *Magnetic Nanostructures in Modern Technology*, B.

Azzerboni, et al., Editors. 2007, Springer Verlag. p. 237-306.

28. Wickert, J.A., *Analysis Of Self-excited Longitudinal Vibration Of A Moving Tape.* Journal of Sound and Vibration, 1993. **160**(3): p. 455-463.

29. Spada, F., *Reported in INSIC TAPE Program Technical Reviews (www.insic.org/tape.htm), also abstract DT-06 of the 52nd Anual MMM Conference, November 2007, Tampa, Florida.* 2007.

30. Chen, C.Y., D.B. Bogy, T. Cheng, and C.S. Bhatia, *Effect of the additive X-1P on the tribological performance and migration behavior of PFPE lubricant at the head-disk interface.* IEEE Transactions on Magnetics, 2000. **36**(5 I): p. 2708-2710.

31. Chen, C.Y., D.B. Bogy, and C.S. Bhatia, *Effects of backbone and endgroup on the decomposition mechanisms of PFPE lubricants and their tribological performance at the head-disk interface.* Journal of Tribology, 2001. **123**(2): p. 364-367.

32. Bhatia, C.S., C.Y. Chen, W. Fong, and D.B. Bogy, *Tribochemistry of ZDOL decomposition on carbon overcoats in Ultra-High Vacuum.* 2000. **593**: p. 397-408.

33. Bhatia, C.S., W. Fong, C.Y. Chen, J. Wei, D.B. Bogy, S. Anders, T. Stammler, and J. Stöhr, *Tribo-chemistry at the head/disk interface.* IEEE Transactions on Magnetics, 1999. **35**(2): p. 910-915.

34. Chen, C.Y., D.B. Bogy, and C.S. Bhatia, *Tribochemistry of monodispersed ZDOL with hydrogenated carbon overcoats.* Journal of Vacuum Science and Technology A: Vacuum, Surfaces and Films, 2000. **18**(4 II): p. 1809-1817.

35. Chen, C.Y., J. Wei, W. Fong, D.B. Bogy, and C.S. Bhatia, *The decomposition mechanisms and thermal stability of ZDOL lubricant on hydrogenated carbon overcoats.* Journal of Tribology, 2000. **122**(2): p. 458-464.

36. Jiang, B., D.J. Keffer, and B.J. Edwards, *A quantum mechanical study of the decomposition of CF3OCF 3 and CF3CF2OCF2CF3 in the presence of AlF3.* Journal of Physical Chemistry A, 2008. **112**(12): p. 2604-2609.

37. Aisenberg, S. and R. Chabot, *Ion-Beam Deposition of Thin Films of Diamondlike Carbon.* Journal of Applied Physics, 1971. **42**(7): p. 2953-2958.

38. Aisenberg, S. and R. Chabot, *Deposition of carbon films with diamond properties.* Carbon, 1972. **10**(3): p. 356.

39. Meyerson, B. and F.W. Smith, *Electrical and optical properties of hydrogenated amorphous carbon films.* Journal of Non-Crystalline Solids, 1980. **35–36, Part 1**(0): p. 435-440.

40. Meyerson, B. and F.W. Smith, *Chemical modification of the electrical properties of hydrogenated amorphous carbon films.* Solid State Communications, 1980. **34**(7): p. 531-534.

41. I. I. Aksenov, S. I. Vakula, V. G. Padalka, V. E. Strel'nitskii, and V.M. Khoroshikh, *High-efficiency source of pure carbon plasma* Sov. Phys.—Tech. Phys., 1980. **25**: p. 1164–1166.

42. Aksenov, I., V. Belous, V. Padalka, and V. Khoroshikh, *Apparatus to rid the plasma of a vacuum arc of macroparticles.* Instruments and experimental techniques, 1978. **21**(5 ): p. 1416-1418.

43. Bhatia, C.S., S. Anders, I.G. Brown, K. Bobb, R. Hsiao, and D.B. Bogy, *Ultra-Thin Overcoats for the Head/Disk Interface Tribology.* Journal of Tribology, 1998. **120**(4): p. 795-799.

44. Anders, A., *Cathodic arcs: from fractal spots to energetic condensation.* Vol. 50. 2009, New York: Springer.

45. Donnet, C. and A. Erdemir, *Tribology of Diamond-Like Carbon Films: Fundamentals and Applications* ed. C. Donnet and A. Erdemir. 2008, New York: Springer US.

46. Ferrari, A.C., J. Robertson, M.G. Beghi, C.E. Bottani, R. Ferulano, and R. Pastorelli, *Elastic constants of tetrahedral amorphous carbon films by surface Brillouin scattering.* Applied Physics Letters, 1999. **75**(13): p. 1893-1895.

47. Pharr, G.M., et al., *Hardness, elastic modulus, and structure of very hard carbon films produced by cathodic-arc deposition with substrate pulse biasing.* Applied Physics Letters, 1996. **68**(6): p. 779-781.

48. Casiraghi, C., A.C. Ferrari, and J. Robertson, *Raman spectroscopy of hydrogenated amorphous carbons.* Physical Review B - Condensed Matter and Materials Physics, 2005. **72**(8): p. 1-14.

49. Erdemir, A. and C. Donnet, *Tribology of diamond-like carbon films: Recent progress and future prospects.* Journal of Physics D: Applied Physics, 2006. **39**(18): p. R311-R327.

50. Charitidis, C. and S. Logothetidis, *Nanomechanical and nanotribological properties of carbon based films.* Thin Solid Films, 2005. **482**(1-2): p. 120-125.

51. Robertson, J., *Ultrathin carbon coatings for magnetic storage technology.* Thin Solid Films, 2001. **383**(1-2): p. 81-88.

52. Robertson, J., *Requirements of ultrathin carbon coatings for magnetic storage technology.* Tribology International, 2003. **36**(4-6): p. 405-415.

53. Guruz, M.U., V.P. Dravid, Y.W. Chung, M.M. Lacerda, C.S. Bhatia, Y.H. Yu, and S.C. Lee, *Corrosion performance of ultrathin carbon nitride overcoats synthesized by magnetron sputtering.* Thin Solid Films, 2001. **381**(1): p. 6-9.

54. Moser, E.M. and C. Müller, *A versatile plasma technique to improve plastic materials against gas and water-vapour permeation.* Journal of Materials Science, 1999. **34**(2): p. 349-353.

55. Casiraghi, C., J. Robertson, and A.C. Ferrari, *Diamond-like carbon for data and beer storage.* Materials Today, 2007. **10**(1-2): p. 44-53.

56. Moser, E.M., R. Urech, E. Hack, H. Künzli, and E. Müller, *Hydrocarbon films inhibit oxygen permeation through plastic packaging material.* Thin Solid Films, 1998. **317**(1-2): p. 388-392.

57. Podgornik, B. and J. Vizintin, *Tribological reactions between oil additives and DLC coatings for automotive applications.* Surface and Coatings Technology, 2005. **200**(5-6): p. 1982-1989.

58. Johnston, S.V. and S.V. Hainsworth, *Effect of DLC coatings on wear in automotive applications.* Surface Engineering, 2005. **21**: p. 67-71.

59. Smietana, M., J. Szmidt, M.L. Korwin-Pawlowski, W.J. Bock, and J. Grabarczyk, *Application of diamond-like carbon films in optical fibre sensors based on long-period gratings.* Diamond and Related Materials. **16**(4-7): p. 1374-1377.

60. Lettington, A.H. and C. Smith, *Optical properties and applications of diamond-like carbon coatings.* Diamond and Related Materials, 1992. **1**(7): p. 805-809.

61. Tiainen, V.-M., *Amorphous carbon as a bio-mechanical coating -- mechanical properties and biological applications.* Diamond and Related Materials, 2001. **10**(2): p. 153-160.

62. Vojs, M., E. Zdravecká, M. Marton, P. Bohác, L. Franta, and M. Veselý, *Properties of amorphous carbon layers for bio-tribological applications.* Microelectronics Journal, 2009. **40**(3): p. 650-653.

63. Robertson, J., *Diamond-like amorphous carbon.* Materials Science and Engineering: R: Reports, 2002. **37**(4-6).

64. Ferrari, A.C., A. Libassi, B.K. Tanner, V. Stolojan, J. Yuan, L.M. Brown, S.E. Rodil, B. Kleinsorge, and J. Robertson, *Density, $sp^3$ fraction, and cross-sectional structure of amorphous carbon films determined by x-ray reflectivity and electron energy-loss spectroscopy.* Physical Review B, 2000. **62**(16): p. 11089-11103.

65. Anders, S., A. Anders, I.G. Brown, B. Wei, K. Komvopoulos, J.W. Ager Iii, and K.M. Yu, *Effect of vacuum arc deposition parameters on the properties of amorphous carbon thin films.* Surface and Coatings Technology, 1994. **68–69**(0): p. 388-393.

66. Anders, S., D.L. Callahan, G.M. Pharr, T.Y. Tsui, and C. Singh Bhatia, *Multilayers of amorphous carbon prepared by cathodic arc deposition.* Surface and Coatings Technology, 1997. **94-95**: p. 189-194.

67. Erdemir, A. and C. Donnet, *Tribology of diamond-like carbon films: recent progress and future prospects.* Journal of Physics D: Applied Physics, 2006. **39**(18): p. R311.

68.    Dischler, B., A. Bubenzer, and P. Koidl, *Bonding in hydrogenated hard carbon studied by optical spectroscopy.* Solid State Communications, 1983. **48**(2): p. 105-108.

69.    Ferrari, A.C., B. Kleinsorge, N.A. Morrison, A. Hart, V. Stolojan, and J. Robertson, *Stress reduction and bond stability during thermal annealing of tetrahedral amorphous carbon.* Journal of Applied Physics, 1999. **85**(10): p. 7191-7197.

70.    McKenzie, D.R., *Tetrahedral bonding in amorphous carbon.* Reports on Progress in Physics, 1996. **59**(12): p. 1611.

71.    Fallon, P.J., V.S. Veerasamy, C.A. Davis, J. Robertson, G.A.J. Amaratunga, W.I. Milne, and J. Koskinen, *Properties of filtered-ion-beam-deposited diamondlike carbon as a function of ion energy.* Physical Review B, 1993. **48**(7): p. 4777-4782.

72.    Anders, S., J. Diaz, J.W. Ager Iii, R.Y. Lo, and D.B. Bogy, *Thermal stability of amorphous hard carbon films produced by cathodic arc deposition.* Applied Physics Letters, 1997. **71**(23): p. 3367-3369.

73.    Anders, S., J.W. Ager Iii, G.M. Pharr, T.Y. Tsui, and I. G. Brown, *Heat treatment of cathodic arc deposited amorphous hard carbon films.* Thin Solid Films, 1997. **308–309**(0): p. 186-190.

74.    Casiraghi, C., A.C. Ferrari, R. Ohr, A.J. Flewitt, D.P. Chu, and J. Robertson, *Dynamic Roughening of Tetrahedral Amorphous Carbon.* Physical Review Letters, 2003. **91**(22): p. 226104.

75.    Luo, J.K. and et al., *Diamond and diamond-like carbon MEMS.* Journal of Micromechanics and Microengineering, 2007. **17**(7): p. S147.

76.    Hultman, L., S. Stafström, Z. Czigány, J. Neidhardt, N. Hellgren, I.F. Brunell, K. Suenaga, and C. Colliex, *Cross-Linked Nano-onions of Carbon Nitride in the Solid Phase: Existence of a Novel C48N12 Aza-Fullerene.* Physical Review Letters, 2001. **87**(22): p. 225503.

77.    Li, D.J., M.U. Guruz, and Y.W. Chung, *Ultrathin CNx overcoats for 1 Tb/in2 hard disk drive systems.* American Society of Mechanical Engineers, Tribology Division, TRIB, 2003(11): p. 61-64.

78.    Zhao, J.F., P. Lemoine, Z.H. Liu, J.P. Quinn, P. Maguire, and J.A. McLaughlin, *A study of microstructure and nanomechanical properties of silicon incorporated DLC films deposited on silicon substrates.* Diamond and Related Materials, 2001. **10**(3–7): p. 1070-1075.

79.    Zhao, J.F., P. Lemoine, Z.H. Liu, J.P. Quinn, and J.A. McLaughlin, *The effects of Si incorporation on the microstructure and nanomechanical properties of DLC thin films.* Journal of Physics: Condensed Matter, 2000. **12**(44): p. 9201.

80.    Cuomo, J.J., D.L. Pappas, J. Bruley, J.P. Doyle, and K.L. Saenger, *Vapor deposition processes for amorphous carbon films with sp3 fractions*

*approaching diamond.* Journal of Applied Physics, 1991. **70**(3): p. 1706-1711.

81. Anders, A., *A Brief History of Cathodic Arc Coating*, in *Cathodic Arcs: From Fractal Spots to Energetic Condensation* A. Anders, Editor. 2009, Springer: New York.

82. Baker Jr, B.B. and D.J. Kasprzak, *Thermal degradation of commercial fluoropolymers in air.* Polymer Degradation and Stability, 1993. **42**(2): p. 181-188.

83. Kasai, P.H., *Perfluoropolyethers: intramolecular disproportionation.* Macromolecules, 1992. **25**(25): p. 6791-6799.

84. Bhatia, C.S., F. Walton, C. Chao-Yuan, W. Jianjun, D.B. Bogy, S. Anders, T. Stammler, and J. Stohr, *Tribo-chemistry at the head/disk interface.* Magnetics, IEEE Transactions on, 1999. **35**(2): p. 910-915.

85. Chen, C.Y., W. Fong, D.B. Bogy, and C. Singh Bhatia, *Initiation of lubricant catalytic decomposition by hydrogen evolution from contact sliding on CHx and CNx overcoats.* Tribology Letters, 2000. **8**(1): p. 25-34.

86. Zieren, V., M. de Jongh, A.B. van Groenou, J.B.A. van Zon, P. Lasinski, and G.S.A.M. Theunissen, *Ultrathin wear-resistant coatings for the tape bearing surface of thin-film magnetic heads for digital compact cassette.* Magnetics, IEEE Transactions on, 1994. **30**(2): p. 340-345.

87. Lee, K.R., K.Y. Eun, K.M. Kim, and K.C. Choi, *Application of diamond-like carbon films for anti-abrasion and low friction properties of VCR head drums.* Surface and Coatings Technology, 1995. **76-77**(PART 2): p. 786-790.

88. Lee, K.-R. and K.Y. Eun. *Measurement of friction coefficients between diamond-like carbon coated VCR head drum and VCR tapes.* 1995.

89. Trakhtenberg, I.S., V.B. Vykhodets, V.L. Arbuzov, S.A. Plotnikov, A.E. Davletshin, J.H. Lee, S.J. Kim, and B.S. Chang, *DLC coating for video head.* Diamond and Related Materials, 1999. **8**(8-9): p. 1770-1775.

90. Bhushan, B., B.K. Gupta, R. Sundaram, S. Dey, S. Anders, A. Anders, I.G. Brown, and P.D. Reader, *Development of hard carbon coatings for thin-film tape heads.* IEEE Transactions on Magnetics, 1995. **31**(6 pt 1): p. 2976-2978.

91. Bhushan, B., S.T. Patton, R. Sundaram, and S. Dey, *Pole tip recession studies of hard carbon-coated thin-film tape heads.* Journal of Applied Physics, 1996. **79**(8 PART 2B): p. 5916-5918.

92. Scott, W.W., B. Bhushan, and A.V. Lakshmikumaran, *Ultrathin diamond-like carbon coatings used for reduction of pole tip recession in magnetic tape heads.* Journal of Applied Physics, 2000. **87**(9 III): p. 6182-6184.

93. Bijker, M.D., E.A. Draaisma, M. Eisenberg, J. Jansen, N. Persat, and E. Sourty, *Future directions in Advanced Digital Recording technology.* Tribology International, 2000. **33**(5): p. 383-390.

94.  Bijker, M.D., J.J.J. Bastiaens, E.A. Draaisma, L.A.M. de Jong, E. Sourty, S.O. Saied, and J.L. Sullivan, *The development of a thin Cr2O3 wear protective coating for the advanced digital recording system.* Tribology International, 2003. **36**(4-6): p. 227-233.

95.  Sourty, E., J.L. Sullivan, and M.D. Bijker, *Chromium oxide coatings applied to magnetic tape heads for improved wear resistance.* Tribology International, 2003. **36**(4-6): p. 389-396.

96.  Sourty, E., J.L. Sullivan, and M.D. Bijker, *Numerical modelling of sub-surface stress in magnetic data tape heads due to the dynamic contact with a tape.* Tribology International, 2002. **35**(3): p. 171-184.

97.  Shi, B., J.L. Sullivan, and S.O. Saied, *A Study of Thin Coating Wear in High Data Density Tape Heads.* Journal of ASTM International, 2008. **5**(3).

98.  Scott, W.W., B. Bhushan, and A.V. Lakshmikumaran, *Ultrathin diamond-like carbon coatings used for reduction of pole tip recession in magnetic tape heads.* Journal of Applied Physics, 2000. **87**(9): p. 6182-6184.

99.  Bhushan, B., G.S.A.M. Theunissen, and X. Li, *Tribological studies of chromium oxide films for magnetic recording applications.* Thin Solid Films, 1997. **311**(1-2): p. 67-80.

100.  Theunissen, G.S.A.M., *Wear coatings for magnetic thin film magnetic recording heads.* Tribology International, 1998. **31**(9): p. 519-523.

101.  Gupta, B.K. and B. Bhushan, *Mechanical and tribological properties of hard carbon coatings for magnetic recording heads.* Wear, 1995. **190**(1): p. 110-122.

102.  Bhushan, B., *Chemical, mechanical and tribological characterization of ultra-thin and hard amorphous carbon coatings as thin as 3.5 nm: recent developments.* Diamond and Related Materials, 1999. **8**(11): p. 1985-2015.

103.  Zhang, H.S. and K. Komvopoulos, *Direct-current cathodic vacuum arc system with magnetic-field mechanism for plasma stabilization.* Review of Scientific Instruments, 2008. **79**(7): p. 073905-7.

104.  Anders, A., *Approaches to rid cathodic arc plasmas of macro- and nanoparticles: a review.* Surface and Coatings Technology, 1999. **120–121**(0): p. 319-330.

105.  Anders, A., *A periodic table of ion charge-state distributions observed in the transition region between vacuum sparks and vacuum arcs.* Plasma Science, IEEE Transactions on, 2001. **29**(2): p. 393-398.

106.  Robertson, J., *Diamond-like amorphous carbon.* Materials Science and Engineering: R: Reports, 2002. **37**(4-6): p. 129-281.

107.  Komvopoulos, K., B. Wei, S. Anders, A. Anders, and I.G. Brown, *Surface modification of magnetic recording heads by plasma immersion ion*

*implantation and deposition.* Journal of Applied Physics, 1994. **76**(3): p. 1656-1664.

108. Ziegler, J.F., J.P. Biersack, and V. Liimark, *The Stopping and Range of Ions in Solids* 1985  New York: Pergamon.

109. D. Briggs and M.P. Seah, *Practical Surface Analysis, Vol. 1. Auger and X-ray Photoelectron Spectroscopy* 2$^{nd}$ ed. 1993, Chichester ; New York: John Willey and sons.

110. Carlson, T.A., *Photoelectron and Auger Spectroscopy.* 1975, New York: Plenum Press.

111. Hedberg, C.L., *Handbook of Auger Electron Spectroscopy*: Physical Electronics, Inc.

112. Shum, P.W., Z.F. Zhou, and K.Y. Li, *Tribological performance of amorphous carbon films prepared on steel substrates with carbon implantation pre-treatment.* Wear, 2004. **256**(3-4): p. 362-373.

113. Tong, H.H., O.R. Monteiro, and I.G. Brown, *Effects of carbon ion pre-implantation on the mechanical properties of ta-C coatings on Ti-6Al-4V.* Surface and Coatings Technology, 2001. **136**(1-3): p. 211-216.

114. Han, H., F. Ryan, and M. McClure, *Ultra-thin tetrahedral amorphous carbon film as slider overcoat for high areal density magnetic recording.* Surface and Coatings Technology, 1999. **120-121**: p. 579-584.

115. Lifshitz, Y., S.R. Kasi, J.W. Rabalais, and W. Eckstein, *Subplantation model for film growth from hyperthermal species.* Physical Review B, 1990. **41**(15): p. 10468.

116. Robertson, J., *The deposition mechanism of diamond-like a-C and a-C: H.* Diamond and Related Materials, 1994. **3**(4-6): p. 361-368.

117. Shirley, D.A., *High-Resolution X-Ray Photoemission Spectrum of the Valence Bands of Gold.* Physical Review B, 1972. **5**(12): p. 4709.

118. Lu, W., K. Komvopoulos, and S.W. Yeh, *Stability of ultrathin amorphous carbon films deposited on smooth silicon substrates by radio frequency sputtering.* Journal of Applied Physics, 2001. **89**(4): p. 2422-2433.

119. Zhang, H.S., J.L. Endrino, and A. Anders, *Comparative surface and nano-tribological characteristics of nanocomposite diamond-like carbon thin films doped by silver.* Applied Surface Science, 2008. **255**(5, Part 2): p. 2551-2556.

120. Robertson, J., *Deposition mechanisms for promoting sp$^3$ bonding in diamond-like carbon.* Diamond and Related Materials, 1993. **2**(5-7): p. 984-989.

121. Hofsäss, H., H. Feldermann, R. Merk, M. Sebastian, and C. Ronning, *Cylindrical spike model for the formation of diamondlike thin films by ion deposition.* Applied Physics A: Materials Science & Processing, 1998. **66**(2): p.

153-181.

122. Malaczynski, G.W., A.A. Elmoursi, C.H. Leung, A.H. Hamdi, and A.B. Campbell, *Surface enhancement by shallow carbon implantation for improved adhesion of diamond-like coatings.* Journal of Vacuum Science & Technology B: Microelectronics and Nanometer Structures, 1999. **17**(2): p. 813-817.

123. Rismani, E., S.K. Sinha, H. Yang, and C.S. Bhatia, *Effect of pretreatment of Si interlayer by energetic $C^+$ ions on the improved nanotribological properties of magnetic head overcoat.* Journal of Applied Physics, 2012. **111**(8): p. 084902-10.

124. Camino, D., A.H.S. Jones, D. Mercs, and D.G. Teer, *High performance sputtered carbon coatings for wear resistant applications.* Vacuum, 1999. **52**(1-2): p. 125-131.

125. Ronkainen, H., S. Varjus, J. Koskinen, and K. Holmberg, *Differentiating the tribological performance of hydrogenated and hydrogen-free DLC coatings.* Wear, 2001. **249**(3-4): p. 260-266.

126. Phetdee, K., A. Pimpin, and W. Srituravanich, *Investigation of wear resistance and lifetime of diamond-like carbon (DLC) coated glass disk in flying height measurement process.* Microsystem Technologies, 2011: p. 1-7.

127. Liu, Z.H., J.F. Zhao, and J. McLaughlin, *A study of microstructural and electrochemical properties of ultra-thin DLC coatings on altic substrates deposited using the ion beam technique.* Diamond and Related Materials, 1999. **8**(1): p. 56-63.

128. Prabhakaran, V. and F.E. Talke, *Wear and hardness of carbon overcoats on magnetic recording sliders.* Wear, 2000. **243**(1-2): p. 18-24.

129. Park, C.K., S.M. Chang, H.S. Uhm, S.H. Seo, and J.S. Park, *XPS and XRR studies on microstructures and interfaces of DLC films deposited by FCVA method.* Thin Solid Films, 2002. **420-421**: p. 235-240.

130. Meyerson, B.S., R.V. Joshi, R. Rosenberg, and V.V. Patel, *Silicon/carbon protection of metallic magnetic structures*, in *US patent*. 1987, International Business Machines Corporation (IBM) United states.

131. Komvopoulos, K., H. Zhang, and C.S. Bhatia, *Systems and Methods for Surface Modification by Filtered Cathodic Vacuum Arc*, in *US Patent*. 2010, UC Berkeley: United States.

132. Zhang, H.S. and K. Komvopoulos, *Synthesis of ultrathin carbon films by direct current filtered cathodic vacuum arc.* Journal of Applied Physics, 2009. **105**(8): p. 083305-7.

133. Anders, A., *Cathodic arcs: from fractal spots to energetic condensation.* 2008, New York: Springer Science.

134. Ponpon, J.P., *Room temperature oxidation of ion bombarded silicon.* Surface

Science, 1985. **162**(1-3): p. 687-694.

135. Manning, I., *Transport-theory approach to ion-beam mixing and recoil implantation.* Physical Review B, 1990. **42**(16): p. 9853.

136. Lifshitz, Y., G.D. Lempert, and E. Grossman, *Substantiation of subplantation model for diamondlike film growth by atomic force microscopy.* Physical Review Letters, 1994. **72**(17): p. 2753-2756.

137. Choi, W.K., T.Y. Ong, L.S. Tan, F.C. Loh, and K.L. Tan, *Infrared and x-ray photoelectron spectroscopy studies of as-prepared and furnace-annealed radio-frequency sputtered amorphous silicon carbide films.* Journal of Applied Physics, 1998. **83**(9): p. 4968-4973.

138. Besling, W.F.A., A. Goossens, B. Meester, and J. Schoonman, *Laser-induced chemical vapor deposition of nanostructured silicon carbonitride thin films.* Journal of Applied Physics, 1998. **83**(1): p. 544-553.

139. Solomon, I., M.P. Schmidt, eacute, C. maud, and M. Driss Khodja, *Band structure of carbonated amorphous silicon studied by optical, photoelectron, and x-ray spectroscopy.* Physical Review B, 1988. **38**(18): p. 13263.

140. Zajícková, L., K. Veltruská, N. Tsud, and D. Franta, *XPS and ellipsometric study of DLC/silicon interface.* Vacuum, 2001. **61**(2-4): p. 269-273.

141. Choi, J., M. Kawaguchi, T. Kato, and M. Ikeyama, *Deposition of Si-DLC film and its microstructural, tribological and corrosion properties.* Microsystem Technologies, 2007. **13**(8): p. 1353-1358.

142. Moulder, J.F., W.F. Stickle, and P.E. Sobol, *Handbook of X Ray Photoelectron Spectroscopy.* 1993, Eden Prairie, Minnesota: Perkin-Elmer, Physical Electronics Division.

143. Gallis, S., M. Huang, H. Efstathiadis, E. Eisenbraun, A.E. Kaloyeros, E.E. Nyein, and U. Hommerich, *Photoluminescence in erbium doped amorphous silicon oxycarbide thin films.* Applied Physics Letters, 2005. **87**(9): p. 091901-3.

144. Wang, Y.H., M.R. Moitreyee, R. Kumar, L. Shen, K.Y. Zeng, J.W. Chai, and J.S. Pan, *A comparative study of low dielectric constant barrier layer, etch stop and hardmask films of hydrogenated amorphous Si-(C, O, N).* Thin Solid Films, 2004. **460**(1-2): p. 211-216.

145. Smith, K.L. and K.M. Black, *Characterization of the treated surfaces of silicon alloyed pyrolytic carbon and SiC.* Journal of Vacuum Science & Technology A: Vacuum, Surfaces, and Films, 1984. **2**(2): p. 744-747.

146. Onneby, C. and C.G. Pantano, *Silicon oxycarbide formation on SiC surfaces and at the SiC/SiO$_2$ interface.* Journal of Vacuum Science & Technology A, 1997. **15**(3 ): p. 1597-1602.

147. Correa, S.A., et al., *Enhancement in interface robustness regarding thermal*

*oxidation in nanostructured Al$_2$O$_3$ deposited on 4H-SiC.* Applied Physics Letters, 2009. **95**(5): p. 051916-3.

148. Klein, T.M., D. Niu, W.S. Epling, W. Li, D.M. Maher, C.C. Hobbs, R.I. Hegde, I.J.R. Baumvol, and G.N. Parsons, *Evidence of aluminum silicate formation during chemical vapor deposition of amorphous Al$_2$O$_3$ thin films on Si(100).* Applied Physics Letters, 1999. **75**(25): p. 4001-4003.

149. Choy, K.-L. and E. Felix, *Functionally graded diamond-like carbon coatings on metallic substrates.* Materials Science and Engineering: A, 2000. **278**(1–2): p. 162-169.

150. Jones, M.I., I.R. McColl, D.M. Grant, K.G. Parker, and T.L. Parker, *Haemocompatibility of DLC and TiC–TiN interlayers on titanium.* Diamond and Related Materials, 1999. **8**(2–5): p. 457-462.

151. Wang, L., S. Wan, S. Wang, R. Wood, and Q. Xue, *Gradient DLC-Based Nanocomposite Coatings as a Solution to Improve Tribological Performance of Aluminum Alloy.* Tribology Letters, 2010. **38**(2): p. 155-160.

152. Liao, J.X., L.F. Xia, M.R. Sun, W.M. Liu, T. Xu, and Q.J. Xue, *The tribological properties of a gradient layer prepared by plasma-based ion implantation on 2024 aluminum alloy.* Surface and Coatings Technology, 2004. **183**(2–3): p. 157-164.

153. Castillo, H.A., E. Restrepo-Parra, and P.J. Arango-Arango, *Chemical and morphological difference between TiN/DLC and a-C:H/DLC grown by pulsed vacuum arc techniques.* Applied Surface Science, 2011. **257**(7): p. 2665-2668.

154. Liao, J.X., L.F. Xia, M.R. Sun, W.M. Liu, T. Xu, and Q.J. Xue, *The structure and tribological properties of gradient layers prepared by plasma-based ion implantation on 2024 Al alloy.* Journal of Physics D: Applied Physics, 2004. **37**(3): p. 392.

155. Avelar-Batista, J.C., E. Spain, G.G. Fuentes, A. Sola, R. Rodriguez, and J. Housden, *Triode plasma nitriding and PVD coating: A successful pre-treatment combination to improve the wear resistance of DLC coatings on Ti6Al4V alloy.* Surface and Coatings Technology, 2006. **201**(7): p. 4335-4340.

156. Lifang, X., Y. Zhaohui, and L. Jiaxuan, *Effects of intermediate layers on the tribological behavior of DLC coated 2024 aluminum alloy.* Wear, 2004. **257**(5–6): p. 599-605.

157. Pang, X., H. Yang, K. Gao, Y. Wang, and A.A. Volinsky, *AlTiN layer effect on mechanical properties of Ti-doped diamond-like carbon composite coatings.* Thin Solid Films, 2011. **519**(16): p. 5353-5357.

158. Logothetidis, S., E.I. Meletis, G. Stergioudis, and A.A. Adjaottor, *Room temperature oxidation behavior of TiN thin films.* Thin Solid Films, 1999. **338**(1–2): p. 304-313.

159. Hassan, M., R.S. Rawat, P. Lee, S.M. Hassan, A. Qayyum, R. Ahmad, G.

Murtaza, and M. Zakaullah, *Synthesis of nanocrystalline multiphase titanium oxycarbide TiC$_x$O$_y$ thin films by UNU/ICTP and NX2 plasma focus devices.* Applied Physics A: Materials Science & Processing, 2008. **90**(4): p. 669-677.

160. Phase, D.M. and S. Vasant, *In situ photoelectron spectroscopy study of TiC x N y films synthesized through reactive ion beam mixing.* Journal of Physics D: Applied Physics, 2004. **37**(12): p. 1696.

161. Bertoncello, R., A. Casagrande, M. Casarin, A. Glisenti, E. Lanzoni, L. Mirenghi, and E. Tondello, *Tin, Tic and Ti(C, N) film characterization and its relationship to tribological behaviour.* Surface and Interface Analysis, 1992. **18**(7): p. 525-531.

162. Schüler, A. and P. Oelhafen, *Titanium aluminum nitride (Ti-Al-N) films were deposited by reactive magnetron cosputtering.* . Physical Review B, 2001. **63**(11): p. 115413

163. Strydom, I. and S. Hofmann, *The contribution of characteristic energy losses in the core-level X-ray photoelectron spectroscopy peaks of TiN and (Ti, Al)N studied by electron energy loss spectroscopy and X-ray photoelectron spectroscopy.* Journal of Electron Spectroscopy and Related Phenomena, 1991. **56**(2): p. 85-103.

164. Rismani, E., S. Sujeet K., Y. H., and B. C. S., *Effect of pre-treatment of Si interlayer by energetic C$^+$ ions on the improved tribo-mechanical properties of magnetic head overcoat.* Journal of Applied Physics (under review), 2011.

165. Catledge, S., R. Vaid, P. Diggins, J. Weimer, M. Koopman, and Y. Vohra, *Improved adhesion of ultra-hard carbon films on cobalt–chromium orthopaedic implant alloy.* Journal of Materials Science: Materials in Medicine, 2011. **22**(2): p. 307-316.

166. Tang, Y., Y.S. Li, C.Z. Zhang, J. Wang, Q. Yang, and A. Hirose, *Synthesis of cobalt/diamond-like carbon thin films by biased target ion beam deposition.* Diamond and Related Materials, 2011. **20**(4): p. 538-541.

167. Zhang, W., A. Tanaka, K. Wazumi, and Y. Koga, *Structural, mechanical and tribological properties of diamond-like carbon films prepared under different substrate bias voltage.* Diamond and Related Materials, 2002. **11**(11): p. 1837-1844.

168. Grill, A., V. Patel, and B. Meyerson, *Tribological behavior of diamond-like carbon: effects of preparation conditions and annealing.* Surface and Coatings Technology, 1991. **49**(1–3): p. 530-536.

169. Liu, Y., A. Erdemir, and E.I. Meletis, *Influence of environmental parameters on the frictional behavior of DLC coatings.* Surface and Coatings Technology, 1997. **94–95**(0): p. 463-468.

170. Andersson, J., R.A. Erck, and A. Erdemir, *Friction of diamond-like carbon films in different atmospheres.* Wear, 2003. **254**(11): p. 1070-1075.

171.  Andersson, J., R.A. Erck, and A. Erdemir, *Frictional behavior of diamondlike carbon films in vacuum and under varying water vapor pressure.* Surface and Coatings Technology, 2003. **163–164**(0): p. 535-540.

172.  Yoon, E.-S., H. Kong, and K.-R. Lee, *Tribological behavior of sliding diamond-like carbon films under various environments.* Wear, 1998. **217**(2): p. 262-270.

173.  Enke, K., H. Dimigen, and H. Hubsch, *Frictional properties of diamondlike carbon layers.* Applied Physics Letters, 1980. **36**(4): p. 291-292.

174.  Jiang, J., S. Zhang, and R.D. Arnell, *The effect of relative humidity on wear of a diamond-like carbon coating.* Surface and Coatings Technology, 2003. **167**(2–3): p. 221-225.

175.  Ronkainen, H. and K. Holmberg, *Environmental and Thermal Effects on the Tribological Performance of DLC Coatings Tribology of Diamond-Like Carbon Films*, C. Donnet and A. Erdemir, Editors. 2008, Springer US. p. 155-200.

176.  Ambekar, P.P. and B. Bhushan, *Effect of operating environment on head–tape interface in a linear tape drive.* Journal of Magnetism and Magnetic Materials, 2003. **261**(1–2): p. 277-294.

177.  Bhushan, B., G.S.A.M. Theunissen, and X. Li, *Tribological studies of chromium oxide films for magnetic recording applications.* Thin Solid Films, 1997. **311**(1–2): p. 67-80.

178.  *Information Storage Industry Consortium (INSIC), International Magnetic Tape Storage Roadmap.* 2008: p. 149.

179.  McKenzie, D.R., Y. Yin, N.A. Marks, C.A. Davis, B.A. Pailthorpe, G.A.J. Amaratunga, and V.S. Veerasamy, *Hydrogen-free amorphous carbon preparation and properties.* Diamond and Related Materials, 1994. **3**(4–6): p. 353-360.

180.  Ronkainen, H., J. Koskinen, J. Likonen, S. Varjus, and J. Vihersalo, *Characterization of wear surfaces in dry sliding of steel and alumina on hydrogenated and hydrogen-free carbon films.* Diamond and Related Materials, 1994. **3**(11–12): p. 1329-1336.

181.  Jung, H.-S., H.-H. Park, S.S. Pang, and S.Y. Lee, *The structural and electron field emission characteristics of pulsed laser deposited diamond-like carbon films with thermal treatment.* Thin Solid Films, 1999. **355–356**(0): p. 151-156.

182.  Erdemir, A., *The role of hydrogen in tribological properties of diamond-like carbon films.* Surface and Coatings Technology, 2001. **146–147**(0): p. 292-297.

183.  Erdemir, A., *Genesis of superlow friction and wear in diamondlike carbon films.* Tribology International, 2004. **37**(11–12): p. 1005-1012.

184.  Gardos, M.N., *Tribology and wear behaviour of diamond*, in *Synthetic*

*Diamond: Emerging CVD Science and Technology*, K.E. Spear, Dismuke, J. P, Editor. 1994, Wiley: New York. p. 419–502.

185.    Bhushan, B., *Introduction to Tribology*. 2002, New York: John Wiley & Sons.

186.    Sourty, E., M. Wild, and J.L. Sullivan, *Pole tip recession and staining at the head to tape interface of linear tape recording systems.* Wear, 2002. **252**(3-4): p. 276-299.

187.    Zhi-Min, Y., L. Bo, Z. Tiejun, G. Chi Keong, O. Chun Lian, C. Choon Min, and W. Li, *Perspectives of Magnetic Recording System at 10 Tb/in$^2$.* Magnetics, IEEE Transactions on, 2009. **45**(11): p. 5038-5043.

188.    Bandic, Z. and R.H. Victora, *Advances in Magnetic Data Storage Technologies* Proceedings of the IEEE  2008. **96**(11): p. 1749 - 1753.

189.    Poh Wei Choong, A., S.N. Piramanayagam, and T.Y.F. Liew, *Overcoat Materials for Magnetic Recording Media*, in *Developments in Data Storage*. 2011, John Wiley & Sons, Inc. p. 167-192.

190.    Casiraghi, C., A.C. Ferrari, J. Robertson, R. Ohr, M.v. Gradowski, D. Schneider, and H. Hilgers, *Ultra-thin carbon layer for high density magnetic storage devices.* Diamond and Related Materials, 2004. **13**(4-8): p. 1480-1485.

191.    Zhong, M., C. Zhang, J. Luo, and X. Lu, *The protective properties of ultra-thin diamond like carbon films for high density magnetic storage devices.* Applied Surface Science, 2009. **256**(Chimica): p. 322-328.

192.    Zhang, H.-S. and K. Komvopoulos, *Surface modification of magnetic recording media by filtered cathodic vacuum arc.* Journal of Applied Physics, 2009. **106**(9): p. 093504.

193.    Samad, M., E. Rismani, H. Yang, S. Sinha, and C. Bhatia, *Overcoat Free Magnetic Media for Lower Magnetic Spacing and Improved Tribological Properties for Higher Areal Densities.* Tribology Letters, 2011. **43**(3): p. 247-256.

194.    Samad, M.A., H. Yang, S.K. Sinha, and C.S. Bhatia, *Effect of carbon embedding on the tribological properties of magnetic media surface with and without a perfluoropolyether (PFPE) layer.* Journal of Physics D: Applied Physics, 2011. **44**(31): p. 315301.

195.    Samad, M.A., S. Xiong, L. Pa, H. Yang, S.K. Sinha, D.B. Bogy, and C.S. Bhatia, *A Novel Approach of Carbon Embedding in Magnetic Media for Future Head/Disk Interface.* IEEE TRANSACTIONS ON MAGNETICS, 2012. **48**(5).

196.    Kawasaki, M., G.J. Vandentop, M. Salmeron, and G.A. Somorjai, *Analysis of the interface of hydrogenated amorphous carbon films on silicon by angle-resolved x-ray photoelectron spectroscopy.* urface Science, 1990. **227**(3): p. I261-267.

197.    García-Méndez, M., F.F. Castillón, G.A. Hirata, M.H. Farías, and G. Beamson,

*XPS and HRTEM characterization of cobalt–nickel silicide thin films.* Applied Surface Science, 2000. **161**(1–2): p. 61-73.

198.   Prabhakaran, K. and T. Ogino, *Behavior of ultrathin layers of Co on Si and Ge systems.* Applied Surface Science, 1996. **100–101**(0): p. 518-521.

199.   Barr, T.L., *Recent advances in x-ray photoelectron spectroscopy studies of oxides.* Journal of Vacuum Science & Technology A: Vacuum, Surfaces, and Films, 1991. **9**(3): p. 1793-1805.

200.   Rismani, E., S.K. Sinha, H. Yang, S. Tripathy, and C.S. Bhatia, *Development of a ta-C Wear Resistant Coating with Composite Interlayer for Recording Heads of Magnetic Tape Drives.* Tribology Letters, 2012. **46**(3): p. 221-232.